两相分流对（微通道式和翅片管式）换热器性能影响及改善措施

Chi-Chuan Wang (王啟川), PhD, FASME, FASHRAE
Professor, Department of Mechanical Engineering,
National Chiao Tung University, Hsinchu, Taiwan

E-mail: ccwang@mail.nctu.edu.tw

Dec. 1, 2017 @ 珠海格力电器

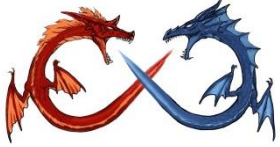

Outline

- Flow distribution in Single phase Flow
- Flow distribution in Two-Phase Flow
- Two-phase Heat Exchanger – microchannels
- Multipass Micro channel HXs
- Improved Designs
- Concluding Remarks

Typical Single Phase Design

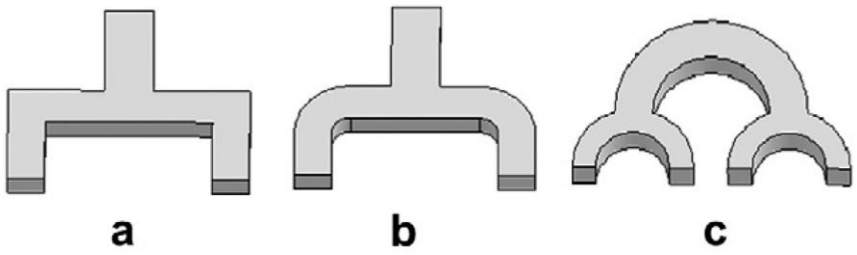

Fig. 2 – Flow channel bifurcation and the structure for a 90-degree channel turning after bifurcation ((a) Turning with sharp corner; (b) Turning with round corner; (c) Circular turning).

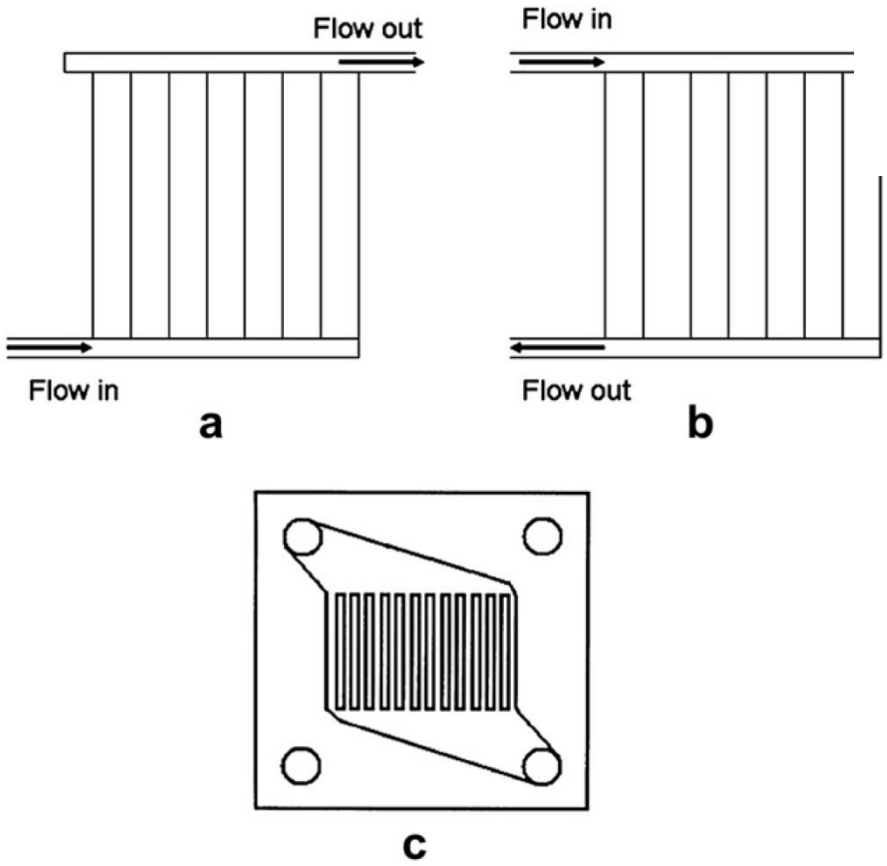

Fig. 1 – Typical flow distribution structures evolved from flute-type manifold.

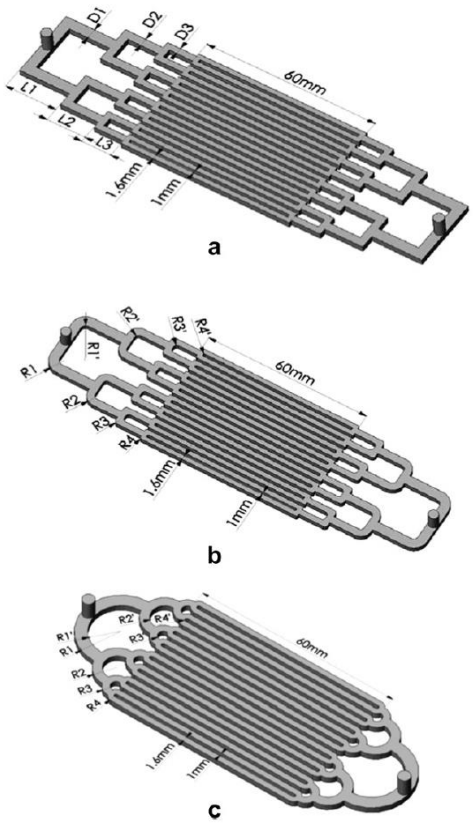

Fig. 3 – Overview of bifurcation flow distributors in different structure of the 90-degree turning of flow channels ((a) Turning with sharp corner; (b) Turning with round corner; (c) Circular turning).

Typical single phase flow distribution for U and Z type header

Fundamentals of Heat exchanger Design, R.K. Shah, Chapter 12

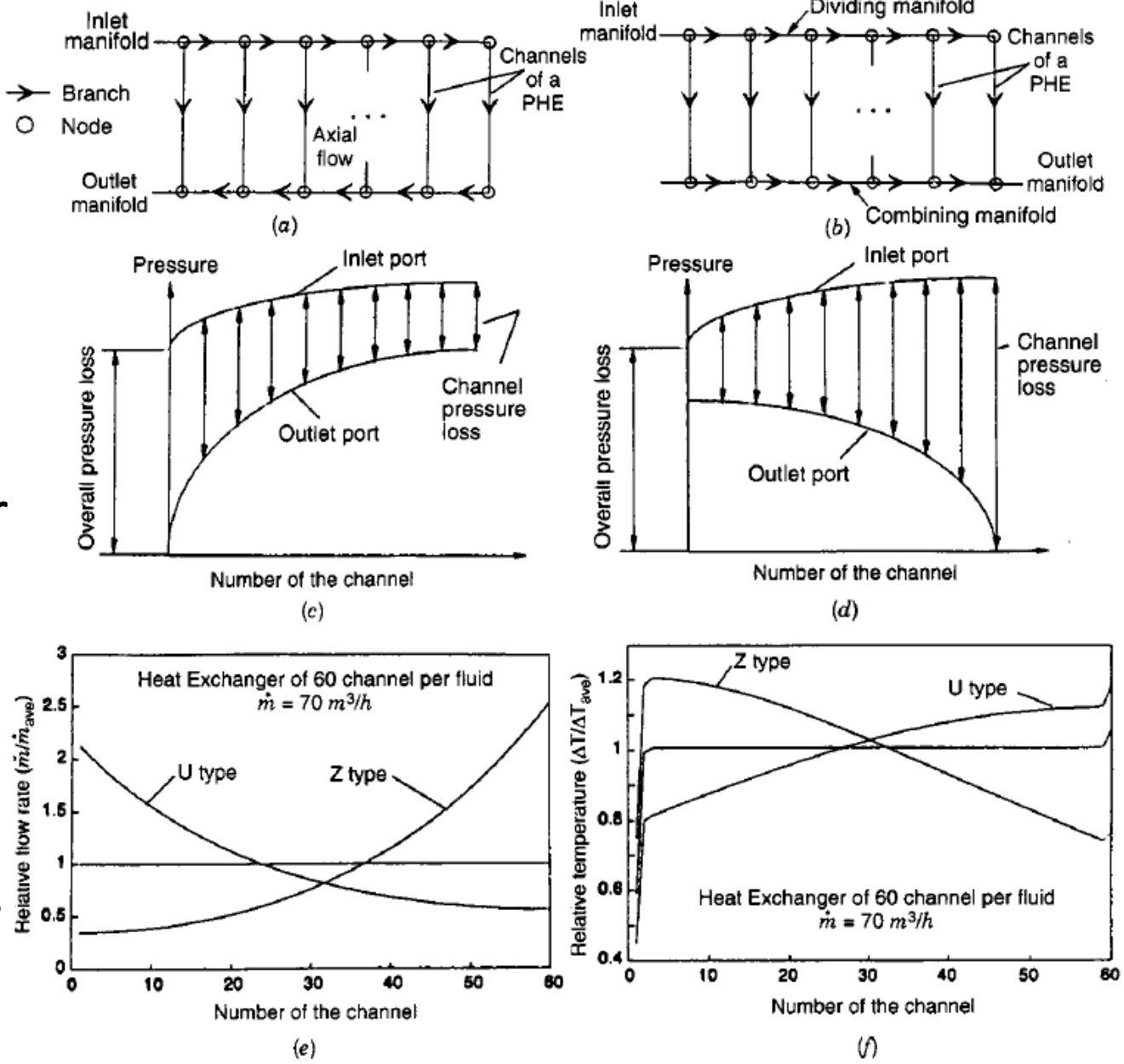

FIGURE 12.7 Manifold configurations: (*a*) U-flow or parallelflow configuration; (*b*) Z-flow, S-flow, or reverse-flow configuration. Pressure profile in (*c*) U-flow configuration, (*d*) Z-flow configuration. In these configurations, (*e*) typical flow distribution, and (*f*) typical temperature distribution. [Parts (e) and (f) from Thonon, 2002.]

Liquid Flow Distribution Characteristics in Compact Parallel Flow Heat Exchangers, Part I: Typical Inlet Header, *Applied Thermal Engineering,* Vol. 31, pp. 3226-3234 (2011).

Liquid Flow Distribution Characteristics in Compact Parallel Flow Heat Exchangers, Part II: Modified Inlet Header," *Applied Thermal Engineering,* Vol. 31, pp. 3025-3242 (2011).

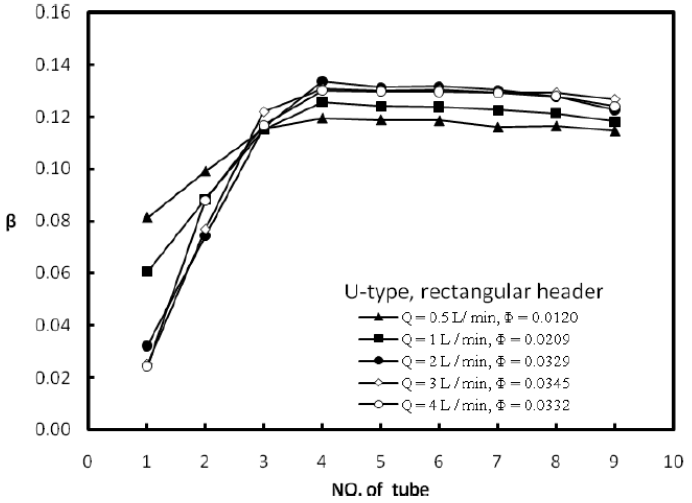

(a) Flow ratio of the typical rectangular header for U-type flow.

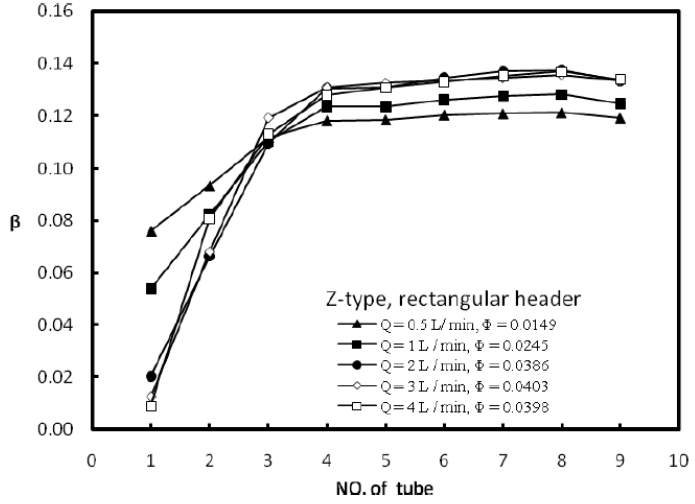

(b) Flow ratio of the typical rectangular header for Z-type flow.

Fig. 2. Flow ratio of the rectangular header for U-type and Z-type flows.

Table 1. The geometric sizes of the test sections.

D mm	H (mm)	W (mm)	AR (mn)	t (mm)	b (mm)	L (mm)
3	12	12	0.442	18.5	6	120
	9	9	0.785	18.5	5	120
				13.5		110
				3.5		90
	7	7	1.298	18.5	5	120
2	12	12	0.196	19	6	120
	9	9	0.349	19	5	120
	7	7	0.557	19	5	120

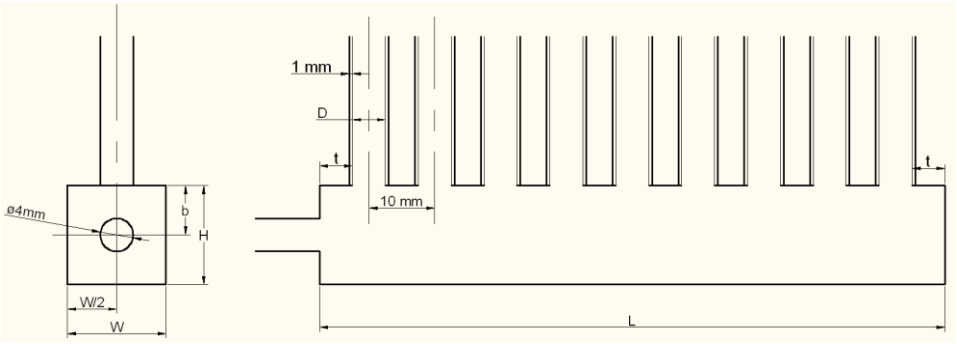

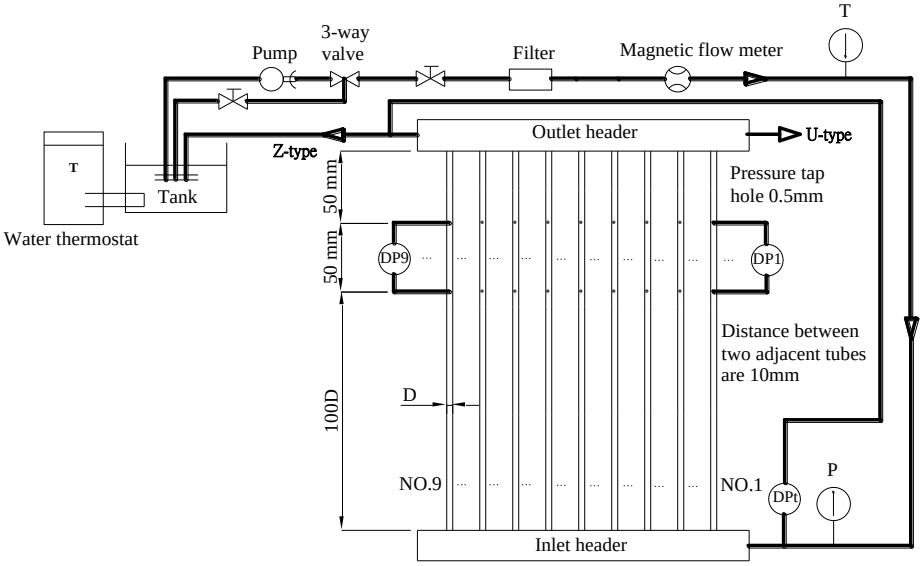

Different flow distribution when jet flow pattern prevails

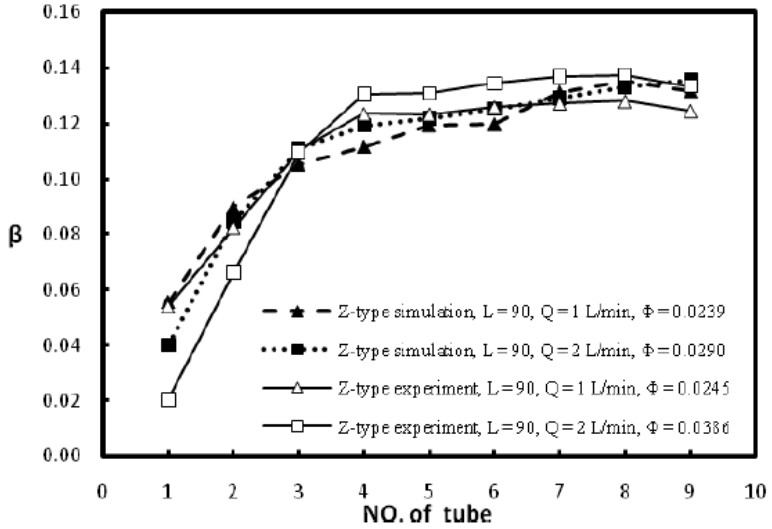

F.ig. 7. Numerical simulation of flow ratio for Z-type flow vs. data.

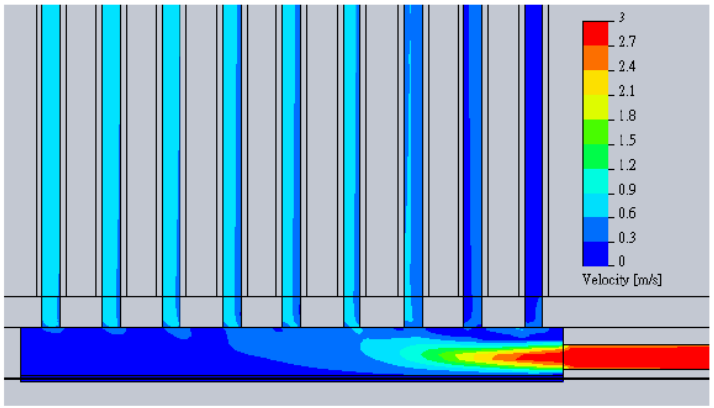

Fig. 8. Velocity simulation in 9×9 mm header with 90 mm length and D = 3 mm tubes

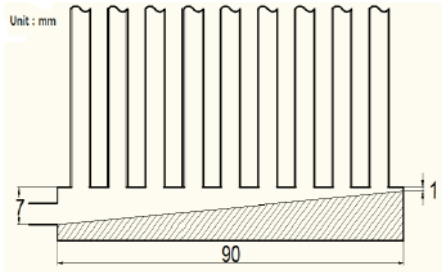

(a) Diagram of the modified header with a trapezoidal blocker.

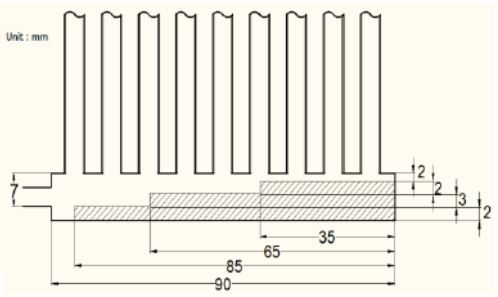

(b) Diagram of modified header with a multi-step blocker.

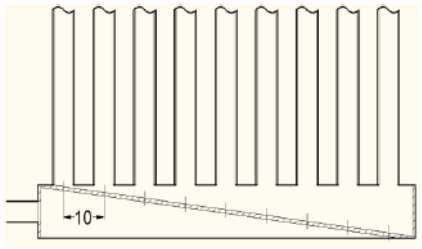

(c.1)The inclined baffle plate installing in the header

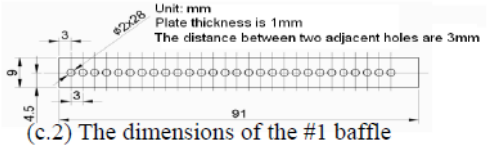

(c.2) The dimensions of the #1 baffle plate.

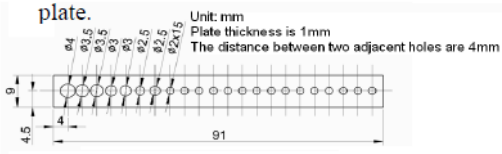

(c.3) The dimensions of the #2 baffle

(c) Diagram of the modified header and baffle plates.

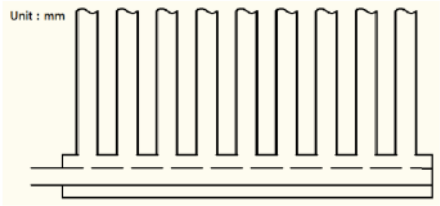

(d) Modified header with installed baffle

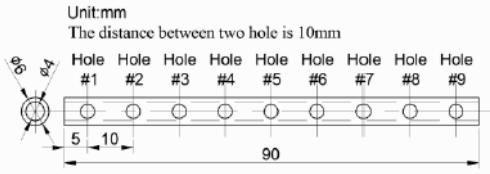

(d.1) Dimensions of baffle tubes.

Baffle tube	Hole #1 (mm)	Hole #2 (mm)	Hole #3 (mm)	Hole #4 (mm)	Hole #5 (mm)	Hole #6 (mm)	Hole #7 (mm)	Hole #8 (mm)	Hole #9 (mm)
#1	4	3.7	3.2	3.2	3.2	3.2	3.2	3.2	3.2
#2	4	3.5	3	3	3	3	3	3	3
#3	3.7	3.2	2.8	2.8	2.8	2.8	2.8	2.8	2.8
#4	3.5	3	2	2	2	2	2	2	2
#5	3	2.2	1.5	1.5	1.5	1.5	1.5	1.5	1.5
#6	2.8	2	1.2	1.2	1.2	1.2	1.2	1.2	1.2
#7	3.8	2.2	1.5	1.5	1.5	1.5	1.5	1.5	1.5

(e) The hole diameters for 7 baffle tubes

Fig. 1. Diagram of the modified headers.

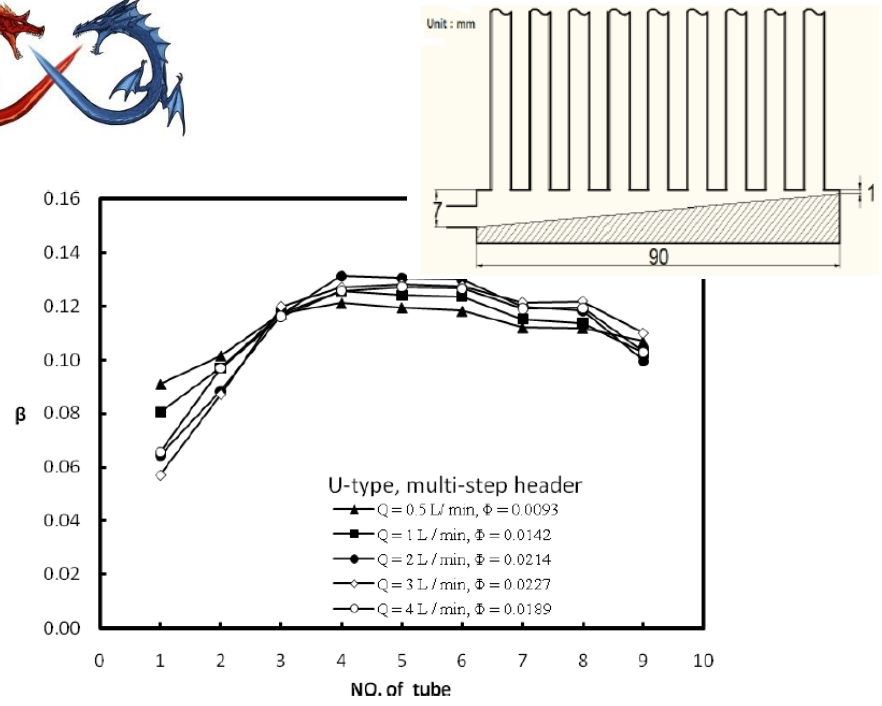

(a) Flow ratio of the multi-step header for U-type flow.

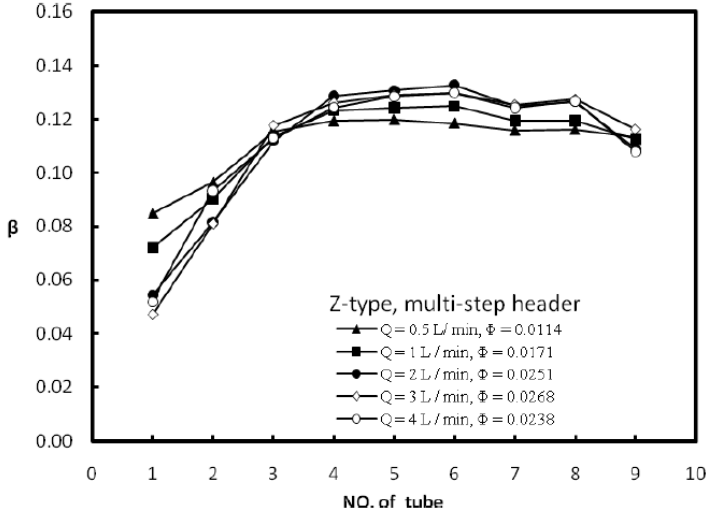

(b) Flow ratio of the multi-step header for Z-type flow.

Fig. 4. Flow ratio of the modified header with multi-step blocker for U-type and Z-type flows.

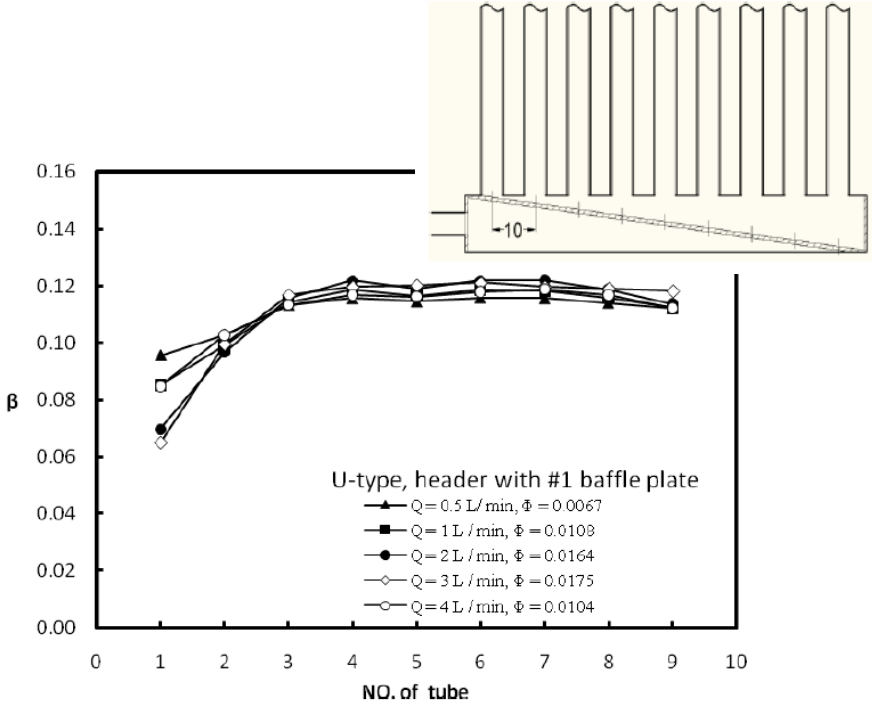

(a) Flow ratio of the modified header with #1 baffle plate for U-type flow.

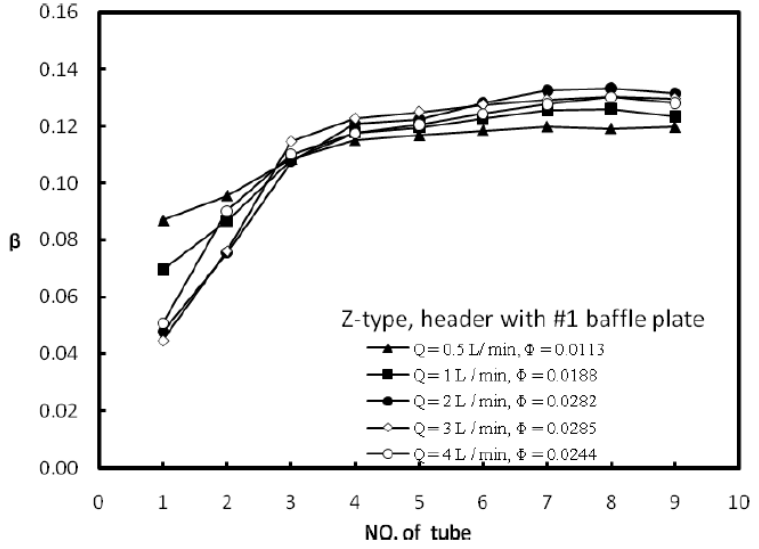

(b) Flow ratio of the modified header with #1 baffle plate for Z-type flow.

Fig. 5. Flow ratio of the modified header with #1 baffle plate for U-type and Z-type flows.

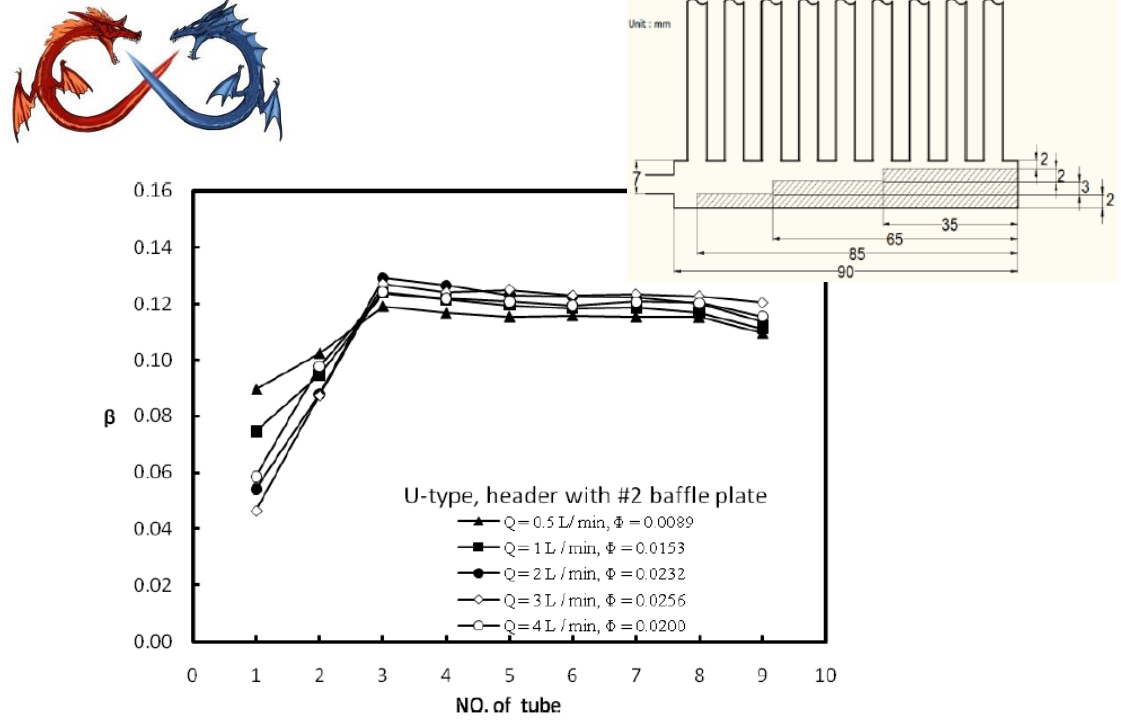

(a) Flow ratio of the modified header with #2 baffle plate for U-type flow.

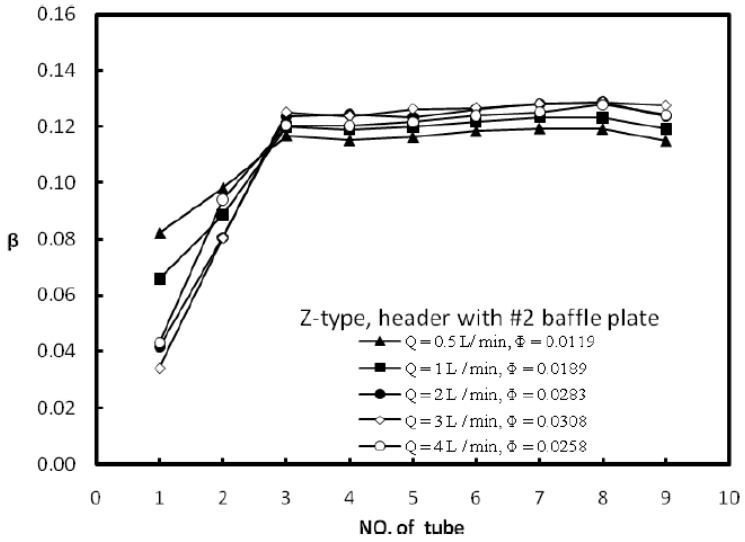

(b) Flow ratio of the modified header with #2 baffle plate for Z-type flow.

Fig. 6. Flow ratio of the modified header with #2 baffle plate for U-type and Z-type flows.

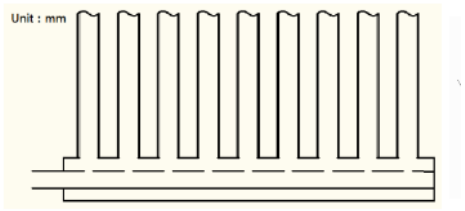

(d) Modified header with installed baffle

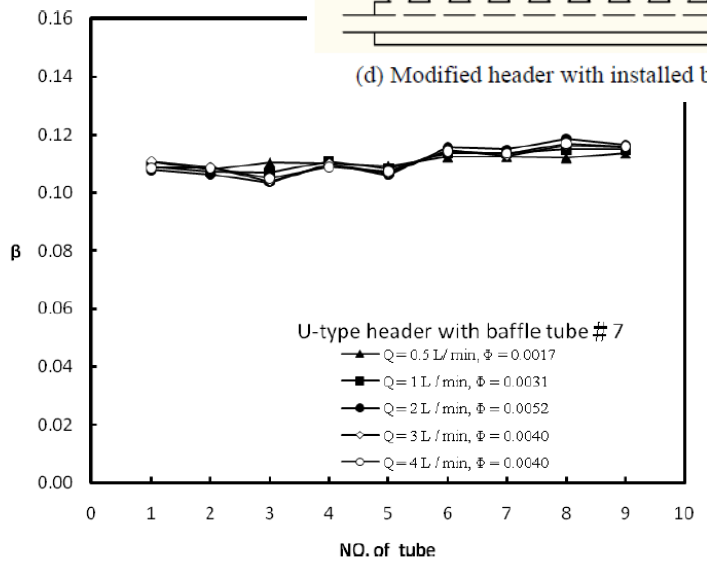

(a) Flow ratio of the modified header with #7 baffle tube for U-type flow.

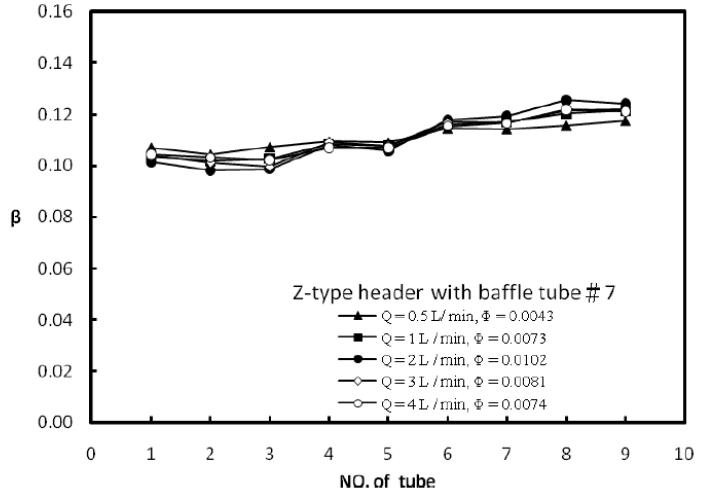

(b) Flow ratio of the modified header with #7 baffle tube for Z-type flow.

Fig. 9. Flow ratio of the modified header with #7 baffle tube for U-type and Z-type flows.

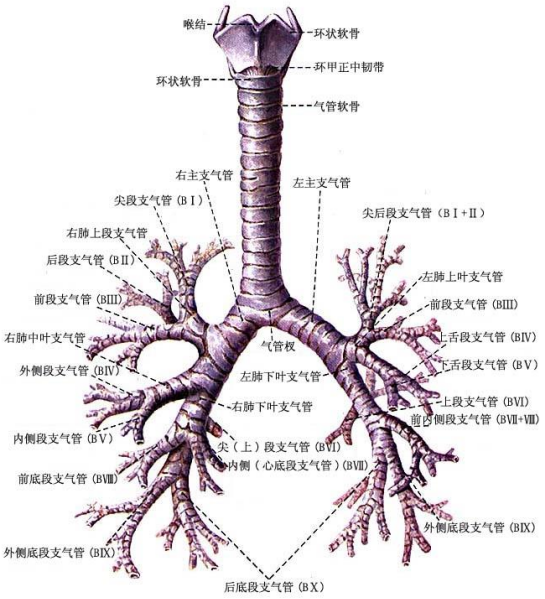

68. 气管和肺段支气管

Flow Distribution Property of the Constructal Distributor and Heat Transfer Intensification in a Mini Heat Exchanger, AIChE J., 2008 Vol. 54, 2796-2807.

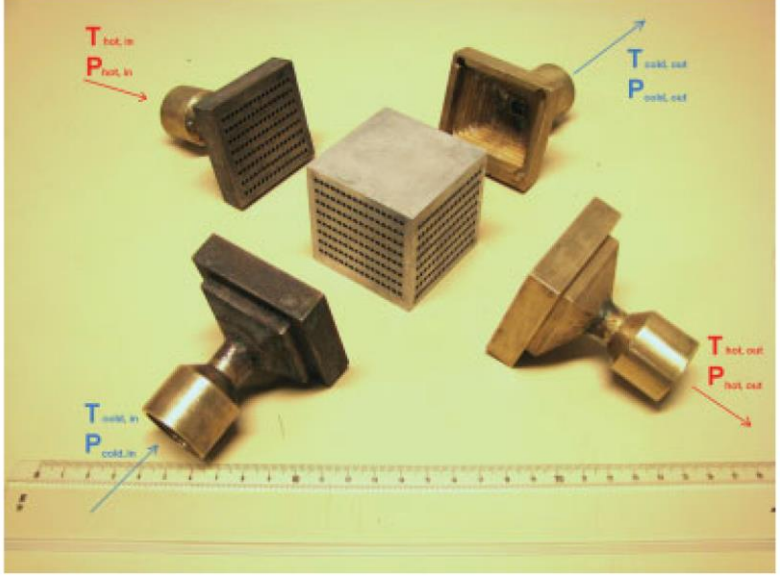

Figure 2. Photo of the test section configuration example (CEP).

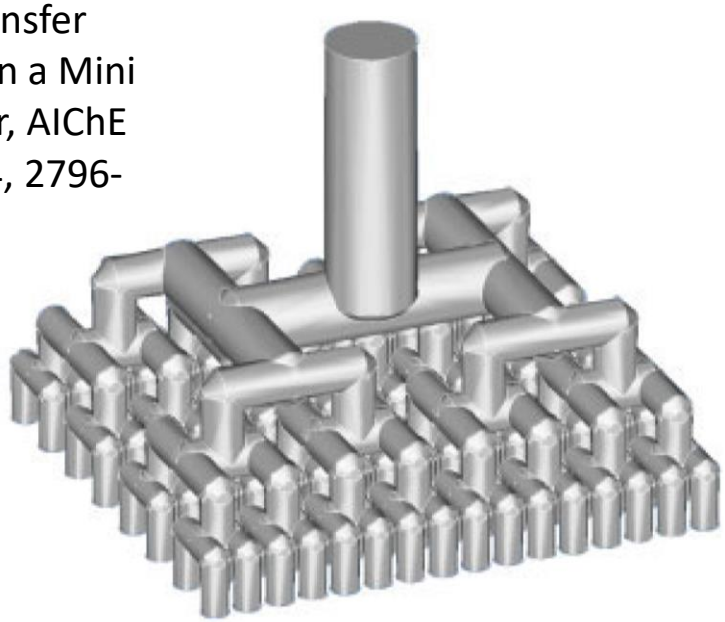

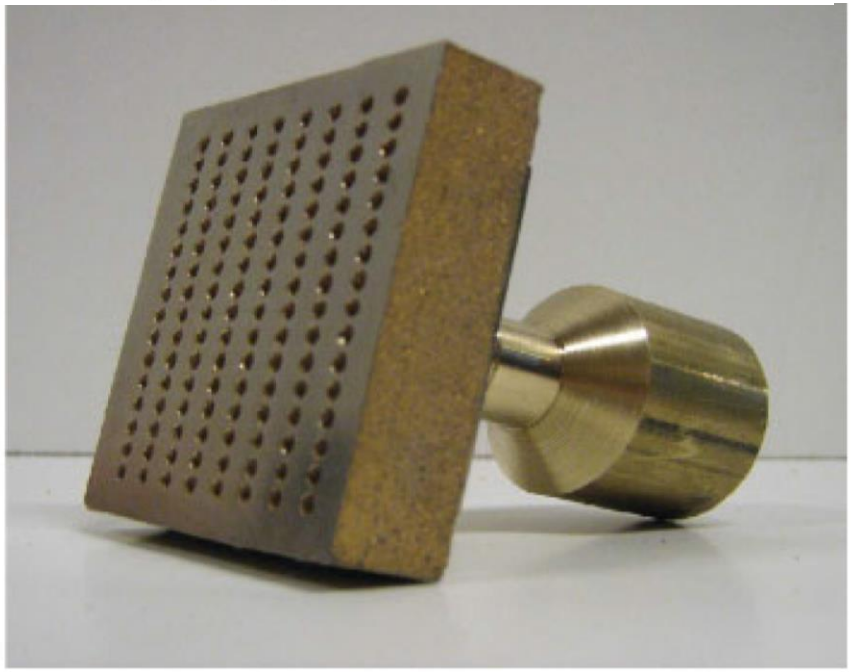

Figure 1. Prototype of the metallic multi-scale flow distributor and its inner channel structure.

[Color figure can be viewed in the online issue, which is available at www.interscience.wiley.com.]

Review on two-phase flow distribution in parallel channels with macro and micro hydraulic diameters: Main results, analyses, trends, applied thermal engng., 59, 2013, 336-353.

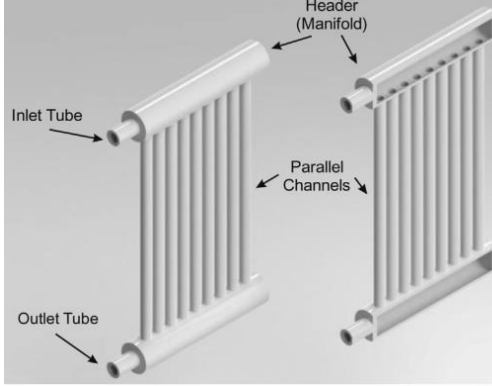

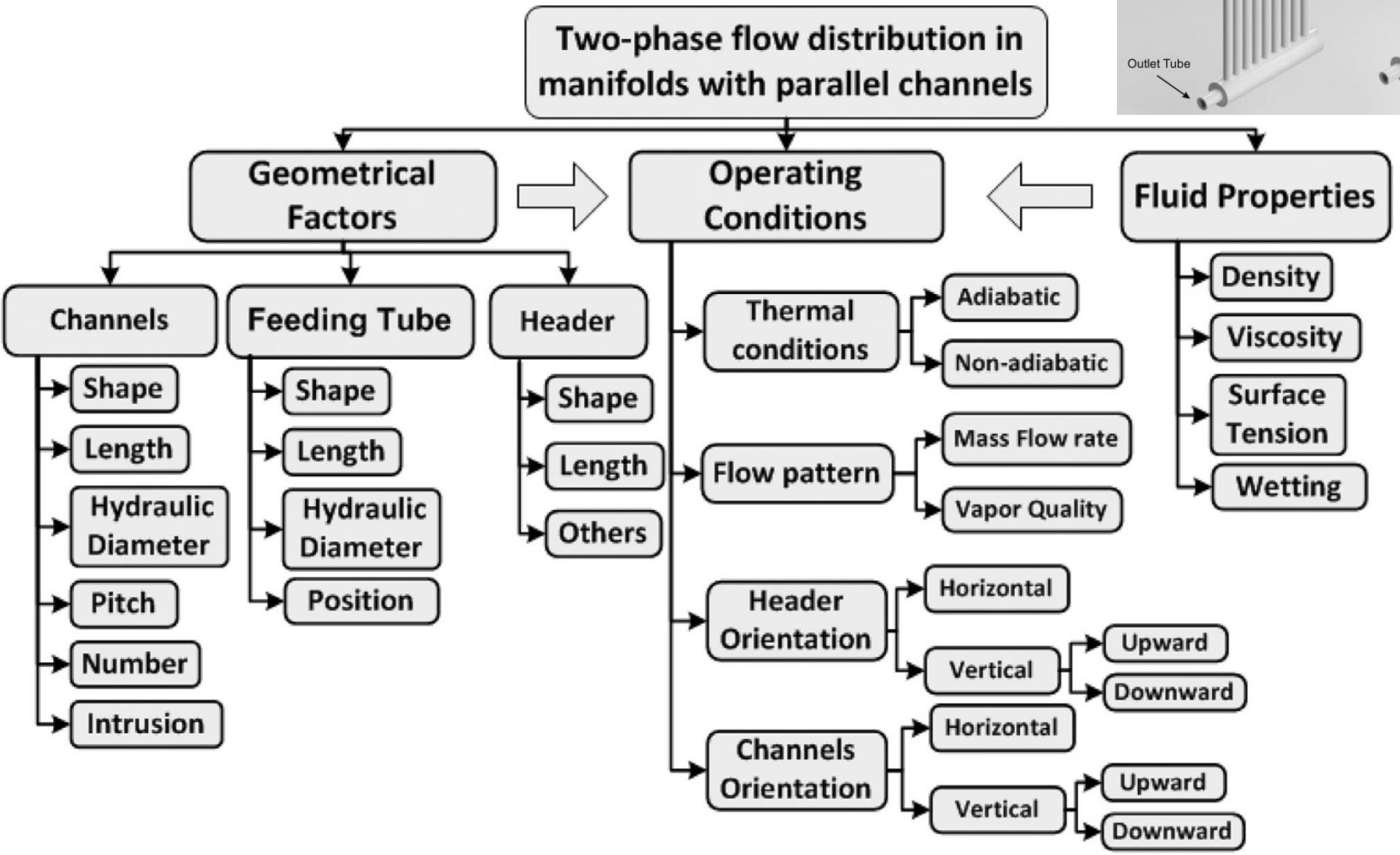

Fig. 2. Factors influencing the two-phase flow distribution in headers with parallel channels.

Causes of mal-distribution for typical Headers

Review on two-phase flow distribution in parallel channels with macro and micro hydraulic diameters: Main results, analyses, trends, applied thermal engng., 59, 2013, 336-353.

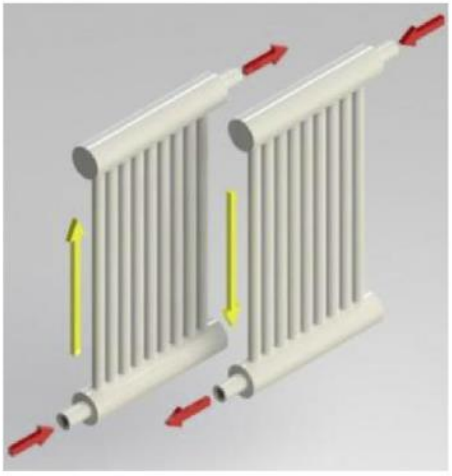

(a) Horizontal Header – Vertical Channels

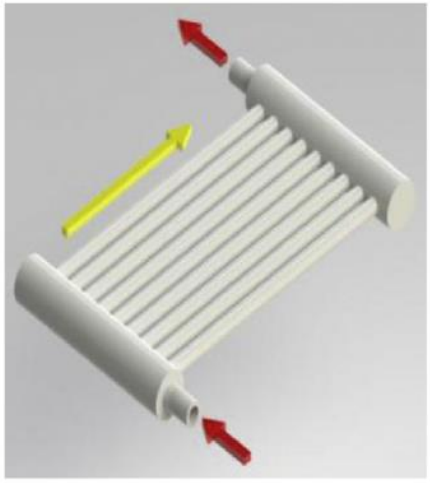

(b) Horizontal Header with Horizontal Channels

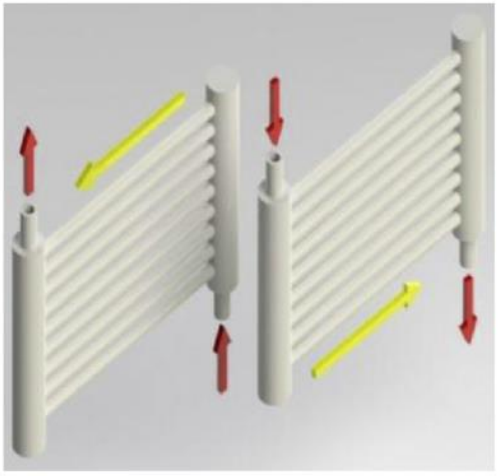

(c) Vertical Header with Horizontal Channels

(a) Uneven local pressure distribution in the inlet/exit headers apparent at the channel entrance/exit caused by the specific placement of the inlet/outlet pipes, fluid distribution in the headers, buoyancy effects, and two-phase separation.

(b) Uneven flow resistances in the parallel channels caused by variations in the channel dimensions, different tube lengths, uneven fouling, density and viscosity variations, and the presence of two or more phases.

Refrigerant Distribution in Minichannel Evaporator Manifolds, HVAC&R Research, Vol. 13, 543-555

- R-410A, upflow, side inlet and end inlet

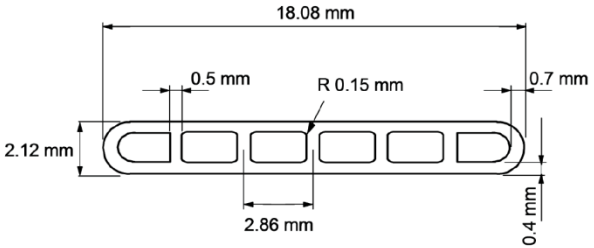

Figure 3. Cross section of minichannel tube.

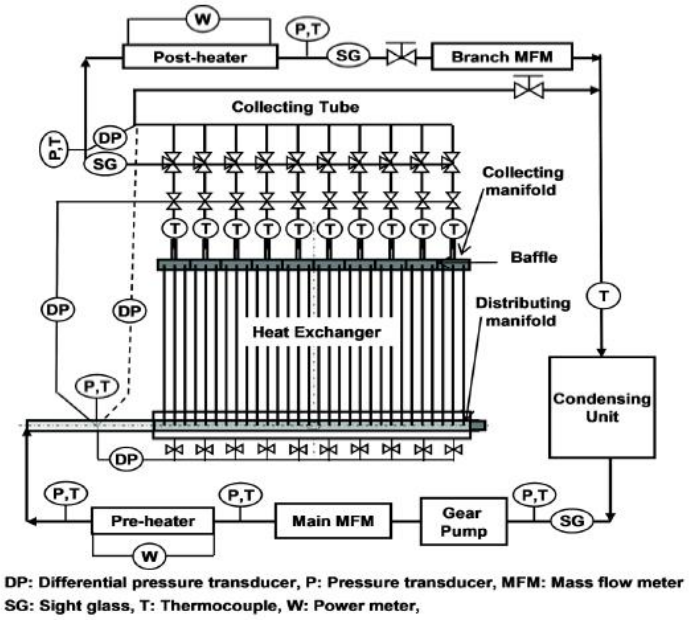

Figure 1. Schematic diagram of experimental setup.

Table 3. Range of Experimental Parameters

Experimental Parameters	Range
Inlet temperature	7.2°C
Inlet quality	0.3
Refrigerant	R-410A
Manifold inlet mass flow rate, g/s	30/45/60
Heat load, kW	0/5/10
Heat exchanger tube pitch, mm/tube	8/10/12
Location of inlet	End/Side
Number of heat exchanger tubes in parallel	18/24/30

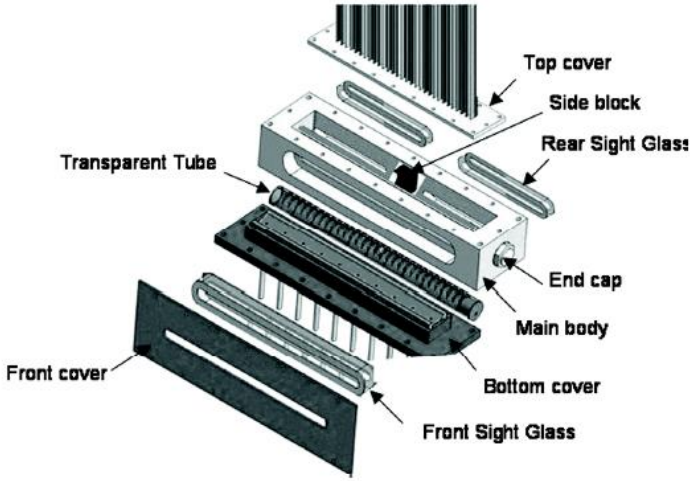

Figure 2. Exploded diagram of flow visualization section.

- Flow distribution for side inlet is better than end inlet

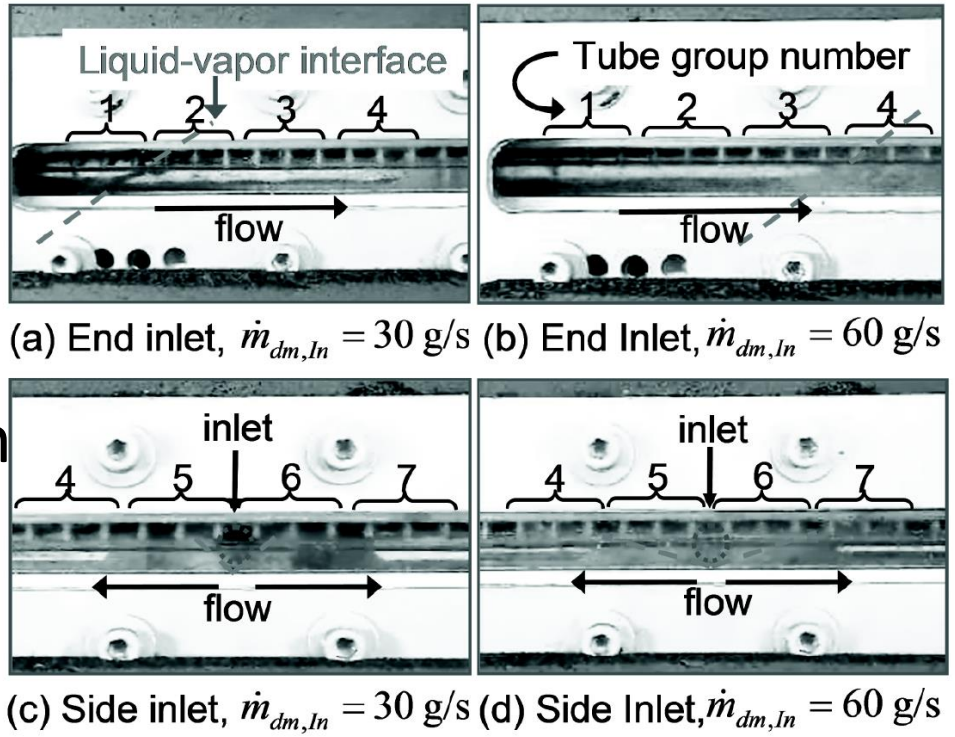

Figure 4. Flow visualization in distributing manifold (10 mm tube pitch, 10 tube groups, adiabatic, $x_{dm,In}$: 0.3).

Table 4. Normalized Standard Deviation of Liquid MFR

MFR	30 g/s		55 g/s	
Inlet Location	End Inlet	Side Inlet	End Inlet	Side Inlet
Branch tube no.: 30 ea	0.408	0.320	0.549	0.286
Branch tube no.: 24 ea	0.450	0.235	0.595	0.202
Branch tube no.: 18 ea	0.466	0.256	0.631	0.249

Heat loading imposes negligible effect on the flow distribution

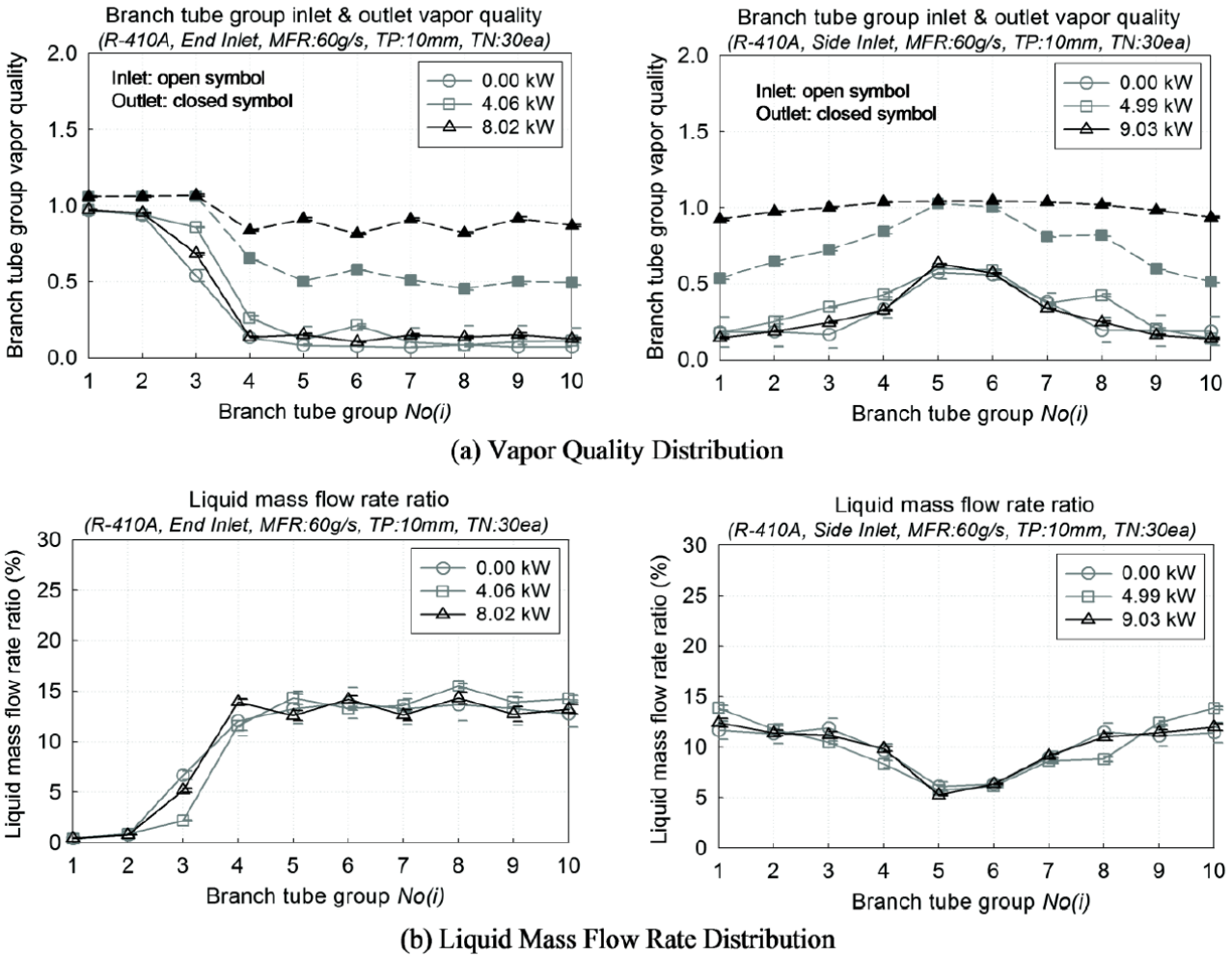

Figure 6. Effects of heat load on refrigerant distribution (10 mm tube pitch, 10 tube groups, MFR: 60 g/s, $x_{dm,In}$:0.3).

- The **gravitational force and the momentum differe**nce between the liquid and the vapor phases affect the phase separation in the horizontal manifold. **Low momentum vapor on the top layer is easily taken off in the branch tubes near the inlet, while the high momentum liquid on the bottom layer travels farther toward the far end of the manifol**d.
- For the **end-inlet location, the profile of the branch tube inlet vapor quality is of a "stepwise" shape**. As the manifold inlet mass flow rate increases, **the number of branch tube groups having almost 100% tube inlet vapor quality also increases because the liquid-vapor interface is located closer to the end of the manifold due to the increased momentum**. (**upflow**)
- For the **side-inlet location, there are no regions with 100% branch tube inlet vapor quality, and the profile of the branch tube inlet vapor quality is symmetric**. **The branch tube inlet vapor quality is about 60% to 70%** near the inlet and about 20% near the end of the manifold. Between these two regions, the branch tube inlet vapor quality decreases steadily along the manifold.

Two-Phase Flow Distribution to Tubes of Parallel Flow Air-Cooled Heat Exchangers, *Heat Transfer Engineering*, 26(4):3–18, 2005

Classification of header flow direction:

(a) horizontal reverse flow,

(b) horizontal parallel flow

(c) horizontal normal flo

(d) vertical reverse flow

(e) vertical parallel flow

(f) vertical normal flow.

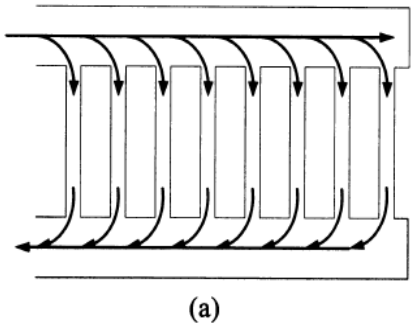

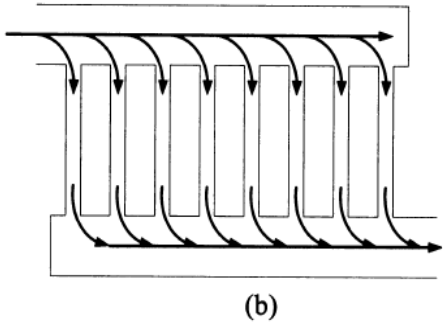

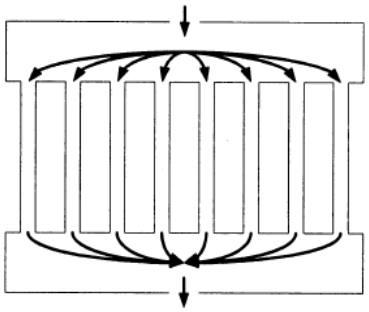

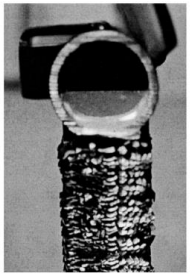

Figure 7 Header shapes and tube end projection: (a) photo of round header cross-section, (b) tube end projection, (c) D-shape header.

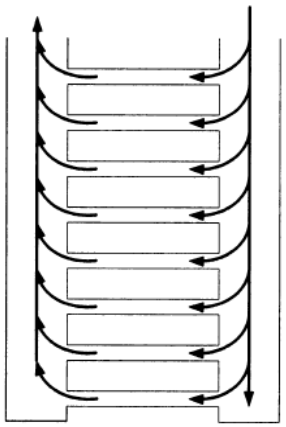

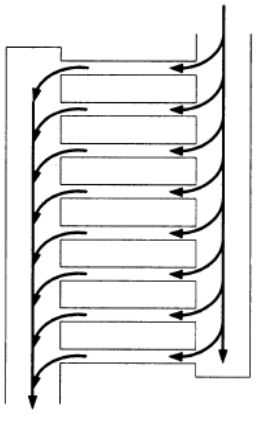

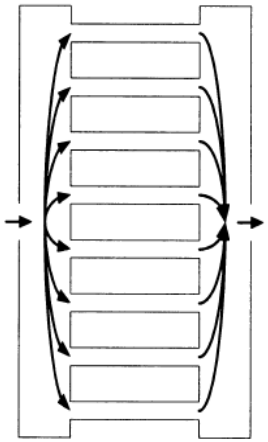

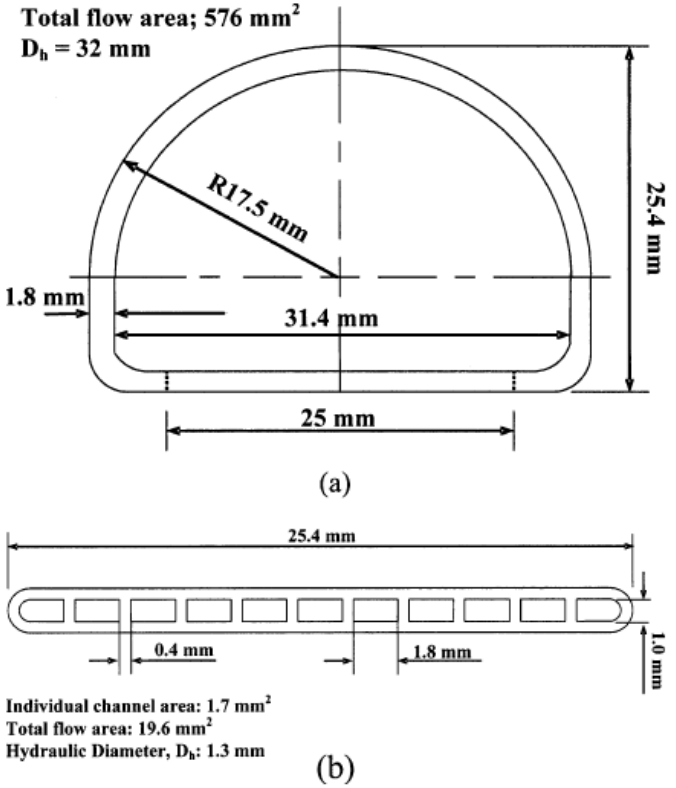

Figure 10 Dimensions of specific header and flat tube: (a) D-shaped header cross-section, (b) tube cross-section.

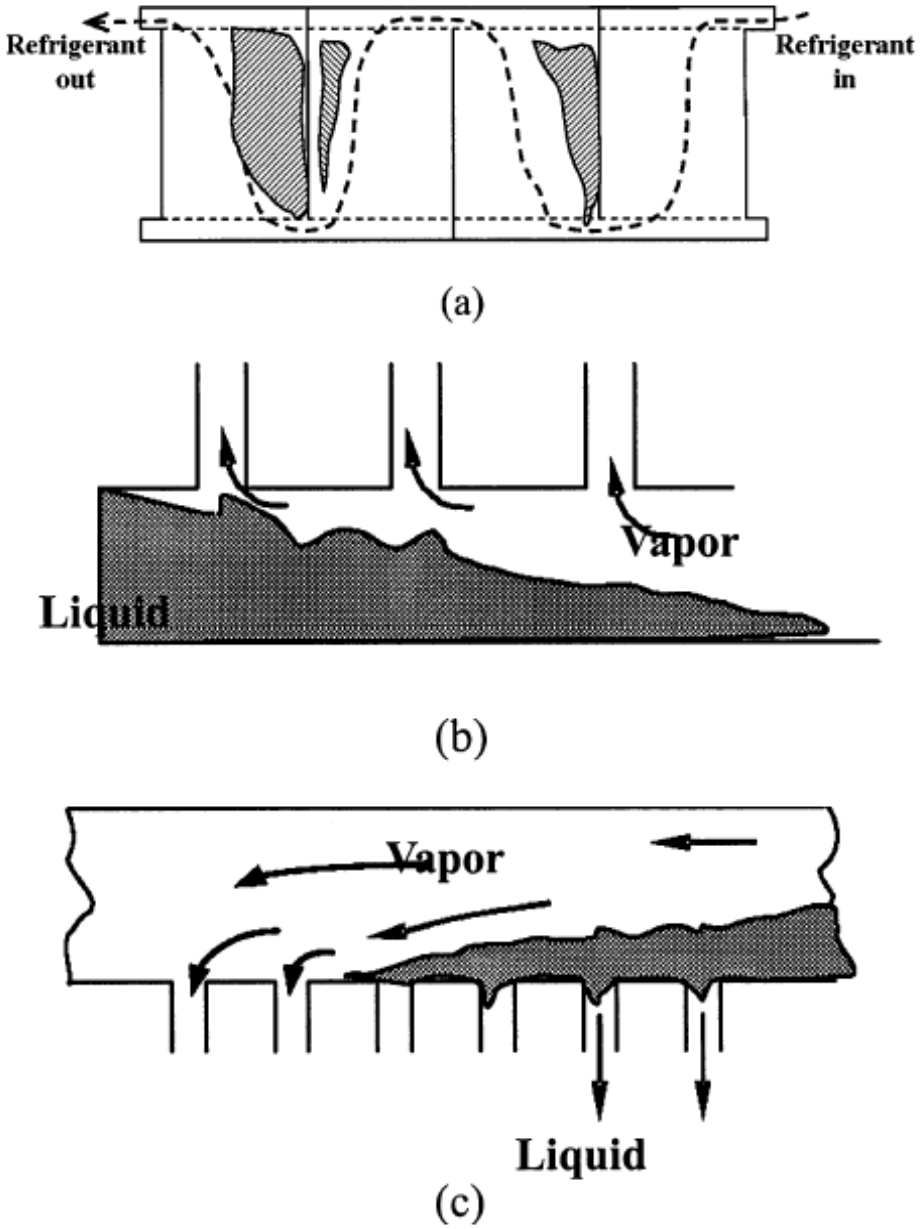

Figure 9 Horizontal Header—Vertical Tube junction (HH–VT): (a) illustration of multi-pass design, (b) bottom-dividing header, (c) top-dividing header.

Down Flow

Reducing the inlet header provide slight improvement

Higher flowrate provide better flow distribution

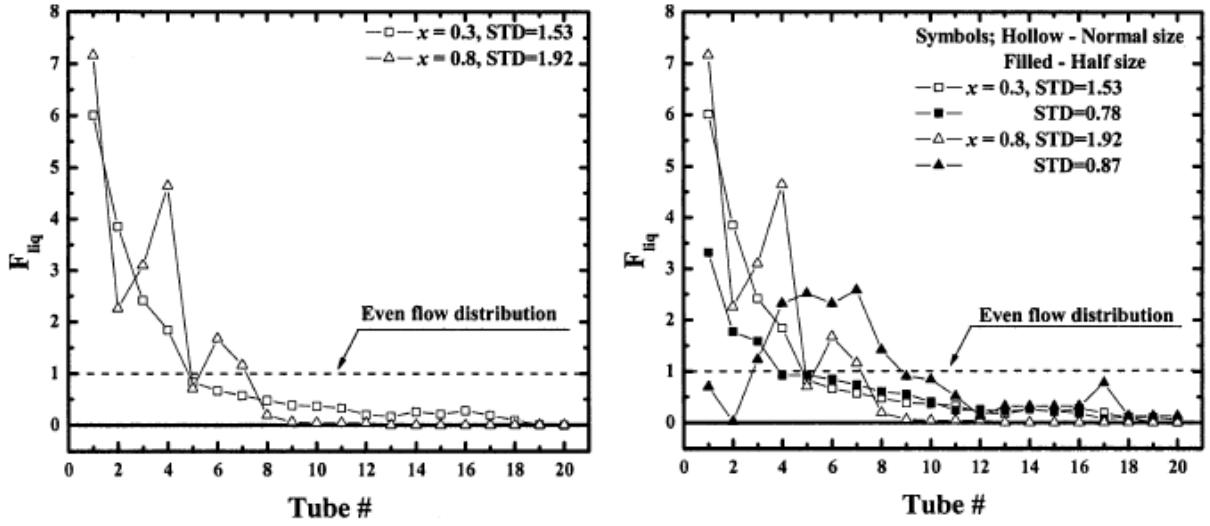

re 11 Liquid flow ratios with various qualities in different size headers: (a) normal size header, (b) normal- and half-size header.

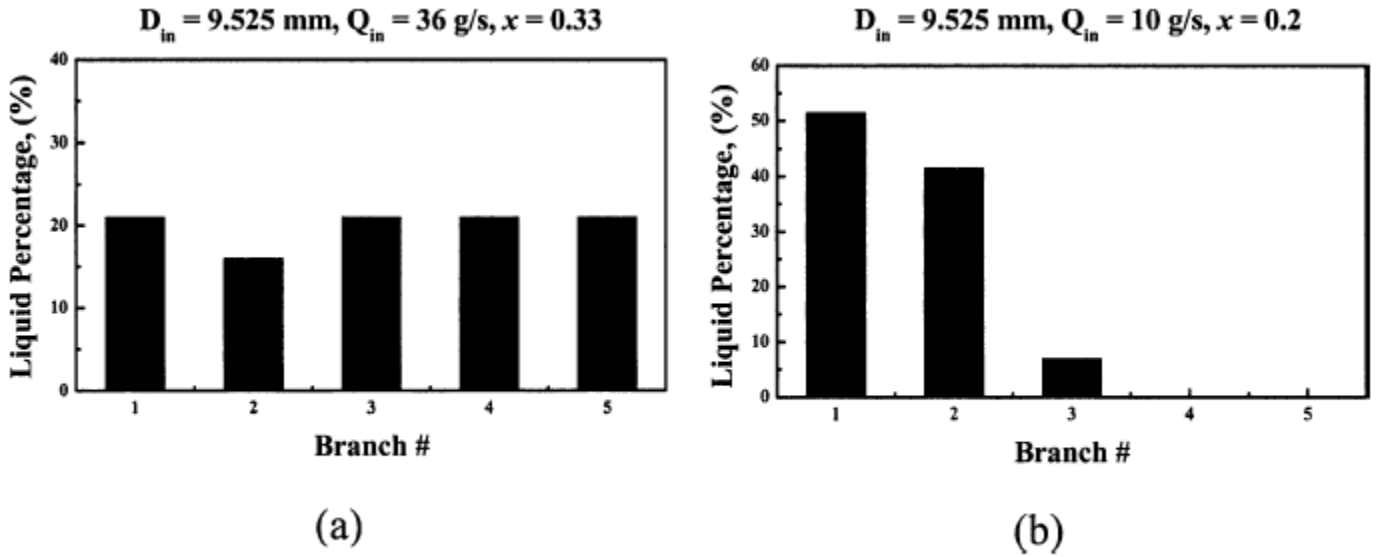

Figure 12 Distribution results for a 9.525 mm-diameter normal inlet as affected by inlet flow rate and vapor quality [10, 11]: (a) good flow distribution, (b) poor

General characteristics of two-phase flow distribution in a compact heat exchanger, Int. J. Heat Mass Transfer, 2009, 52, 442-450, HFE-7100**, 4 different flow patterns in header, stratified, stratified jet, liquid jet, liquid film (For down flow)**

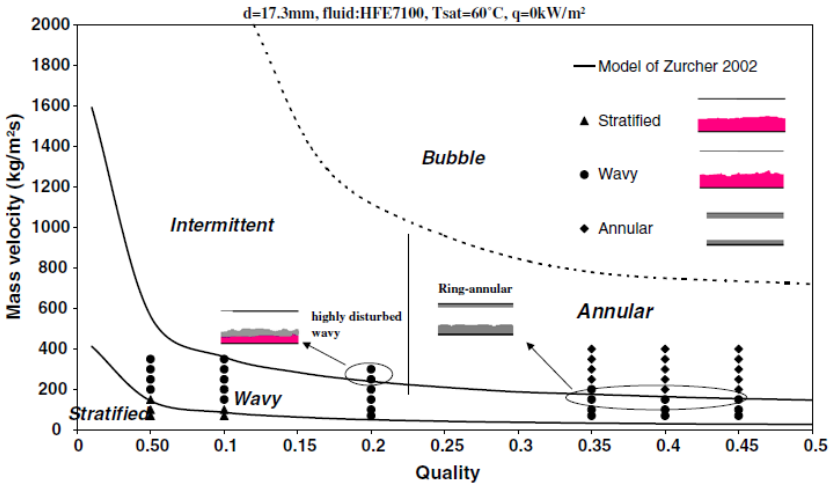

Fig. 4. Flow pattern data at the manifold inlet.

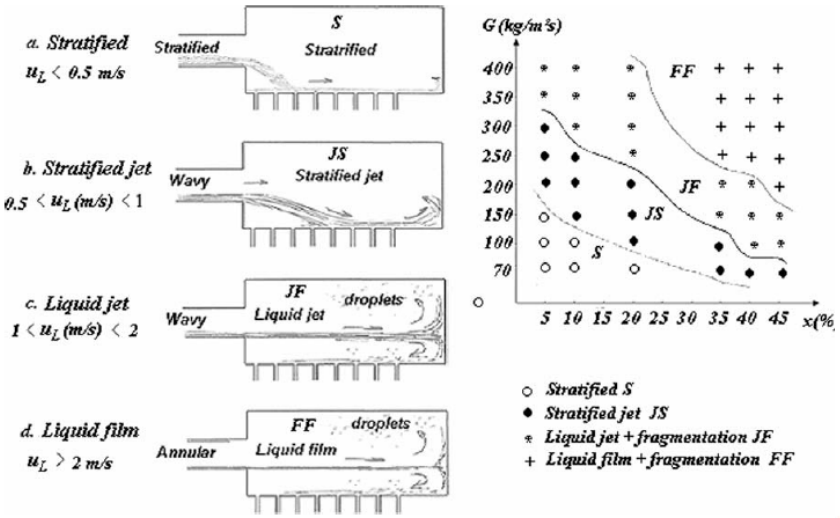

Fig. 5. Flow structure in the 50-mm diameter header.

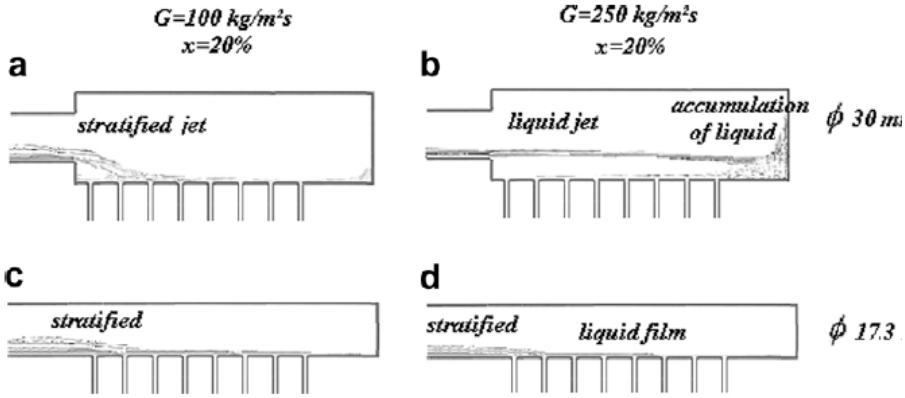

Fig. 8. Flow structure in the header of smaller diameters.

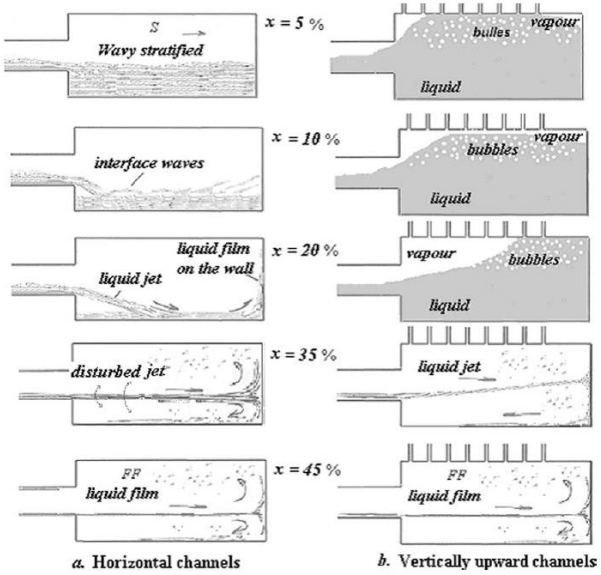

For up flow

Fig. 9. Different flow structures in the manifold for different channels' orientation (G = 200 kg/m² s). (a) Horizontal channels and (b) vertically upward channels.

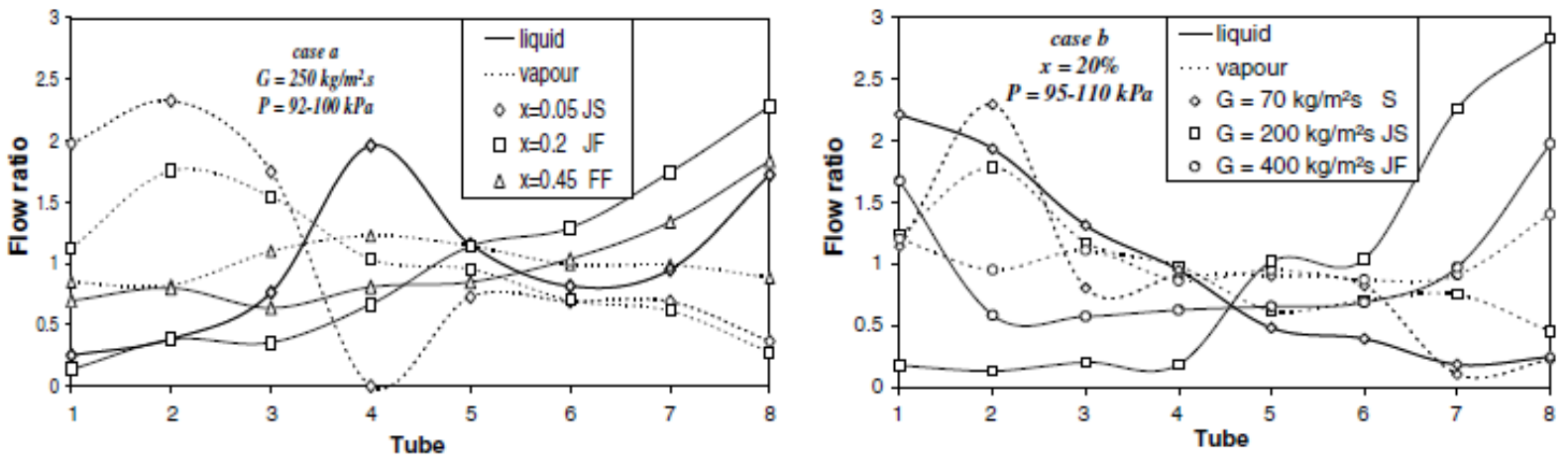

Fig. 6. Influence of the inlet quality and flow rate on the two-phase distribution. Vertically downward channel (ϕ_{header} = 50 mm).

- Higher inlet quality provide better flow distribution
- Higher mass flowrate into the header give better flow distribution
- Vapor phase distribution in larger header is better than smaller diameter
- For low mass flux, liquid phase distribution is not significantly changed with header diameter
- For high mass flux, significant change of the flow distribution is seen.

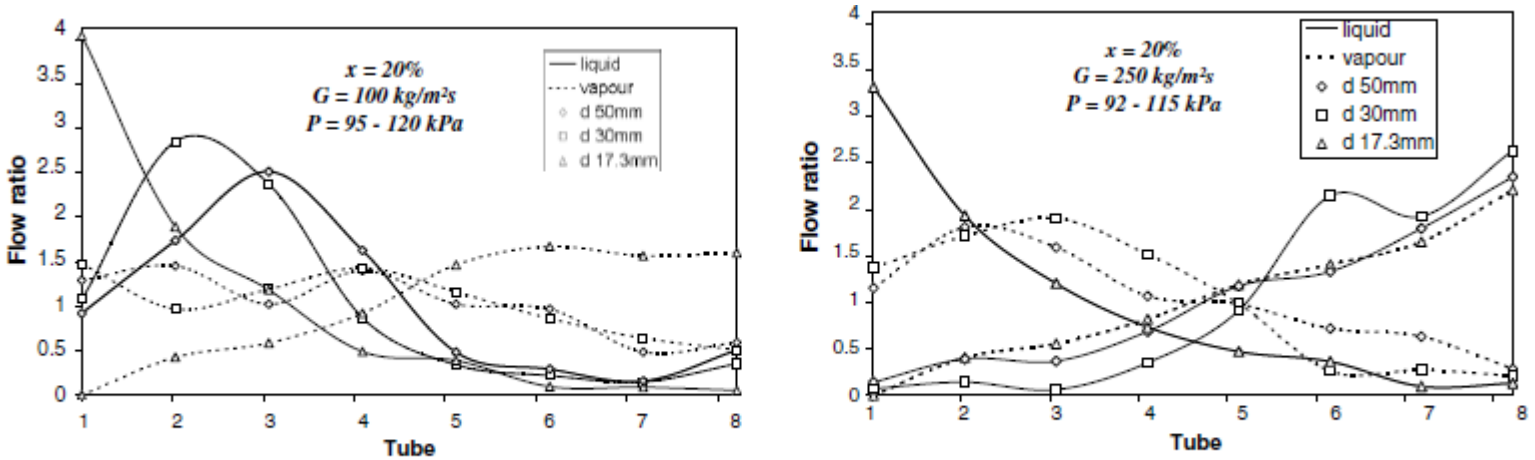

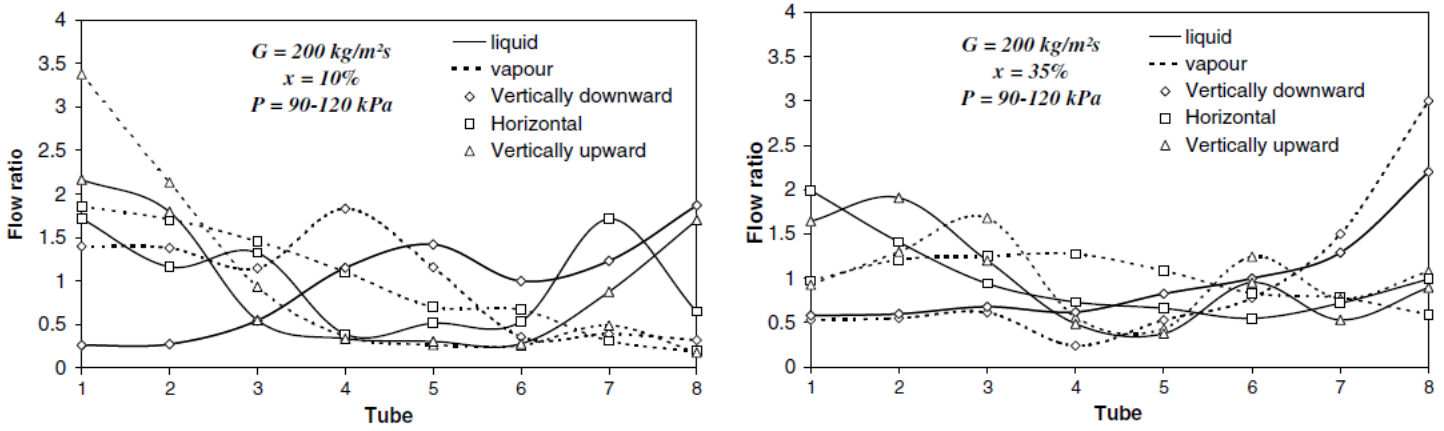

Fig. 10. Flow distribution for different channels orientation.

Place restriction at the header inlet lead to jet flow and improve the flow distribution

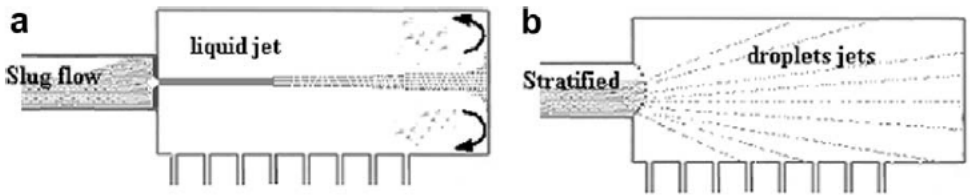

Fig. 13. Flow patterns after the two expansion devices. (a) Expansion orifice and (b) splashing grid.

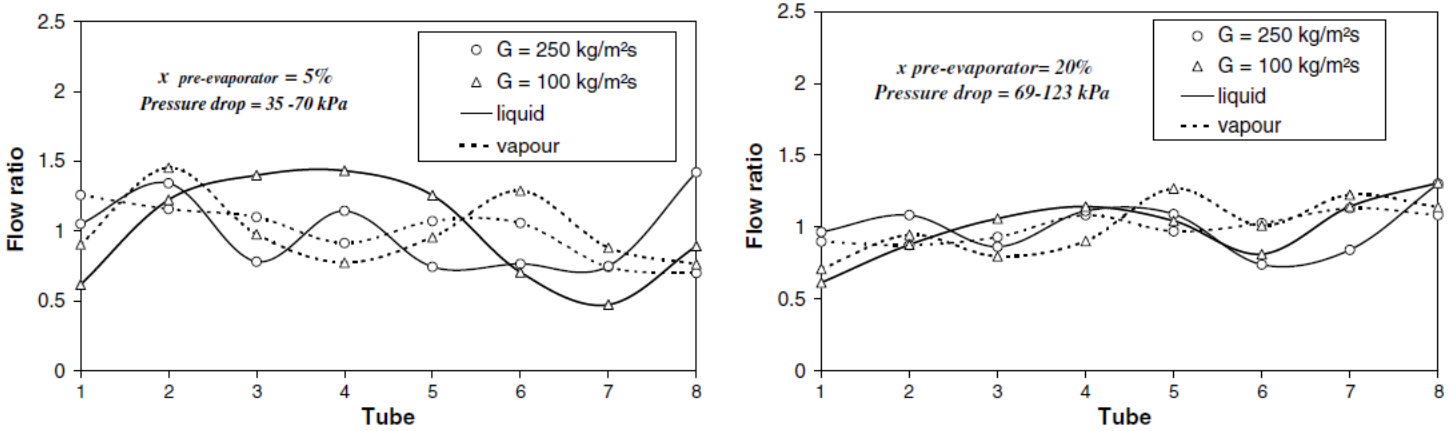

Fig. 14. Distribution profile in the presence of a splashing grid for certain inlet flow rates and qualities.

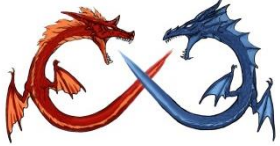

- **For vertically downward channels, better distribution for both phases as mass quality increases.**
  - **Influence of the mass inlet velocity - more visible at high mass velocity. Reducing the header diameter deteriorated the two-phase distribution.**
- **Horizontal distribution channels showed enhanced vapour and liquid distribution even at low inlet mass quality.**
- **For vertically upward channels**, no improvement even for high inlet mass quality.
- **Expansion devices has a great influence on the flow structure** by forming a liquid jet in the header. **High jet velocities rendered the distribution more homogeneous and improves the two-phase distribution.**
- The presence of **high-momentum phases and especially that of liquid favours the occurrence of impacts, fragmentation of liquid phase, the presence of a homogenized multidirectional** two-phase structure and this renders the distribution more homogeneous. **(Disperse the liquid phase is the key..)**

Two-phase flow behavior inside a header connected to multiple parallel channels, Experimental Thermal and Fluid Science 33 (2009) 195–202

- Air/Water System

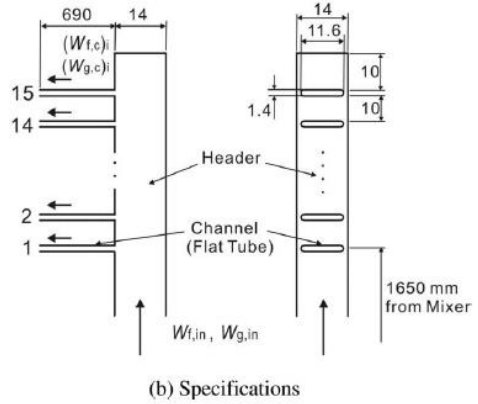

(b) Specifications

Fig. 2. Configuration of the test section without membranes.

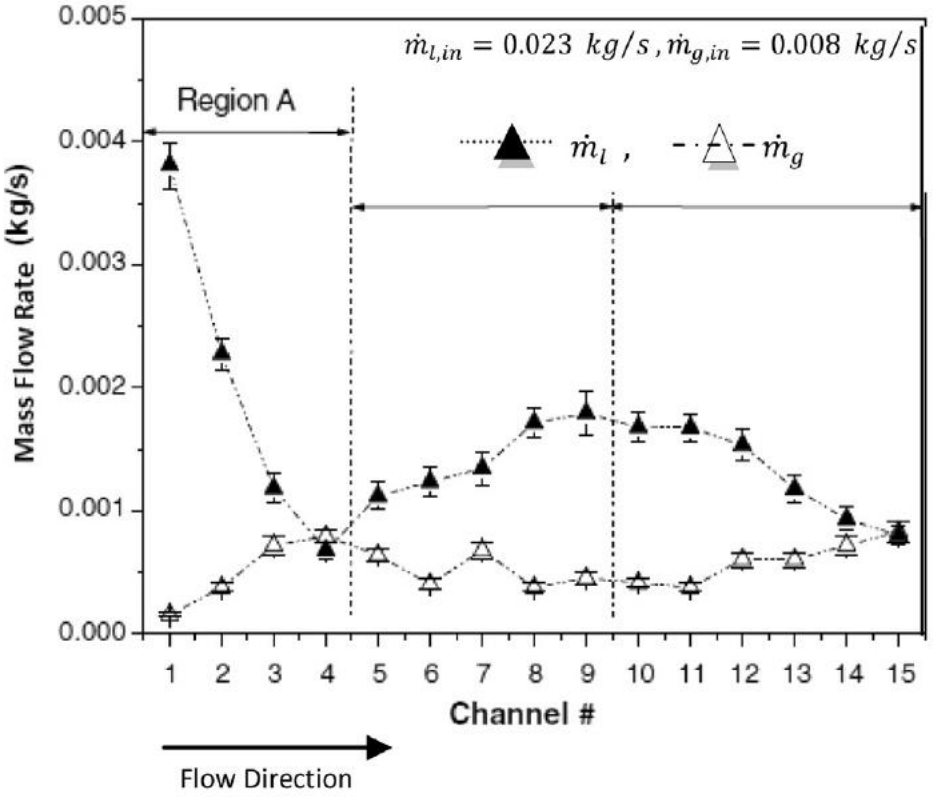

(a) Two-phase Flow distribution

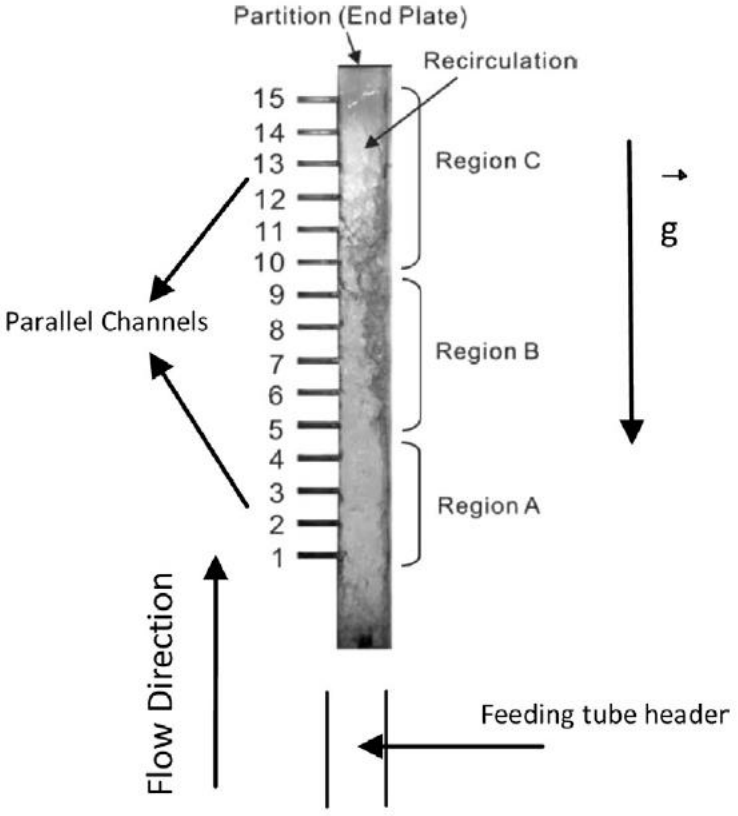

(b) Two-phase Flow visualization

Fig. 4. Effect of the end plate on the flow configuration inside the header (after Lee [12]).

Flow pattern inside the header

Adiabatic Developing Two-Phase Refrigerant
Flow in Manifolds of Heat Exchangers, ACRC TR225, R-134a (Down flow)

Downflow

Placing the expansion valve near the header to result in expansion or developing region help to produce mist flow and a better distribution

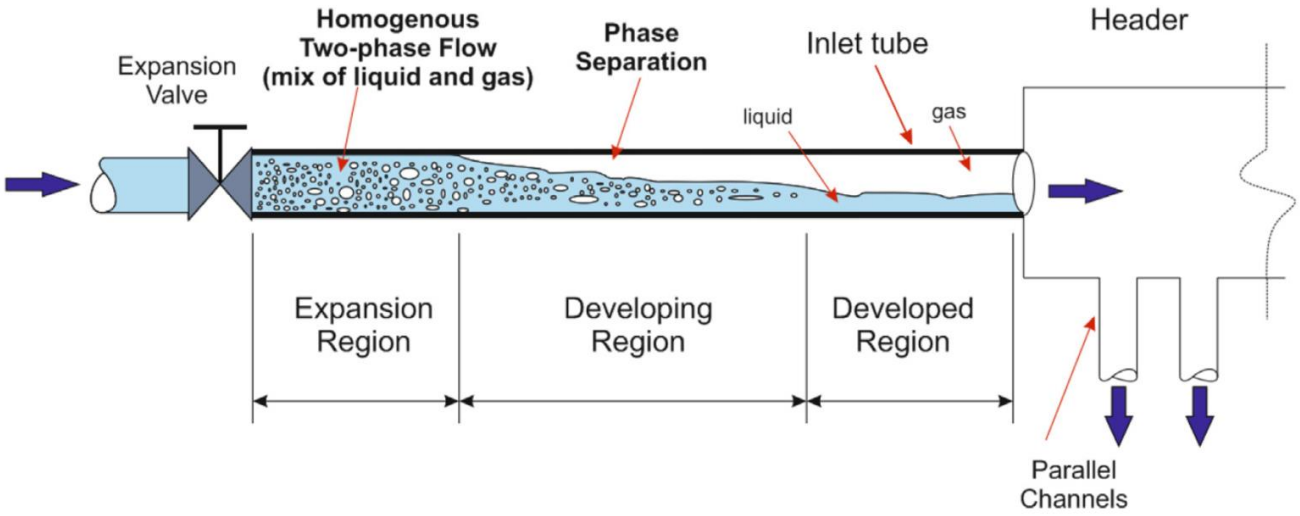

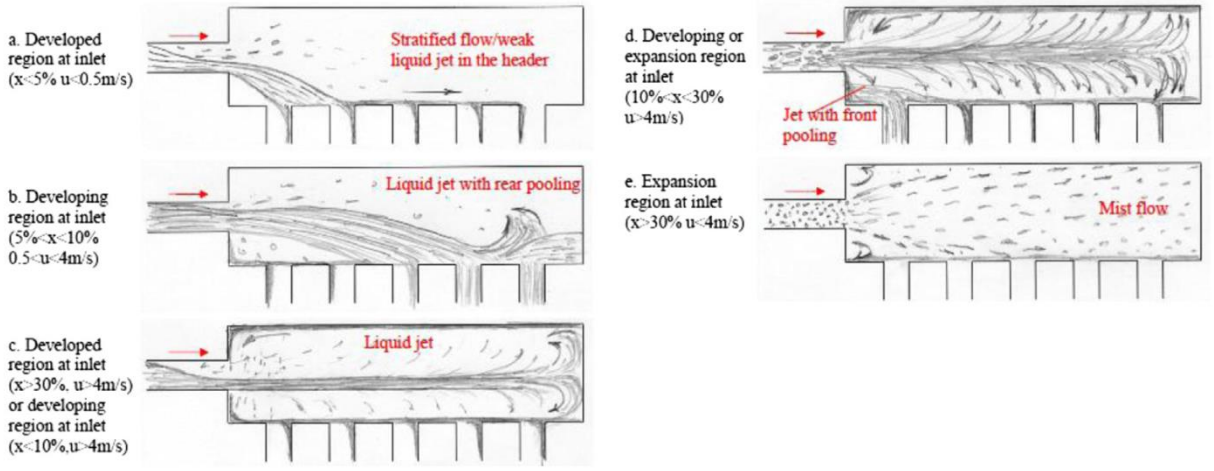

Fig. 8. Influence of inlet flow pattern on the flow structure in the horizontal header for downward flow (after Fei and Hrnjak [47]).

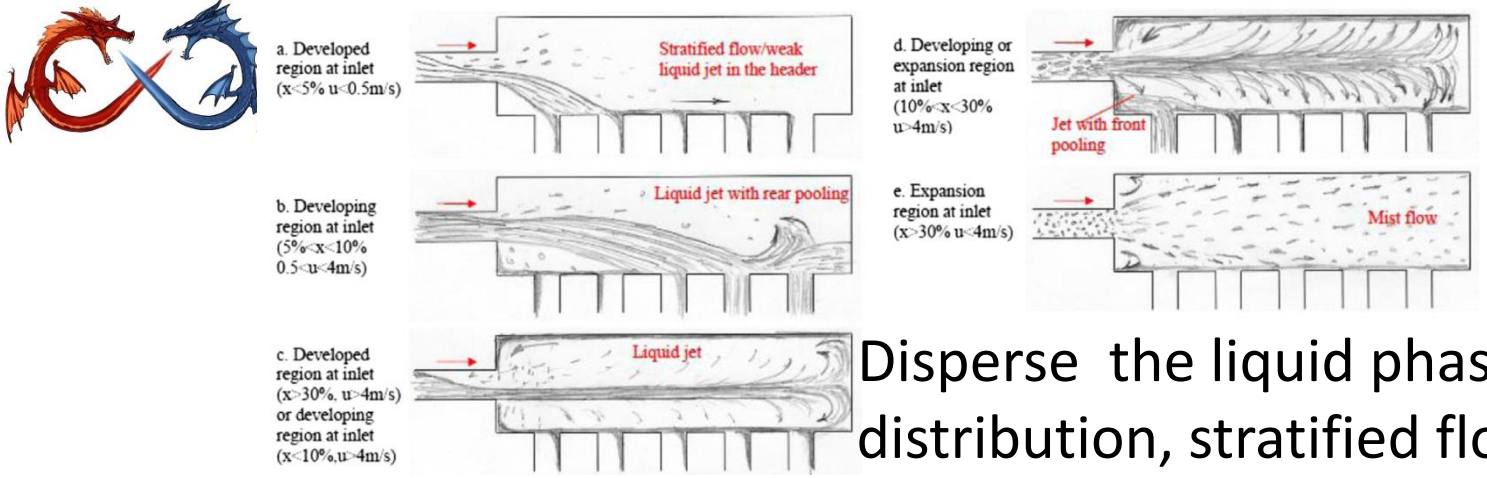

Disperse the liquid phase gives the best distribution, stratified flow shows worse distribution, jet flow with front pooling is slightly better than at rear pooling

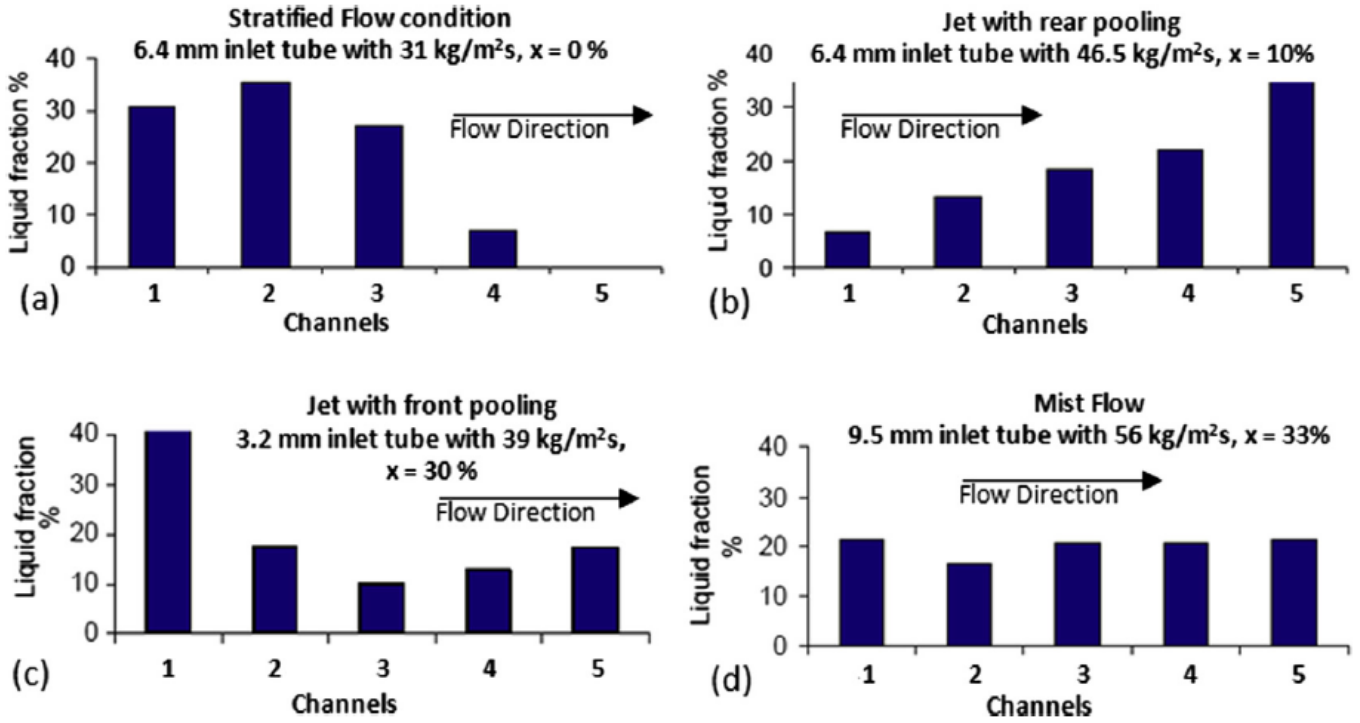

Fig. 9. Liquid fraction in parallel channels for the typical flow pattern. (a) and (b) feeding tube diameter 6.4 mm; (c) feeding tube diameter 3.2 mm; (d) feeding tube diameter 9.5 mm (after Fei and Hrnjak [47]).

Distribution of two-phase annular flow at header–channel junctions, Experimental Thermal and Fluid Science 28 (2004) 217–222

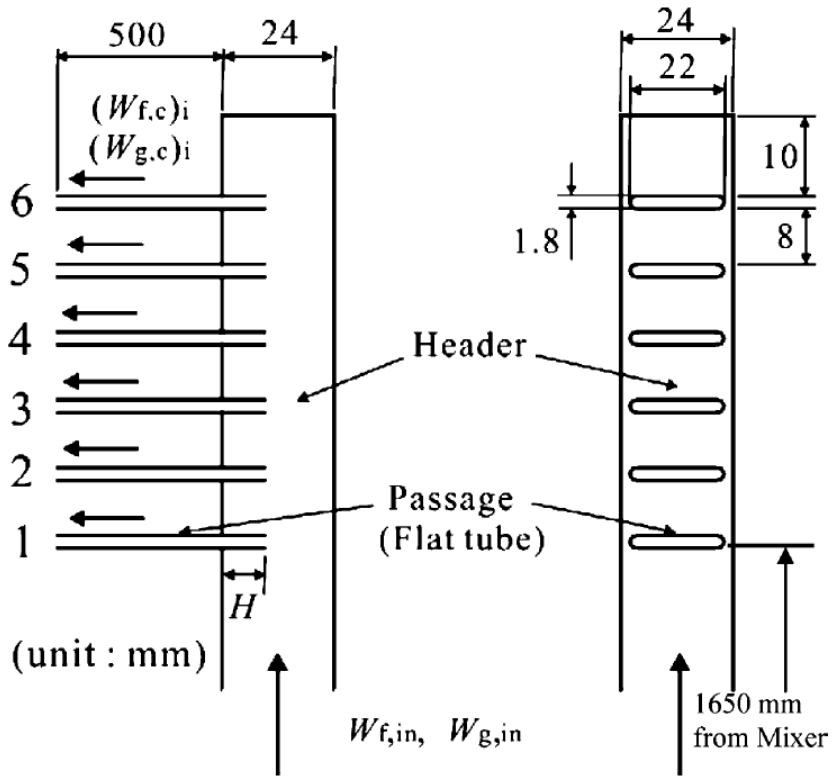

Fig. 2. Configuration of the test section.

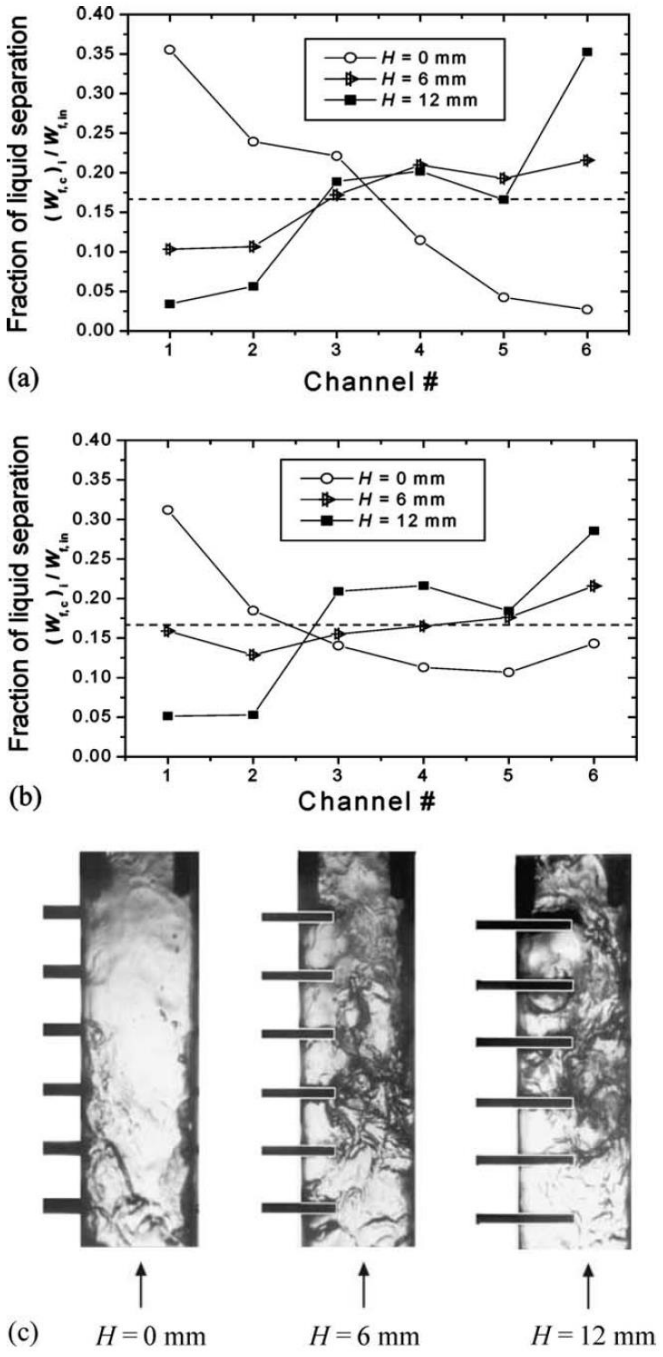

Fig. 3. Effect of intrusion depth on liquid flow distribution. (a) and (c) $G_{in} = 54$ kg/m^2 s, $x_{in} = 0.5$, (b) $G_{in} = 70$ kg/m^2 s, $x_{in} = 0.25$.

Air-water, G = 70 - 130 kg/m^{2}s, x = 0.2-0.6. The flow in the header inlet was annular. D = 17 mm), 30 vertical flat tubes (hydraulic diameter, Dh = 1.32 mm)
Int. J. of Multiphase Flow 32 (2006) 1340–1353

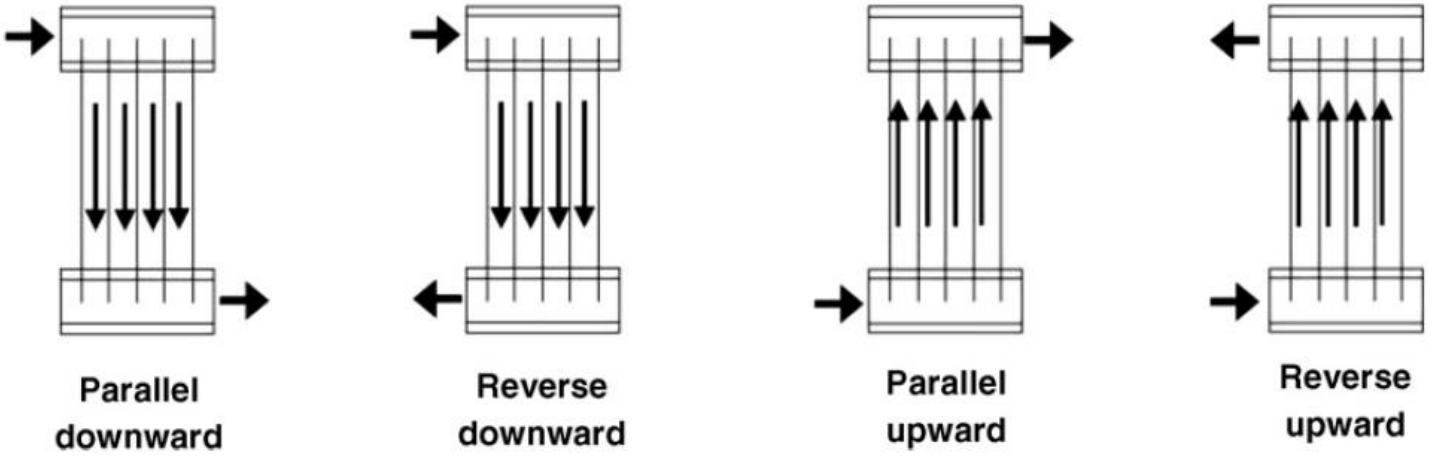

Fig. 1. Four different methods of flow distribution.

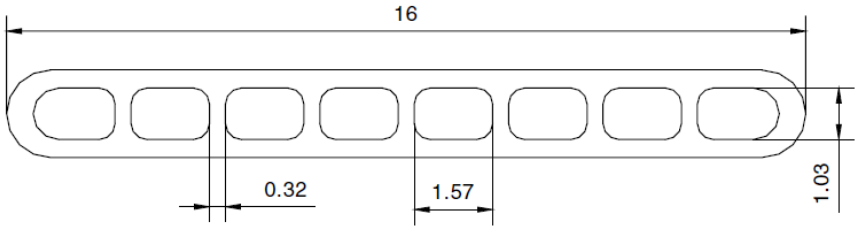

Fig. 3. Cross sectional view of the flat tube used in this study (unit: mm).

- Downflow

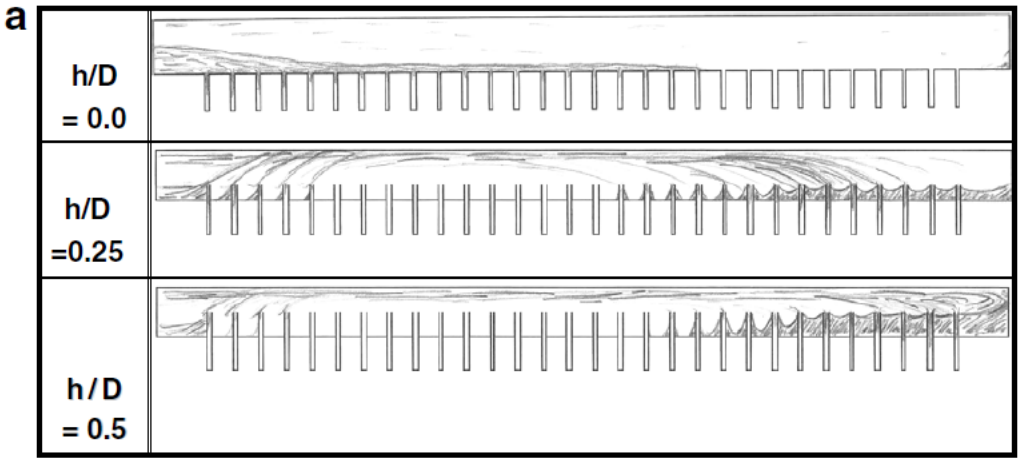

Down flow, stratified flow pattern

As the protrusion increases, more water is forced to rear part of the header with stronger intensity, slightly improve the inlet but the middle part is deteriorated and the rear part is improved.

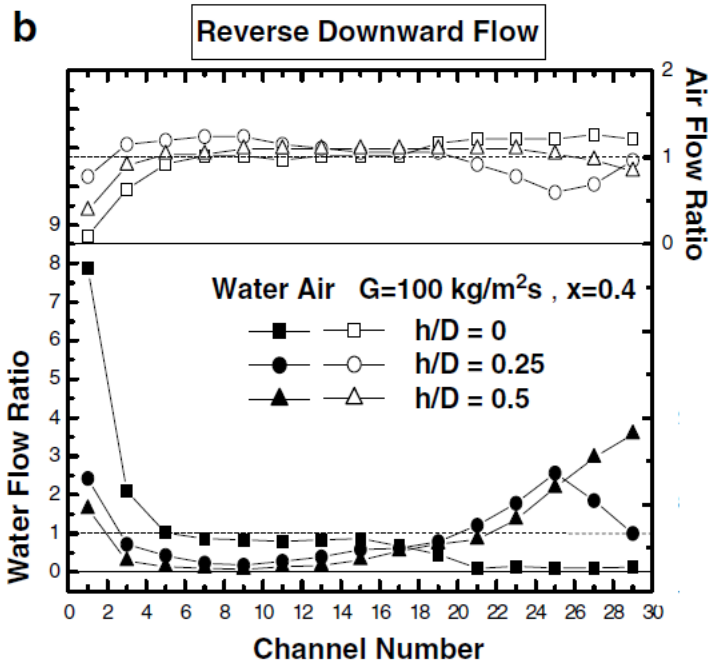

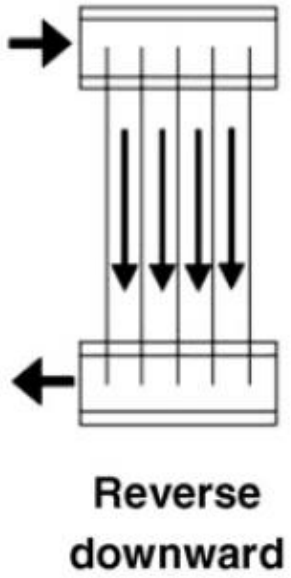

Fig. 6. (a) Typical flow pattern in an upper header with downward flow configuration and (b) corresponding water and air distribution.

Down Flow arrangement

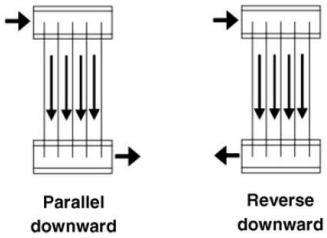

Parallel flow

The air flow rate slightly increases or remains the same as the flow travels downstream.

Reverse flow

the air flow rate decreases significantly as the flow travels downstream. This is due to the opposing trend of the header pressure difference between the reverse and the parallel flow.

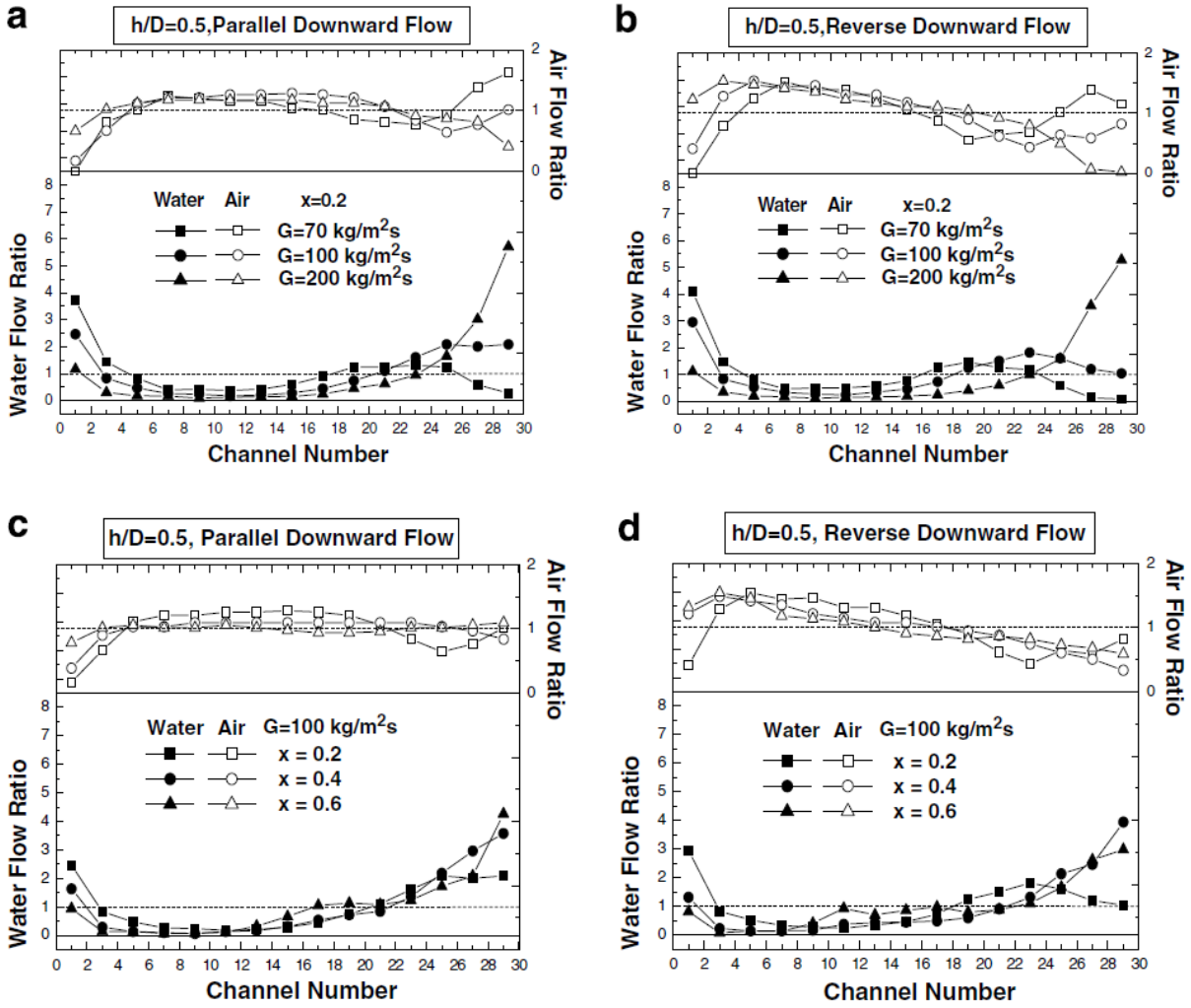

Fig. 7. Graphs showing the effect of tube outlet configuration on water and air distribution for a downward flow configuration: (a flow ($x = 0.2$), (b) reverse flow ($x = 0.2$), (c) parallel flow ($G = 100$ kg/m^2 s) and (d) reverse flow ($G = 100$ kg/m^2 s).

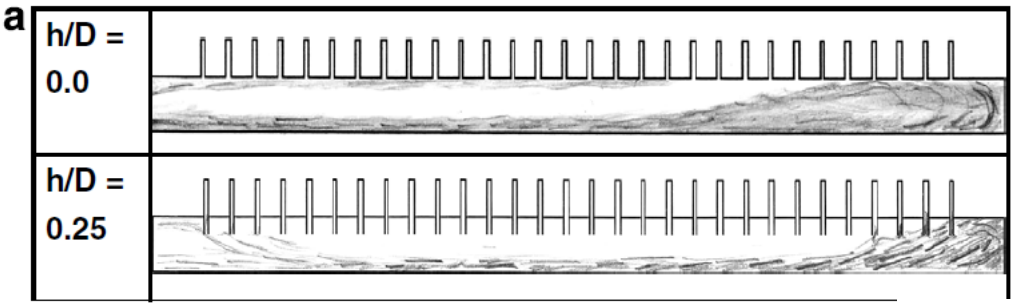

Comparatively less influence on flow distribution as compared to downward arrangement.

Liquid accumulated at the rear part of the flow channels

Air flow distribution is not significantly affected

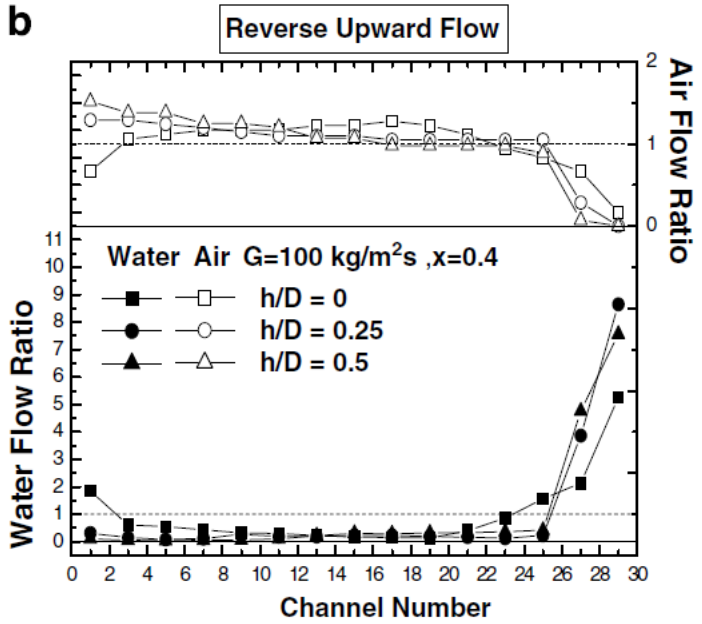

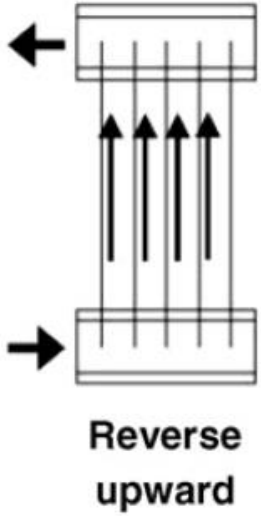

Fig. 10. (a) Typical flow pattern in a lower header with upward flow configuration and (b) corresponding water and air distribution.

Effect of quality

- Except for the low quality (x = 0.2), the quality does not significantly affect the water or air distribution for x > 0.4.
- At x = 0.2, stagnant water region forms at the rear part of the upper header, and no flow is observed. The stagnant region disappears at higher quality. Fig. 12c shows that no stagnant region exists at h/D =0.

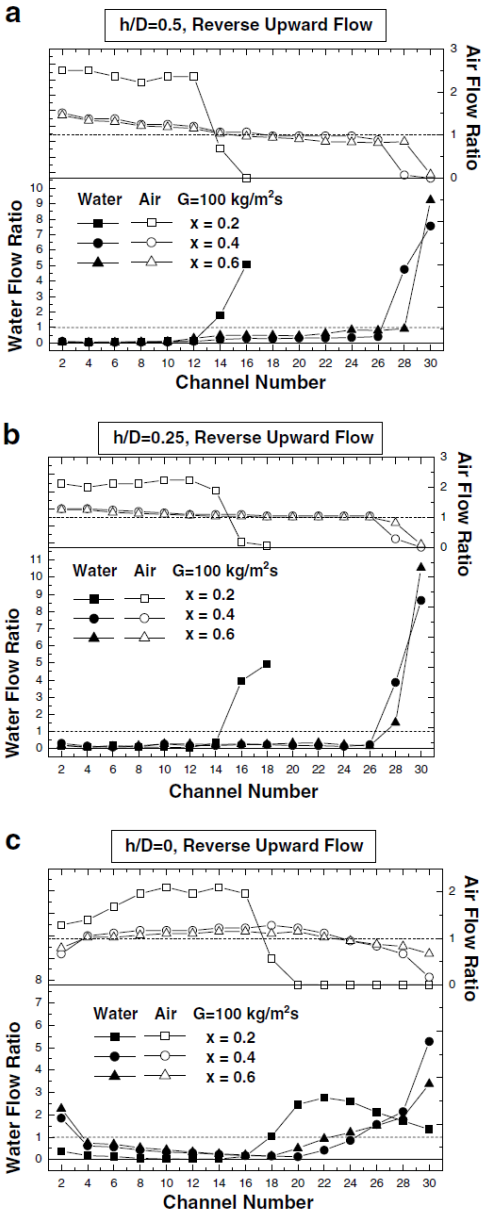

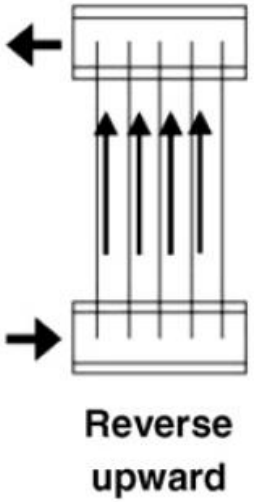

Fig. 12. Effect of quality on air and water distribution in the header of upward configuration at $G = 100\ \mathrm{kg/m^2\,s}$: (a) $h/D = 0.5$, (b) $h/D = 0.25$ and (c) $h/D = 0.0$.

MASS FLOW RATE DISTRIBUTION AND PHASE SEPARATION OF R-22 IN MULTI-MICROCHANNEL TUBES UNDER ADIABATIC CONDITION, Microscale Thermophysical Engineering, 8:129–139, 2004

- R-22 in multi-microchannel tubes under adiabatic condition.
- The test section consisted of inlet and outlet headers with the inner diameter of 19.4 mm and 15 parallel multi-microchannel tubes.
- Each microchannel tube had 8 rectangular ports with hydraulic diameter of 1.32 mm.
- The key experimental parameters were the orientation of the header (horizontal and vertical), flow direction of refrigerant into the inlet header (in-line, parallel and cross flow), and inlet quality (0.1, 0.2, and 0.3)

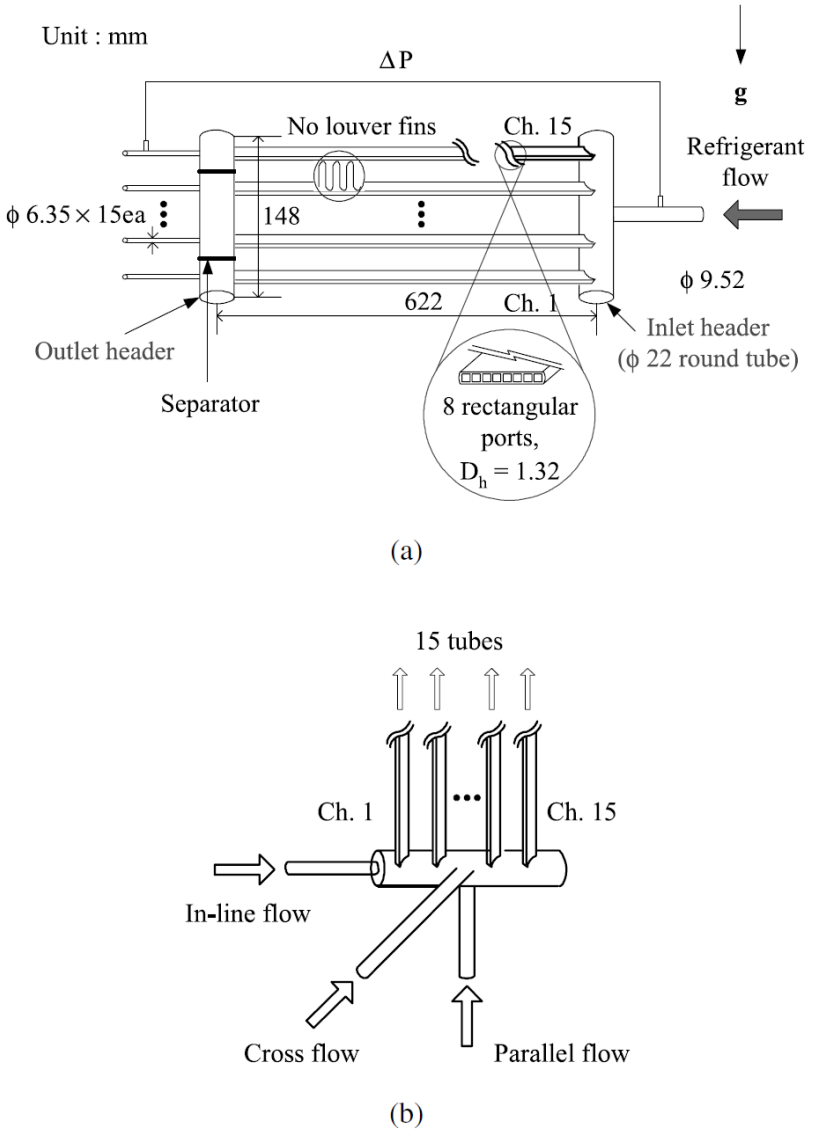

Figure 2. Details of the test section. (a) Headers and microchannel tubes (vertical header); (b) Flow direction into the inlet header (horizontal header).

Results

1. The effect of inlet quality on the mass flow rate distribution and phase separation in the microchannel tubes was negligible.
2. The effect of the orientation of the header on the mass flowrate distribution and phase separation was the largest among the test parameters.
3. Horizontal header showed better mass flow rate distribution and phase separation characteristics than vertical header.
4. Both parallel and cross-flow conditions showed better mass flow rate distribution and phase separation than in-line flow condition.

Table 1. Standard deviation of the phase separation ratio

Header	Flow direction	x_{in} 0.1	x_{in} 0.2	x_{in} 0.3
Vertical	In-line	2.24	0.72	0.64
	Parallel	3.06	0.78	0.68
	Cross	2.11	0.71	0.62
Horizontal	In-line	1.68	0.78	0.71
	Parallel	—	0.75	0.66
	Cross	—	0.79	0.70

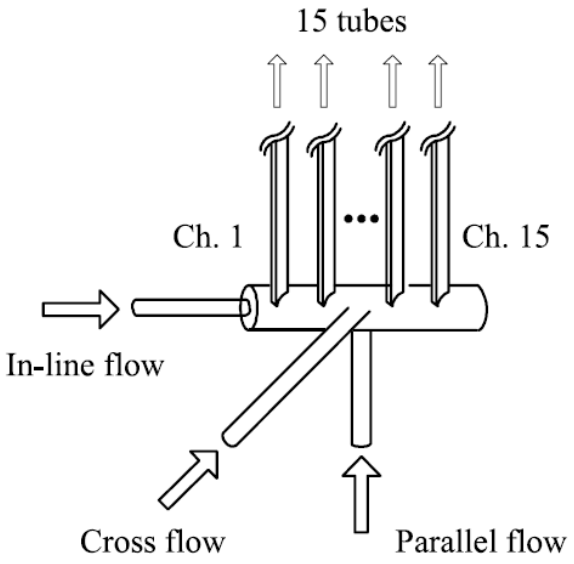

Horizontal header is for upflow

Normally horizontal header is better than vertical header

Vertical header shows worse liquid distribution

Vapor quality shows very minor influence

No significant variation (in terms of SD) for vertical or horizontal subject to different flow inlets

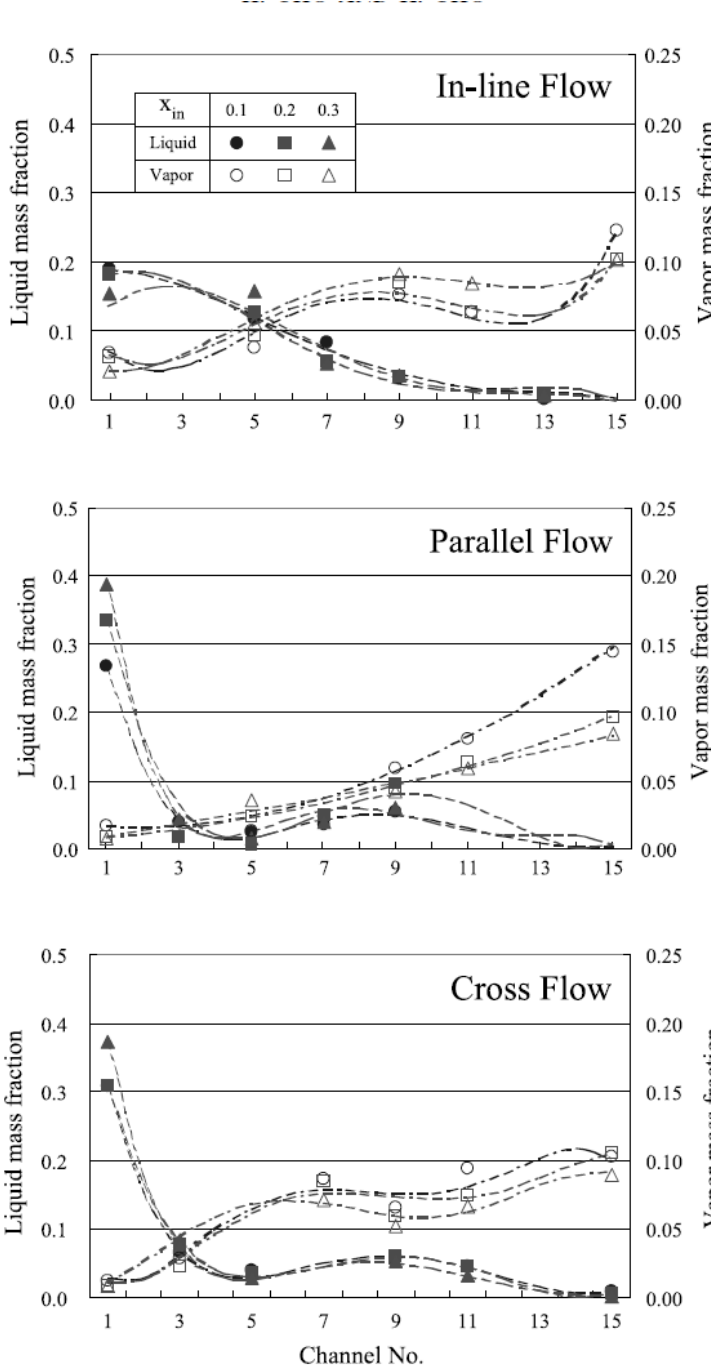

Figure 3. Liquid and vapor mass fraction for the vertical header.

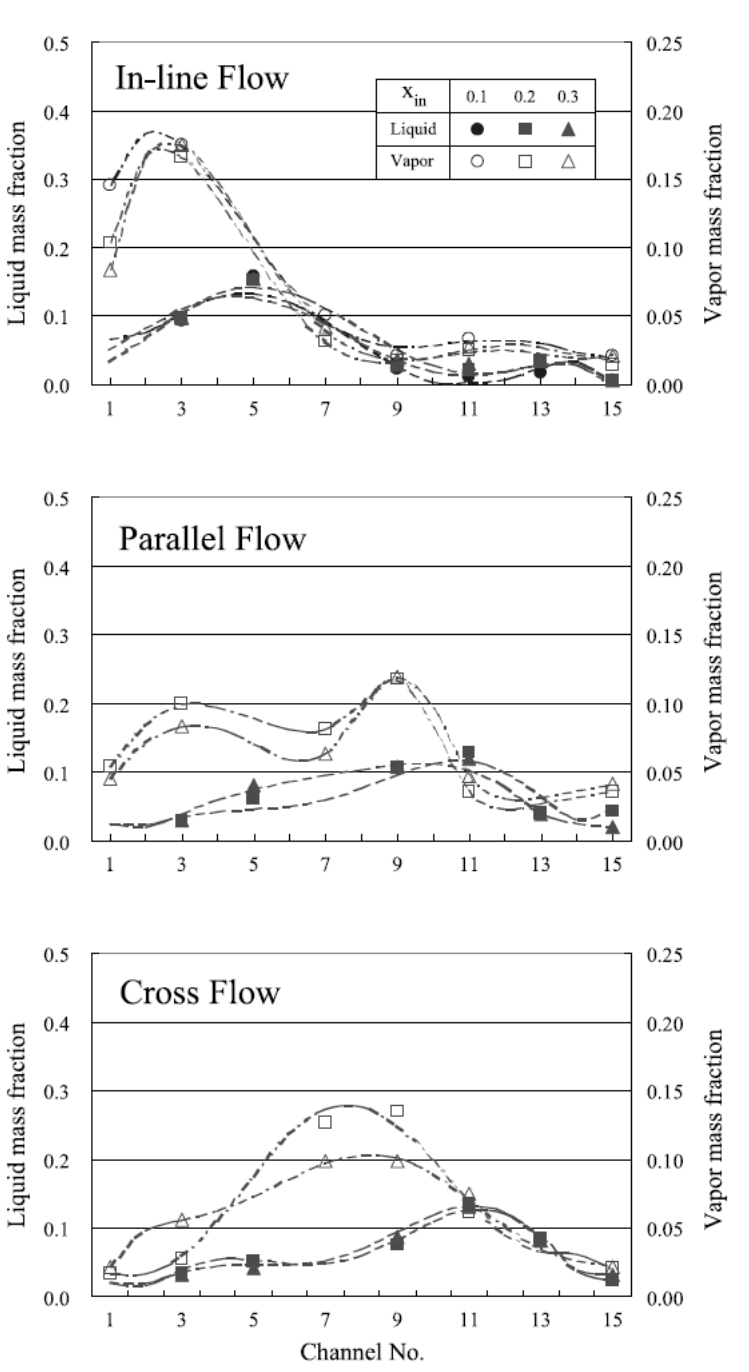

Figure 4. Liquid and vapor mass fraction for the horizontal header.

Two-phase flow distribution in compact heat exchanger manifolds, Experimental thermal and fluid sciences, 2004, 28:209-215

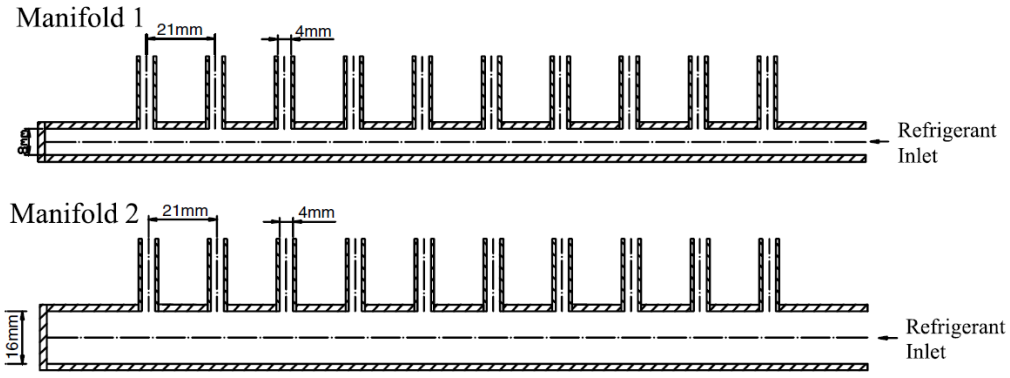

Fig. 2. Schematic of the two inlet manifolds used in the present study.

Evaporator tube = 4 mm

For larger diameter header, saturation temperature shows no influences, and smaller diameter manifold shows very small variations

No mass flowrate effect, probably the mass flowrate is not high enough to alter the stratified flow pattern

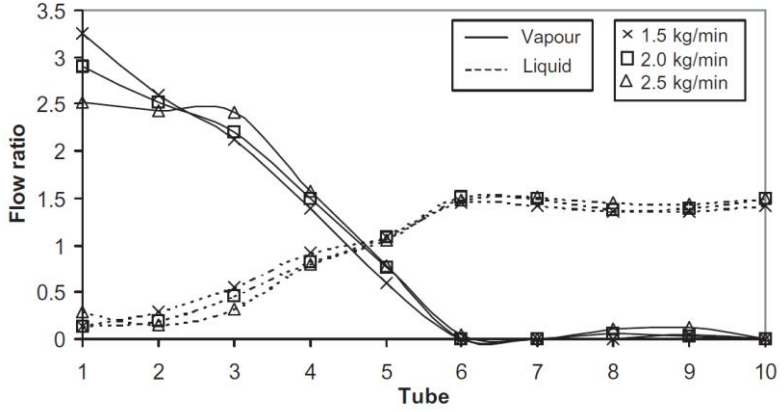

Fig. 3. Influence of mass flow rate on liquid and vapour distribution in a 16 mm manifold, upward flow in heat exchanger tubes.

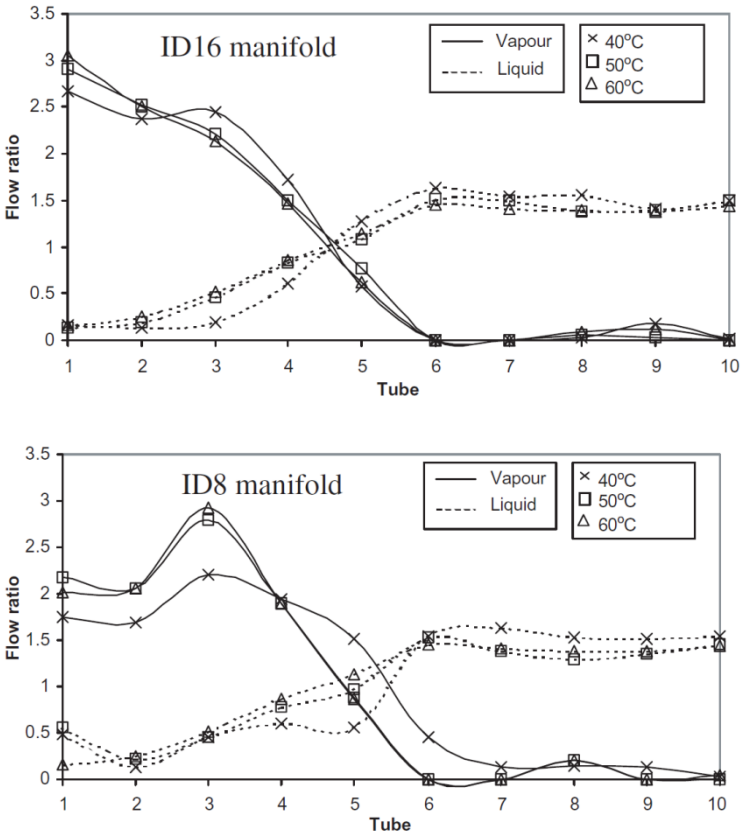

Fig. 4. Influence of evaporator water temperature on liquid and vapour distribution, upward flow in heat exchanger tubes.

At low quality (x~0.1), significant variation in liquid flow distribution is seen either for upflow or downflow but no significant change in vapor distribution.

Further increase the vapor fraction shows very minor change in distribution for both liquid and vapor phase.

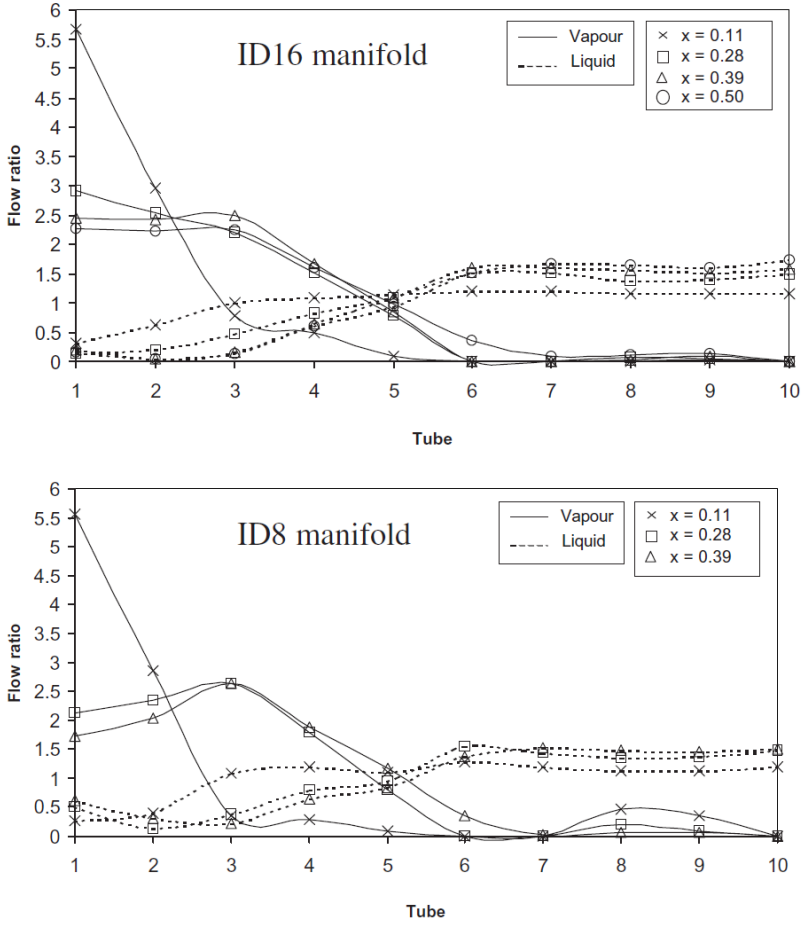

Fig. 5. Influence of inlet vapour fraction on liquid and vapour distribution, upward flow in heat exchanger tubes.

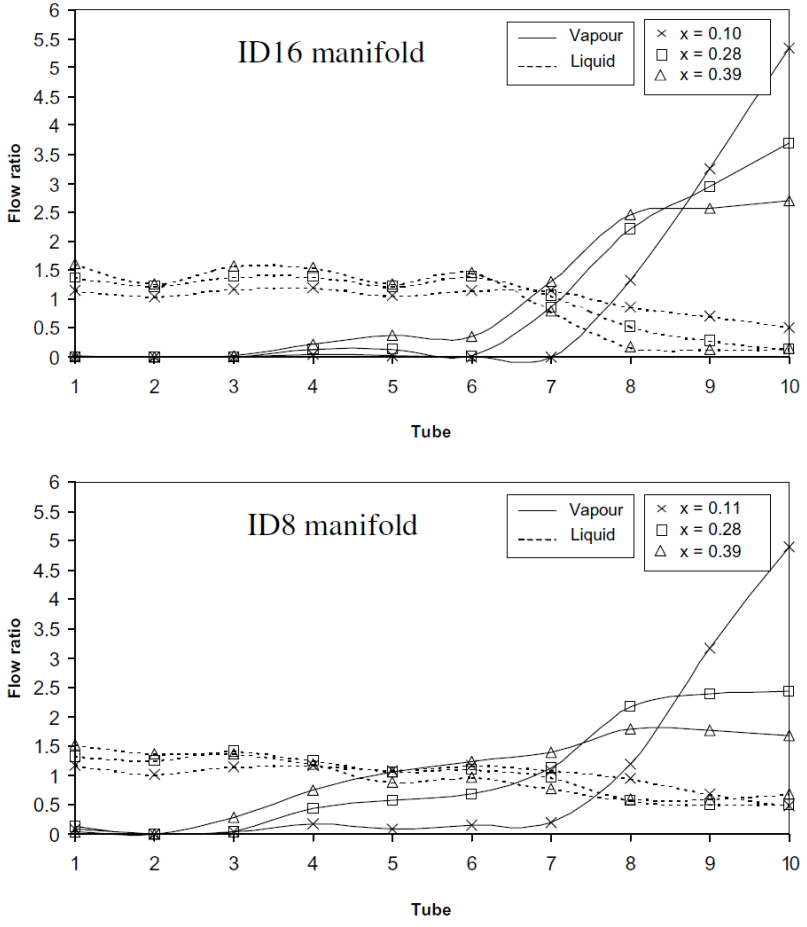

Fig. 6. Influence of inlet vapour fraction on liquid and vapour distribution, downward flow in heat exchanger tubes.

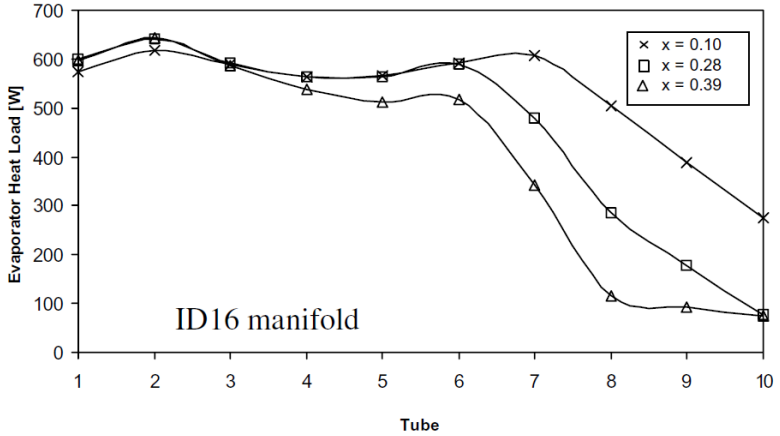

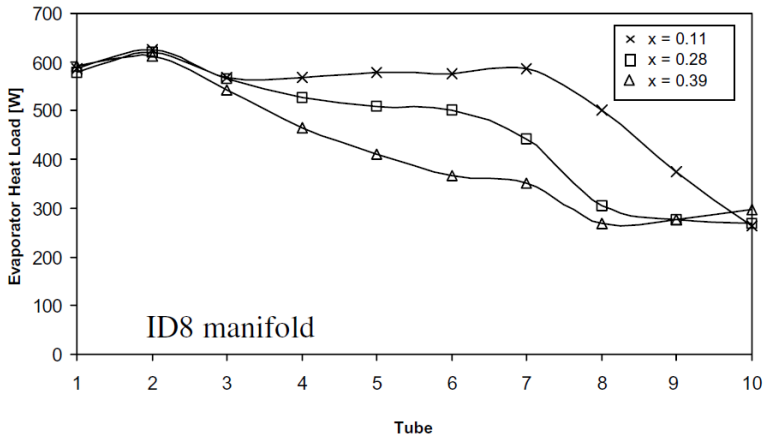

Fig. 8. Measured evaporator tube heat load as function of inlet vapour fraction, downward flow in heat exchanger tubes.

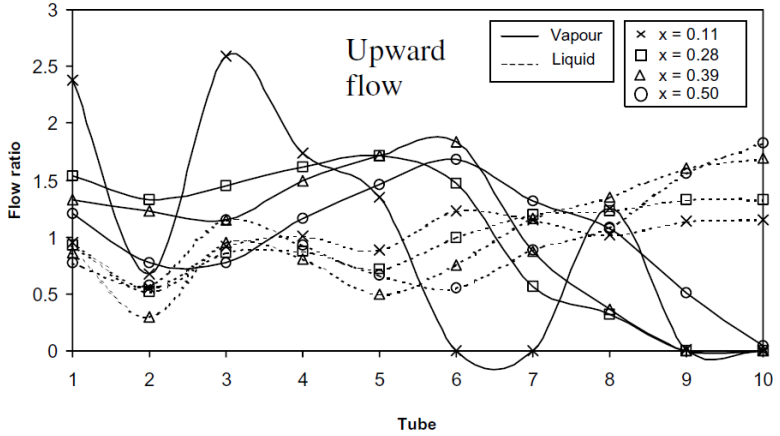

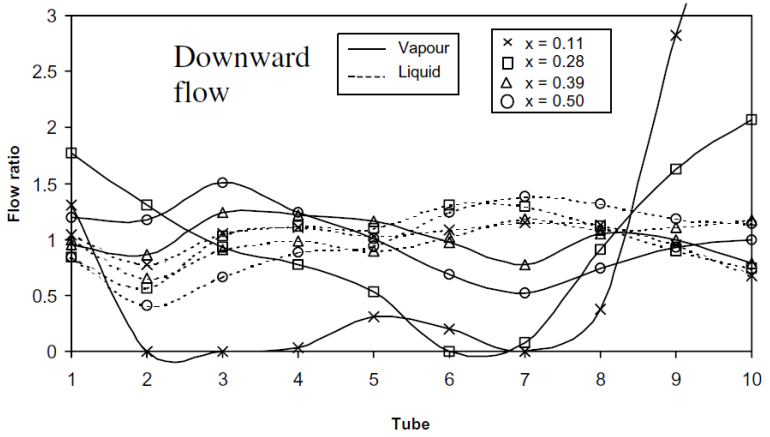

Fig. 9. Influence of inlet vapour fraction on liquid and vapour distribution, ID8 mm manifold, short manifold inlet tube (50 mm).

a short inlet tube of 50 mm was used in some experiments (in contrast to the original inlet tube length of 250 mm)

Effect of inlet configuration on upward branching of two-phase refrigerant in a parallel flow heat exchanger, Int. J. Refrig., 36 (2013) 1062-1077, 1- flat tubes, 70 to 130 kg/m^{2}s and quality from 0.2 to 0.6

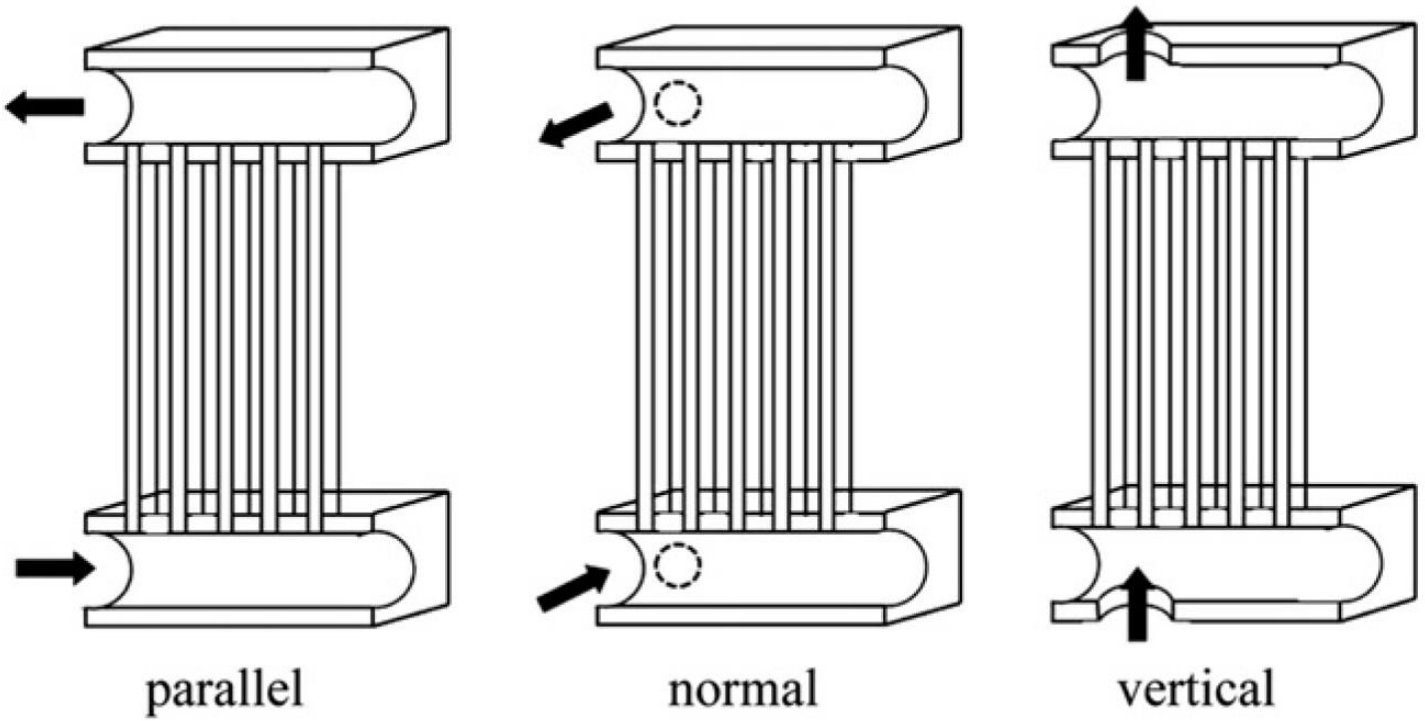

Fig. 1 – Flow inlet configurations.

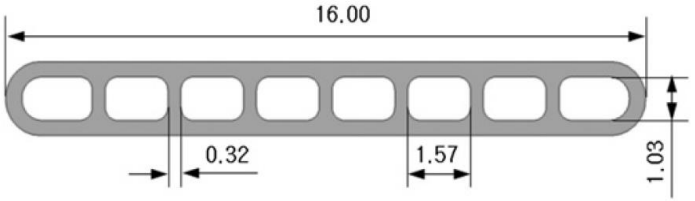

Fig. 2 – Cross-sectional view of the flat tube used in this study (unit: mm).

For Upflow,
Vertical inlet is the best,
Normal inlet is the worst

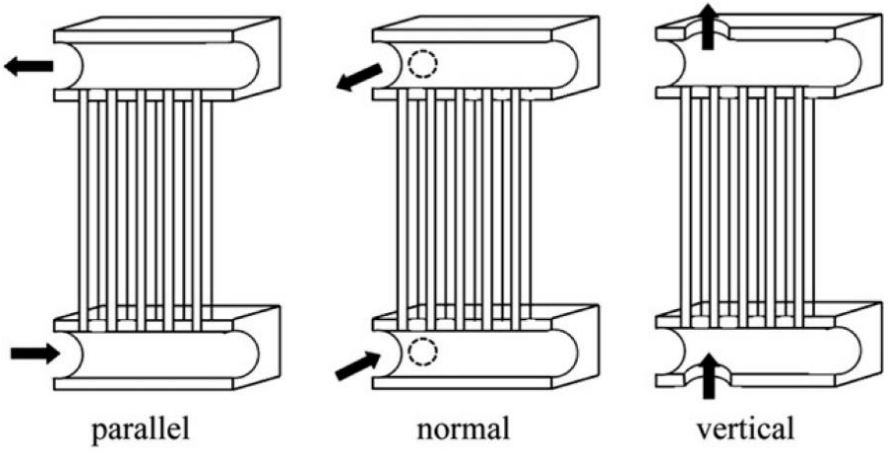

Fig. 1 – Flow inlet configurations.

$$SD = \sqrt{\frac{\sum_{i=i}^{N}(CFR_i - 1.0)^2}{N}}$$

Table 3 – Standard deviations of the liquid and gas flow ratio.

G (kg m^{-2} s^{-1})	x	Standard deviation					
		Parallel		Normal		Vertical	
		Liquid	Gas	Liquid	Gas	Liquid	Gas
70	0.4	0.41	0.70	0.40	0.62	0.24	0.29
100	0.2	0.19	0.45	0.38	0.75	0.26	0.33
100	0.4	0.29	0.69	0.53	0.50	0.27	0.25
100	0.6	0.36	0.81	0.56	0.37	0.20	0.23
130	0.4	0.44	0.61	0.54	0.42	0.35	0.31
Average		0.34	0.65	0.48	0.53	0.26	0.28

Downflow shows much worse distribution, no influence on vapor flow, parallel is the worst for downflow, vertical and normal is about the same.

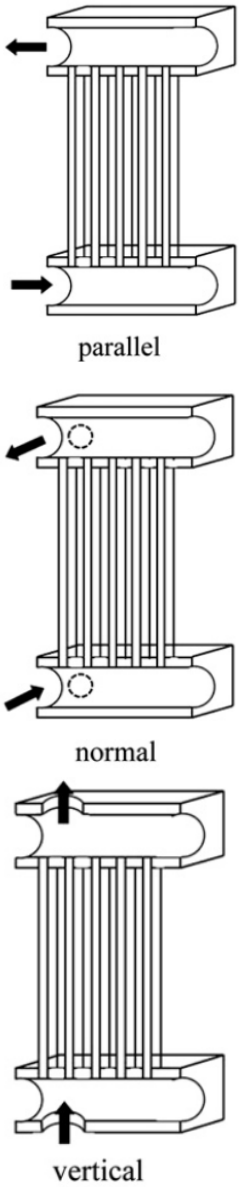

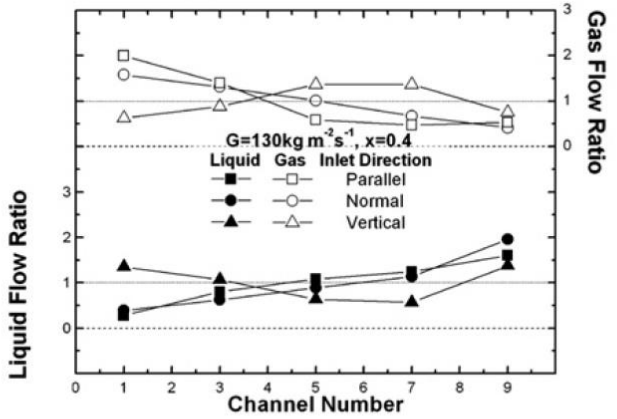

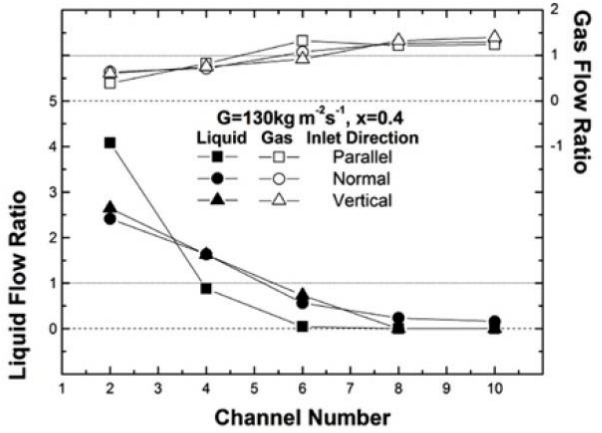

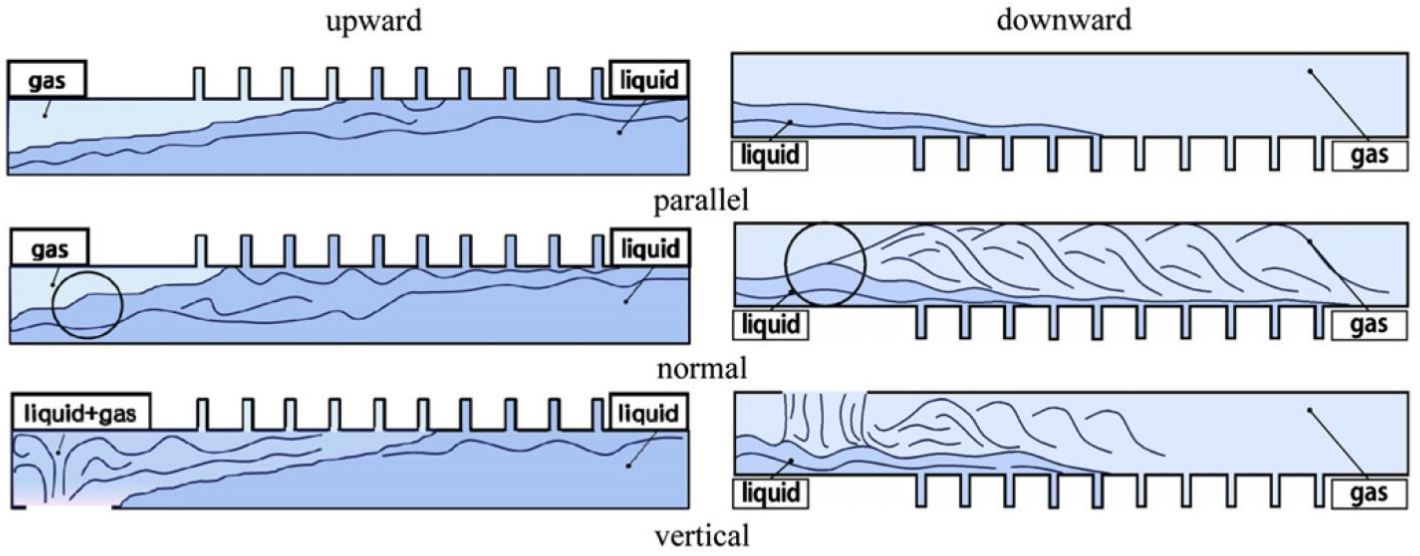

Fig. 12 – Flow distribution data for upward and downward flow at $G = 130$ kg m^{-2} s^{-1} and $x = 0.4$.

Difference between air/water & R-134a (downflow)

High inertia of air/water leads to two higher mass flowrate at front and rear part. R-134a shows continuous drop

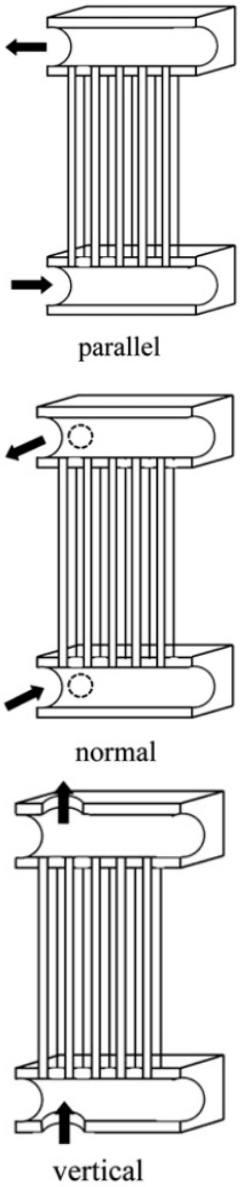

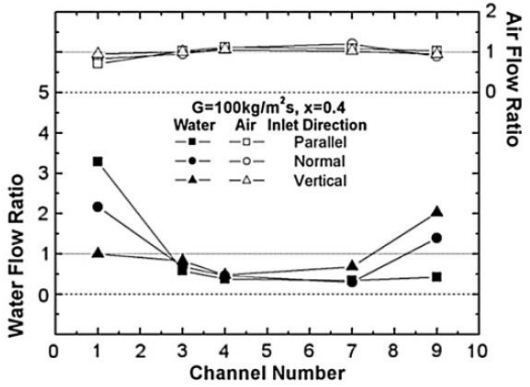

Air-water

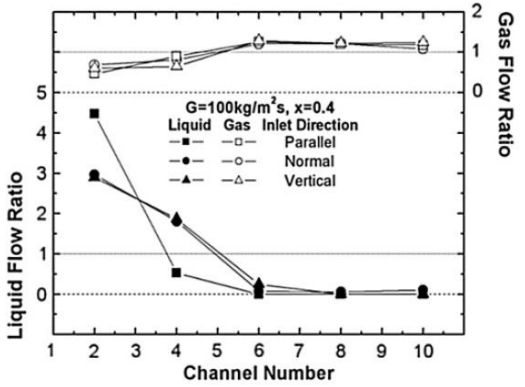

R-134a

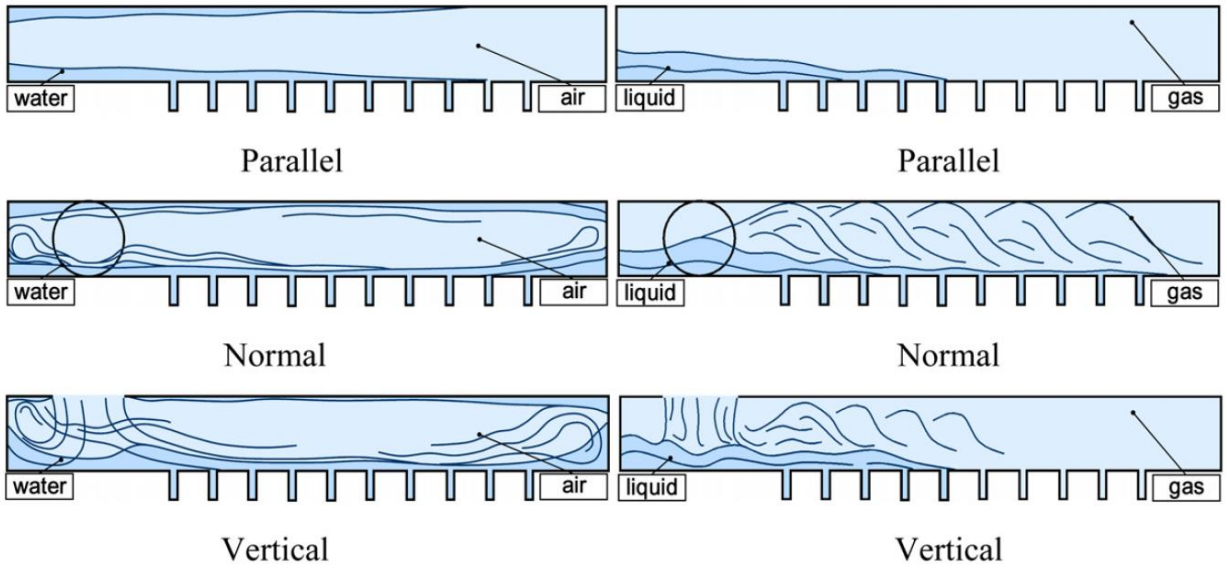

Fig. 12 – Air–water and R-134a flow distribution data at $G = 100\ kg\ m^{-2}\ s^{-1}$ and $x = 0.4$.

Effect of outlet header diameter

Effect of the header pressure drop induced flow maldistribution on the microchannel evaporator performance, Int. J. refrig., 36 (2013), 2176-2186

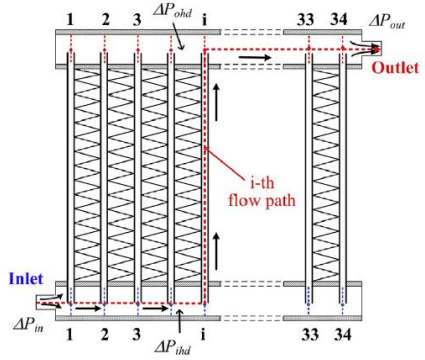

Fig. 4 – Schematic drawing of flow paths in microchannel evaporator.

Larger outlet header is better because refrigerant vapor velocity at the outlet header and corresponding pressure drop gradually decreases. The pressure drop across each microchannel tube becomes more uniform.

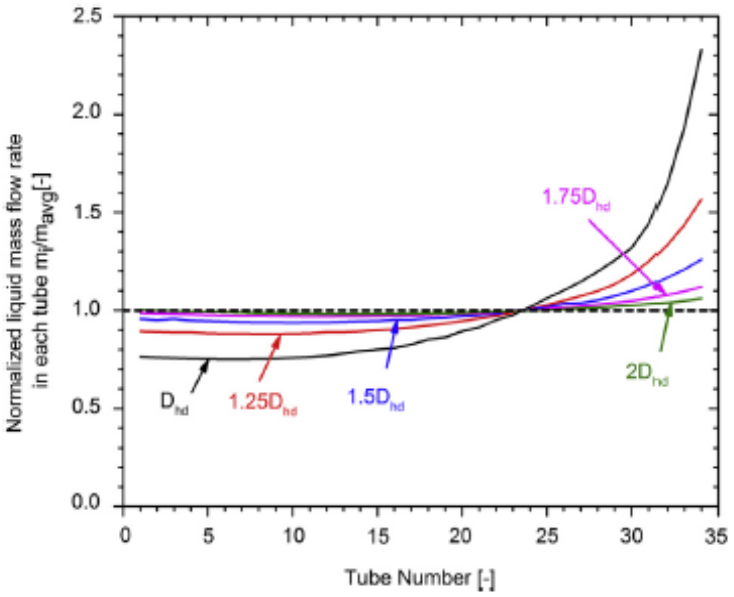

Fig. 10 – Liquid distribution among parallel channels as a function of outlet header diameter.

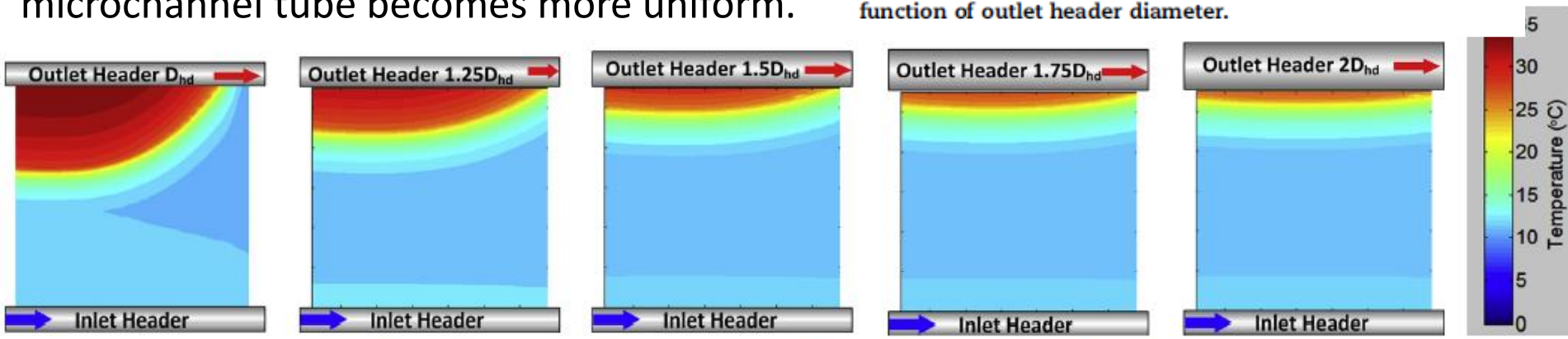

Fig. 12 – Evaporator surface temperature profiles at a fixed bulk exit superheat of 5 °C.

Effect of Microchannel Diameter

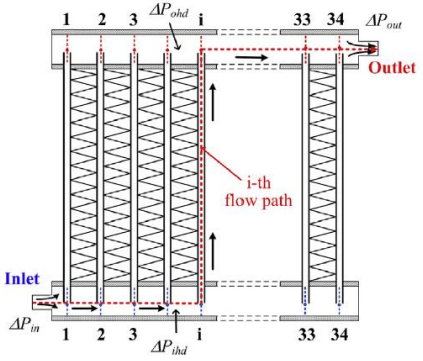

Fig. 4 – Schematic drawing of flow paths in microchannel evaporator.

- microchannel hydraulic diameter varies from 0.8 mm (baseline) to 0.4 mm while keeping other parameters and operating conditions constant.
- A smaller microchannel diameter the normalized liquid mass flow rate becomes more uniform among parallel tubes. This is because the tube pressure drop increases, and therefore the ratio of outlet header DP to total evaporator DP is reduced, as shown in Fig. 14

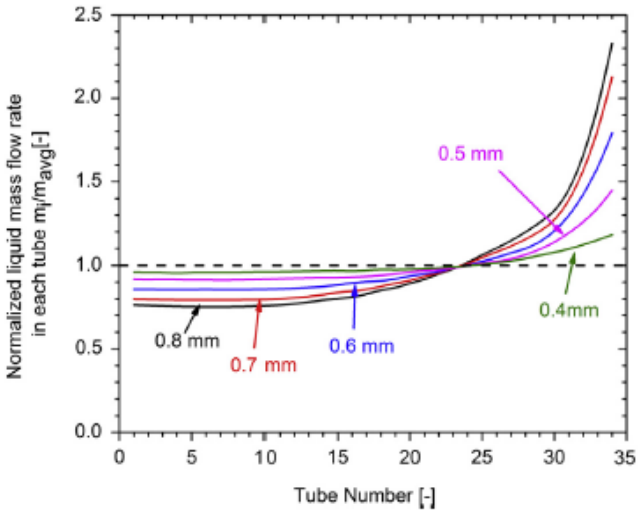

Fig. 13 – Liquid flow rate distribution as a function of microchannel diameter.

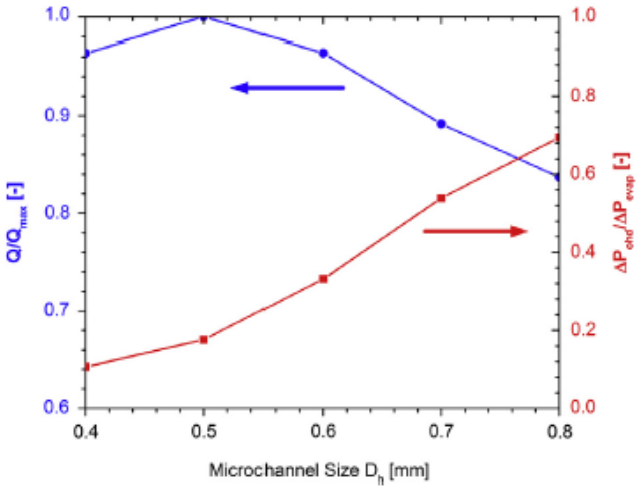

Fig. 14 – Variation of normalized cooling capacity and pressure drop ratio with microchannel size.

Effect of Aspect Ratio

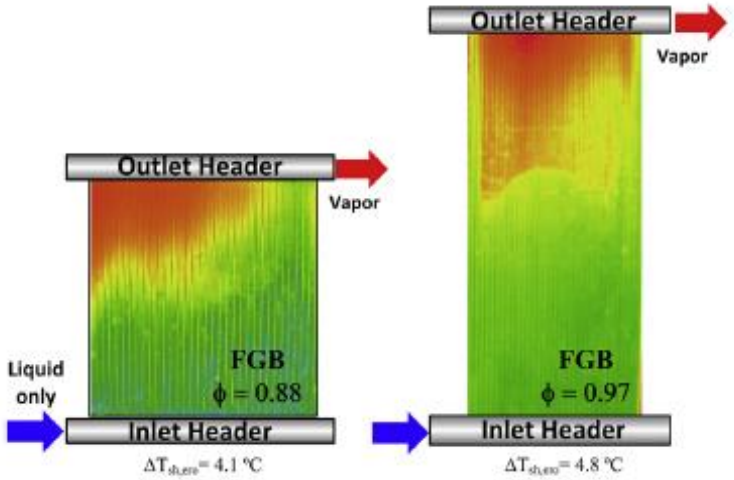

Fig. 18 – Comparison of surface temperature profiles of two different microchannel evaporators.

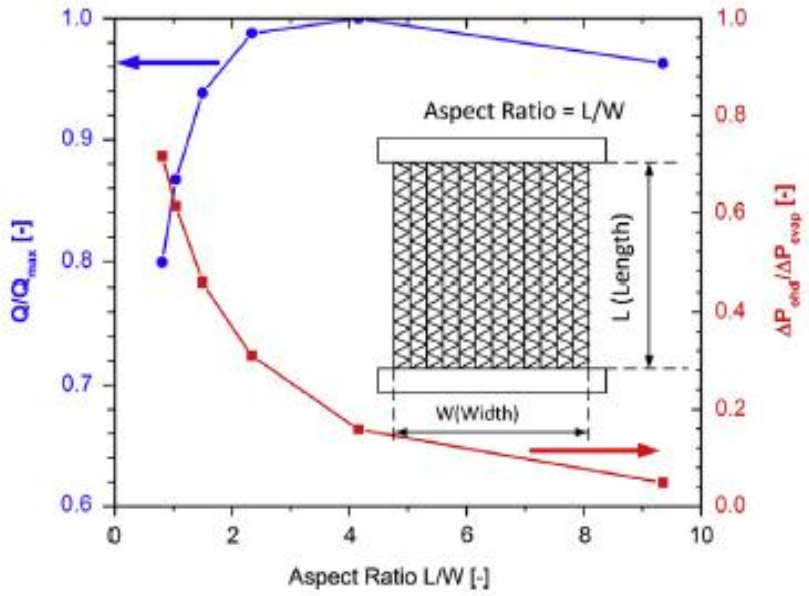

Fig. 17 – Effect of the evaporator aspect ratio on the cooling capacity and the pressure drop ratio.

Table 3 – Geometric parameters of#1 (baseline) and#2 (new) microchannel evaporator.

	#1	#2
Port diameter (mm)	0.8	0.55
Port No. (per tube)	19	21
Tube No.	34	35
Tube length (mm)	275	490
Outlet header diameter (mm)	21	37.5
Aspect ratio	0.79	2.24

Better flow distribution can be achieved via

1) Enlarging outlet header diameter;
2) Increasing heat exchanger aspect ratio (ratio of length to width);
3) Reducing microchannel port size.

Two-phase refrigerant distribution in a two row/four pass parallel flow minichannel heat exchanger, Experimental Thermal and Fluid Science 77 (2016) 10–27

- Multi-pass, R-410A

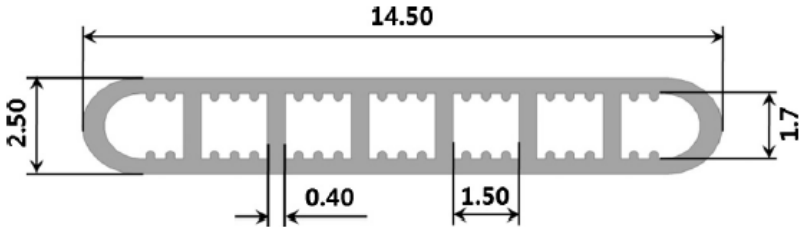

Fig. 2. Cross-sectional geometry of the flat tube (unit: mm).

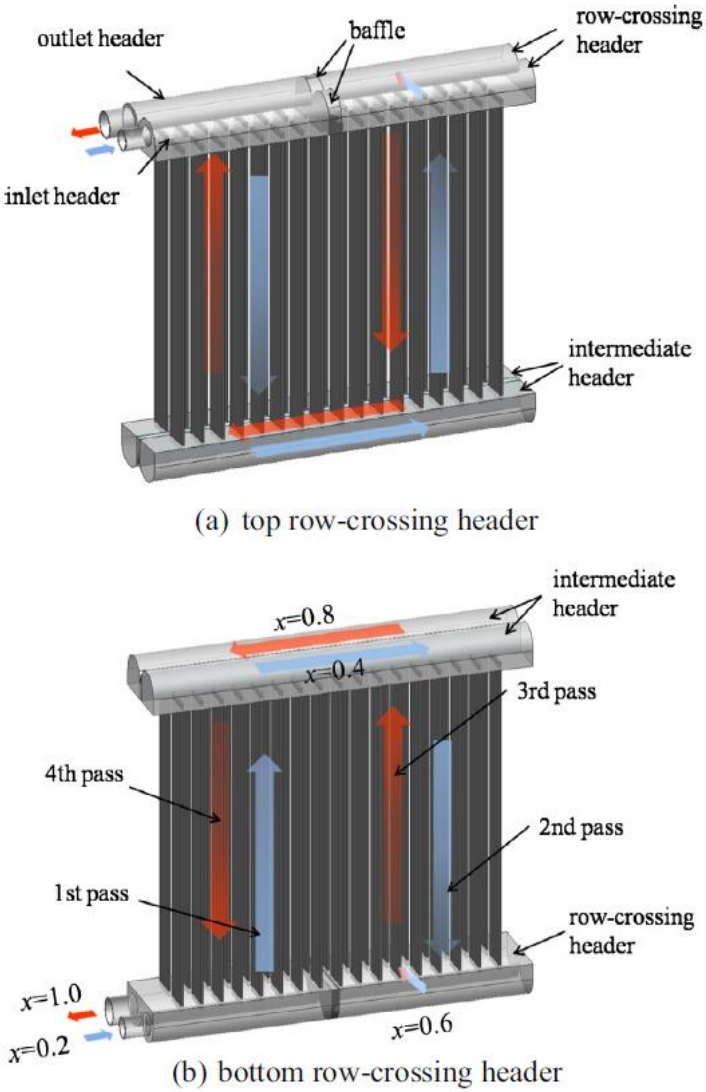

Fig. 1. Refrigerant-side circuiting (top row-crossing header, bottom row-crossing header) investigated in this study.

Inlet on top

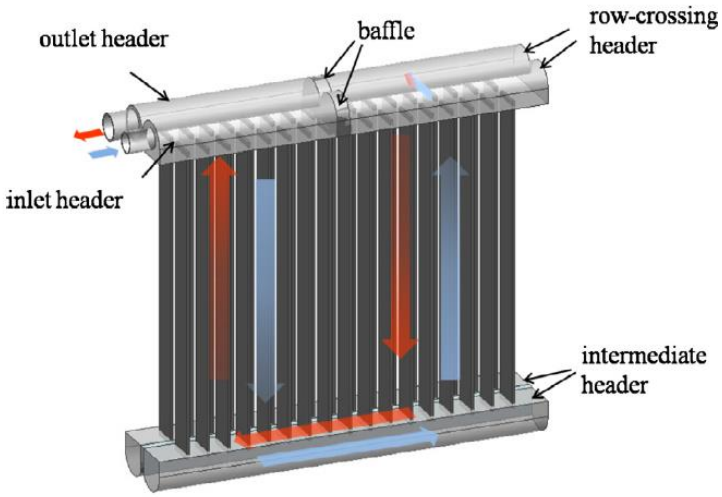

(a) top row-crossing header

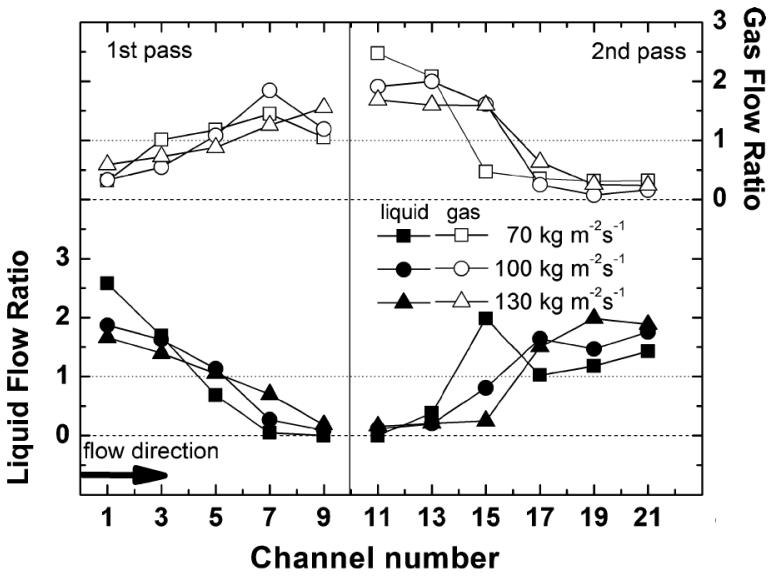

(a) Flow distribution data

- 1st pass shows worse distribution, the first few tubes of 2nd pass shows very poor liquid distribution.
- At subsequent pass, normally downstream tube tubes shows more refrigerant
- The 4th pass shows very worse liquid distribution.

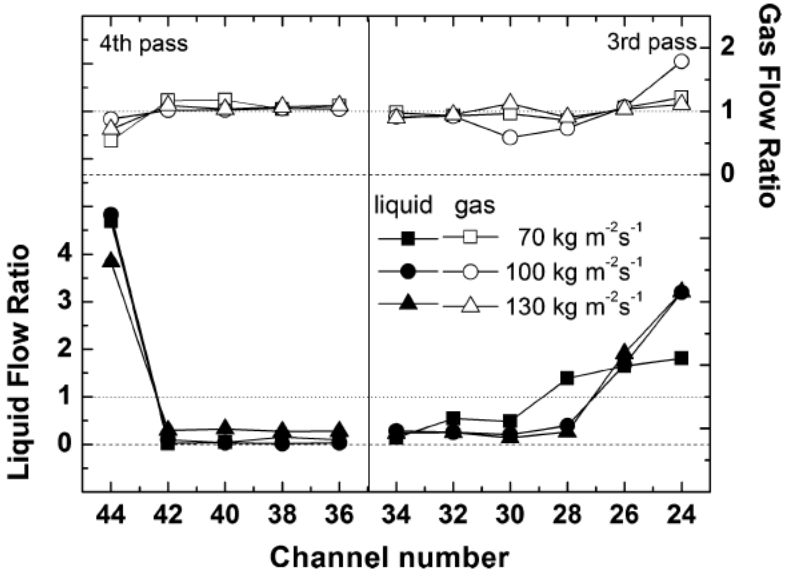

(a) Flow distribution data

Inlet at the bottom

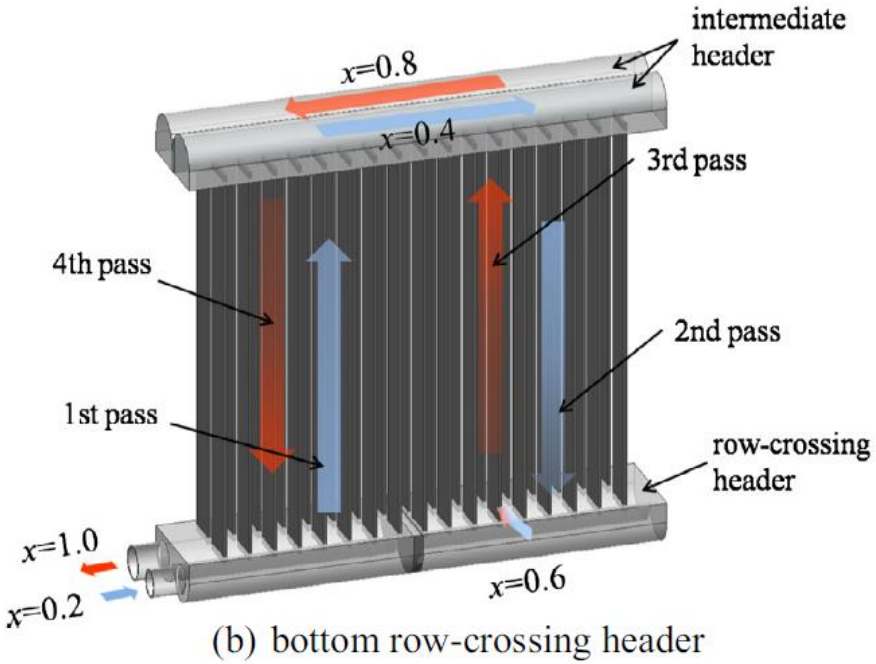

(b) bottom row-crossing header

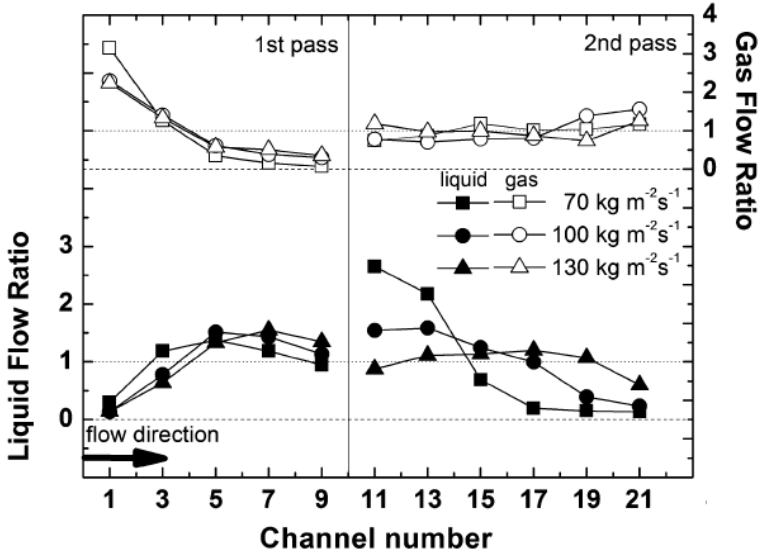

(a) Flow distribution data

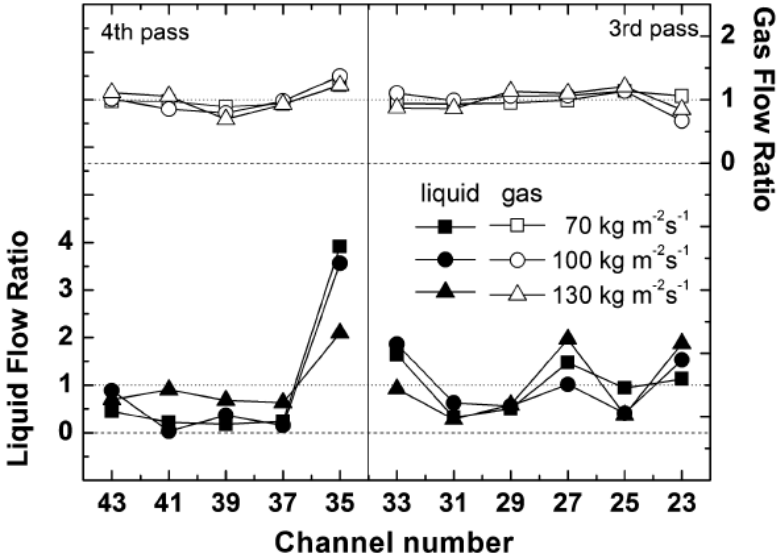

(a) Flow distribution data

Slightly improved even flow distribution

Normally upflow pass gives better distribution

Two-Phase Flow Distribution to Tubes of Parallel Flow Air-Cooled Heat Exchangers, Heat Transfer Engineering, 26(4):3–18, 2005

- Previous research and the patent literature show two basic approaches to improved flow distribution:
  - install obstacles (weir, inserts, or throttle plates) at the inlet end of the header or adjust the tube projection in the header
  - install special distributor devices in the header, which locally feeds the fluid to the branch tubes. The use of a small diameter distributor tube (or similar) with small spaced exit holes along its length appears to be a viable concept to obtain good flow distribution.

Refrigerant distribution in a parallel flow heat exchanger having vertical headers and heated horizontal tubes, Experimental Thermal and Fluid Science 35 (2011) 920–932

- Vertical headers, two passes with a target capacity of 1.0 kW.
- Refrigerant (R-410A) enters the left header,
- To simulate an actual evaporator, tubes are heated to yield a test section outlet superheat of 5 °C. Inlet and out-let locations were systematically varied in a search for an optimum position.

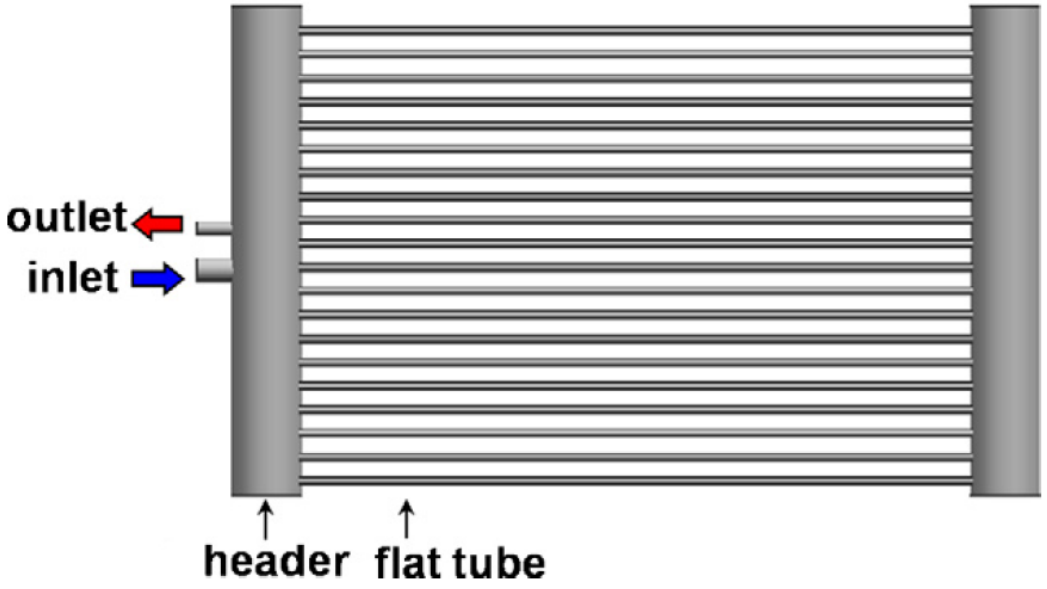

Fig. 2. Schematic drawing of the parallel flow heat exchanger considered in the present study.

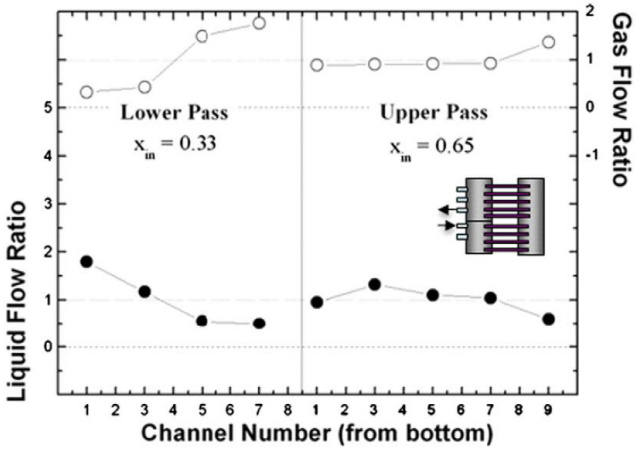

(a) flow distribution data

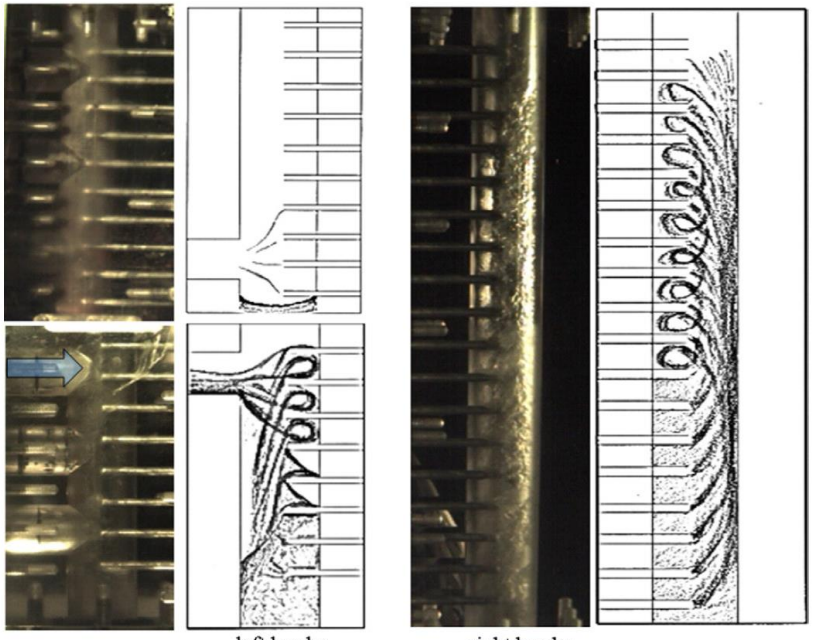

(b) flow pattern

Fig. 8. Typical flow distribution data and flow pattern photos and sketches, data taken at $G = 60$ kg/m^2 s with top inlet and bottom outlet.

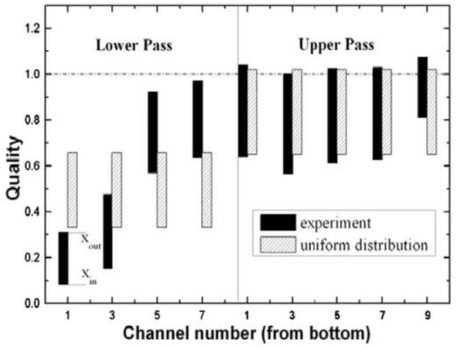

(a) channel inlet and outlet

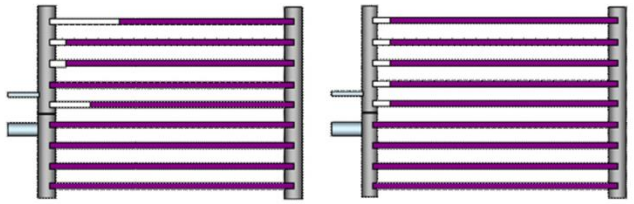

(b) sketches showing channel dryout

Fig. 10. Vapor quality at channel inlet and outlet of each tube and a sketch showing channel dryout, data taken at $G = 60$ kg/m^2 s with top inlet and bottom outle

2-pass

Inlet at the top portion gives better distribution

Table 4
Thermal performance degradation by mal-distribution.

Inlet	Top					Middle		
Outlet	Bottom			Middle	Top	Bottom	Middle	Top
G (kg/m^2 s)	50	60	70	60	60	60	60	60
deg (%)	5.52	2.15	5.5	6.49	1.57	13.2	9.63	13.4
ΔP (kPa)	6.14	6.21	6.83	9.45	6.76	6.83	10.1	8.27

Effect of inlet location

- Lower mass flowrate at the top due to gravity influence
- Lower tube at the 1st pass conatins more liquid due to gravity force

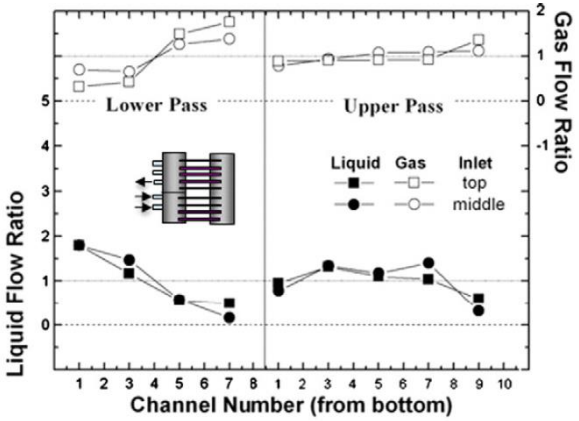

(a) flow distribution data

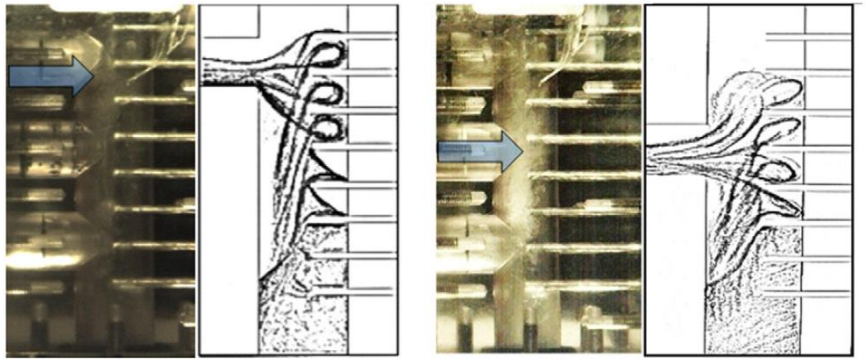

(b) corresponding photos and sketches

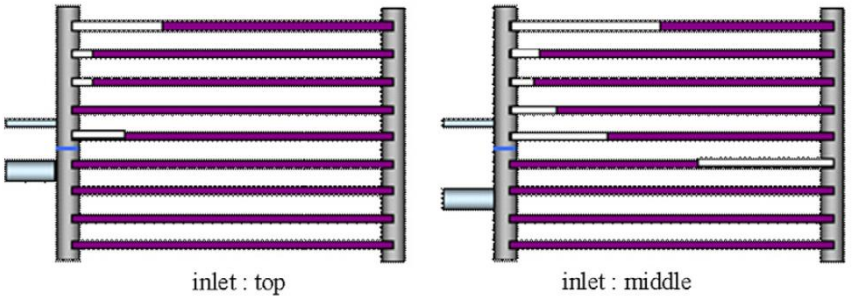

(c) sketches showing channel dryout

Fig. 12. Effect of inlet location on the flow distribution, corresponding photos and flow distribution sketches, sketches showing channel dryout, data taken at $G =$

Effect of Mass flowrate

- Higher mass flowrate does not significantly improved the mass flowrate distribution
- Lower tube at the 1st pass conatins more liquid due to gravity force
- Note that the liquid phase in the 2nd pass is better distributed

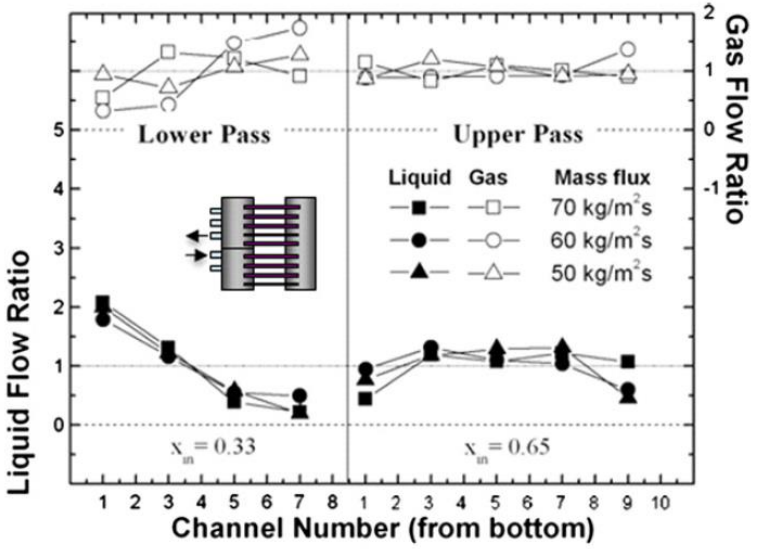

(a) flow distribution data

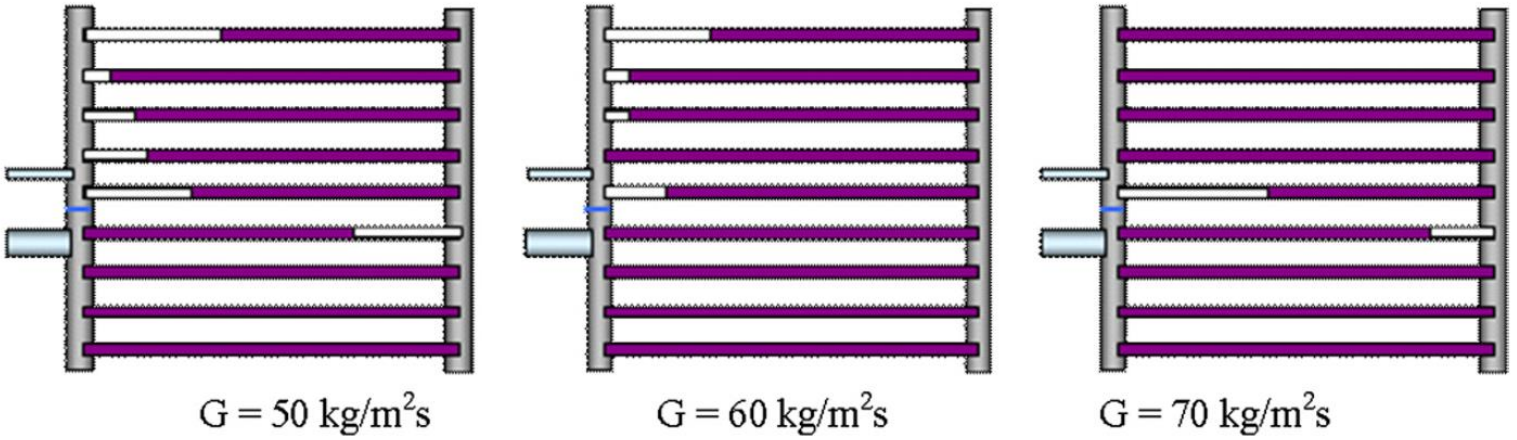

(b) sketches showing channel dryout

Fig. 11. Effect of mass flux on the flow distribution and correspond sketch showing channel dryout, data taken with top inlet and bottom outlet.

Effect of outlet location

- For outlet header (2nd pass), outlet at the bottom is slightly better

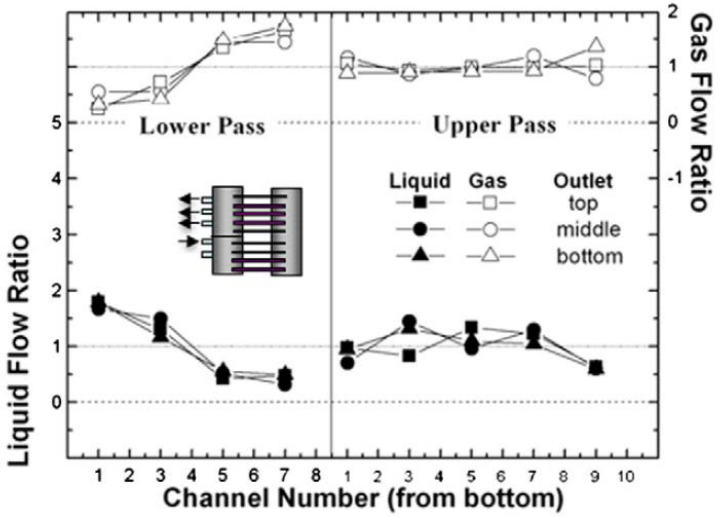

(a) flow distribution data

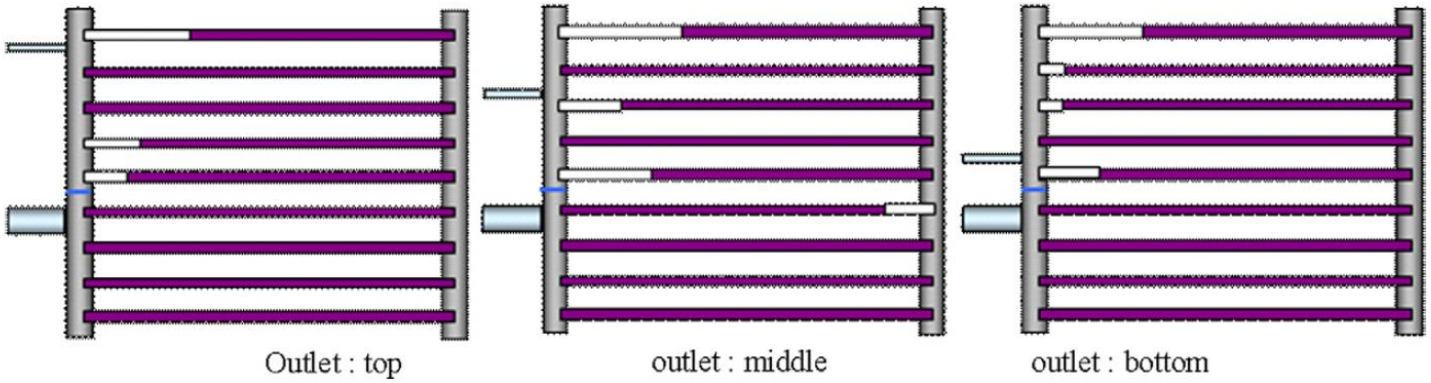

(b) sketches showing channel dryout

Fig. 13. Effect of outlet location on the flow distribution and corresponding sketches showing channel dryout, data taken at $G = 60$ kg/m^2 s.

The effect of the flow direction inside the header on two-phase flow distribution in parallel vertical channels, Applied Thermal Engineering 36 (2012) 245-251

- Air-water system

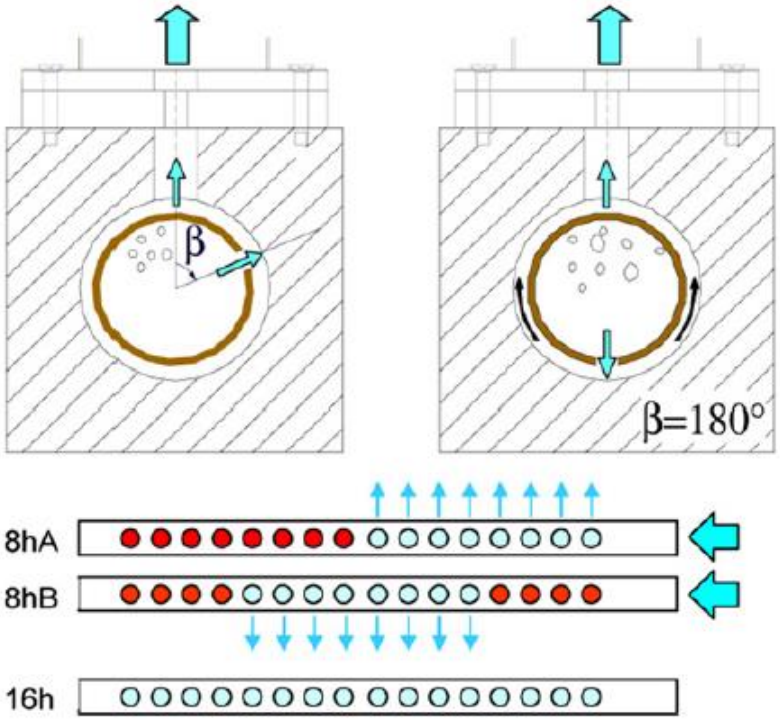

Fig. 3. Flute fitting operating modes.

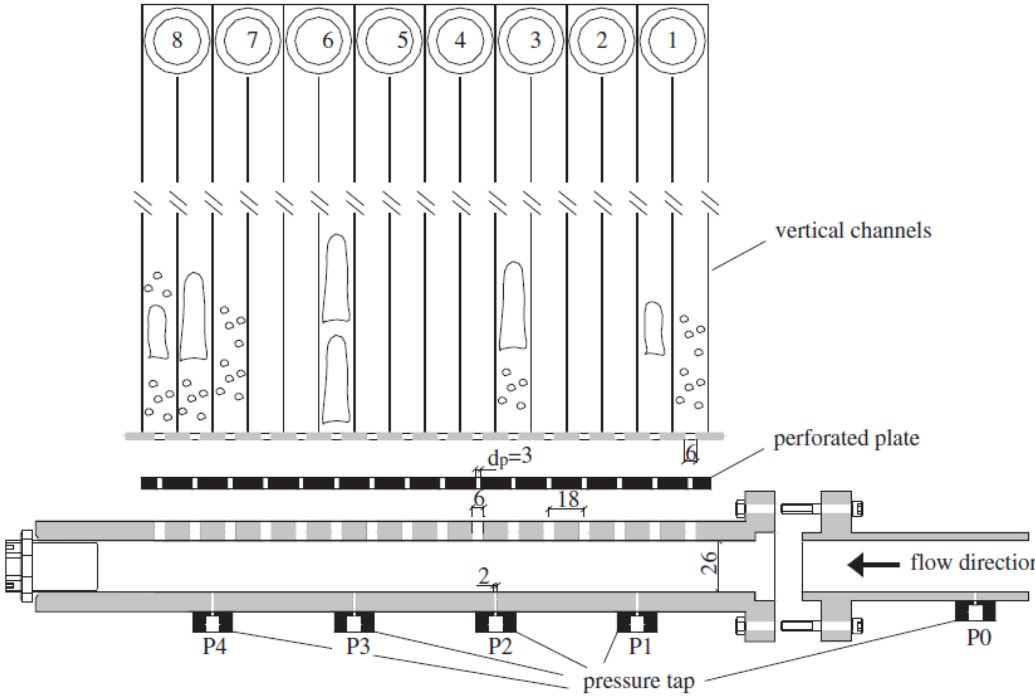

Fig. 2. Test section and channel pairs.

The effect of the flute orientation in terms of the β angle, showed an optimum operating condition, for all the flow rates here investigated, when the flow from the flute is downward (β = 180°). On the other hand, flute exits upward (β = 0°) do not yield meaningful flow distribution enhancements.
The best results were obtained when the flute holes were facing in the opposite direction to the vertical channel inlet, i.e. for β = 180°.

The effect of the flow direction inside the header on two-phase flow distribution in parallel vertical channels, Applied Thermal Engineering 36 (2012) 245-251

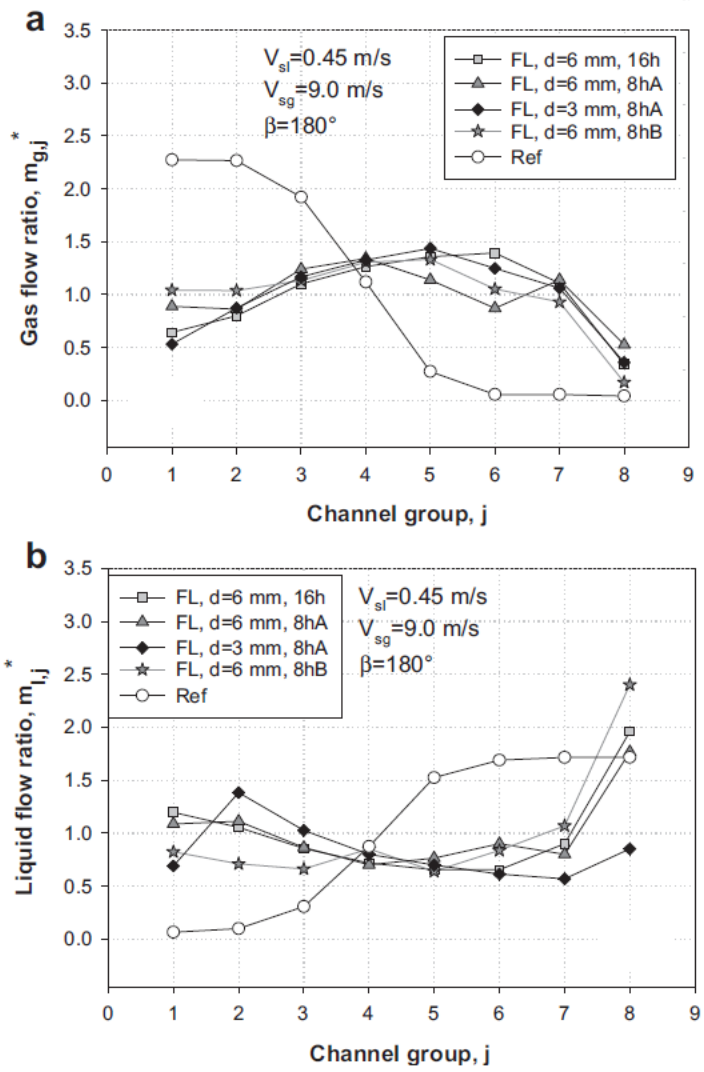

Fig. 4. a and b. Gas and liquid flow ratios inside parallel channels. Comparison between Reference, 16 holes and 8 holes working modes (8hA and 8hB).

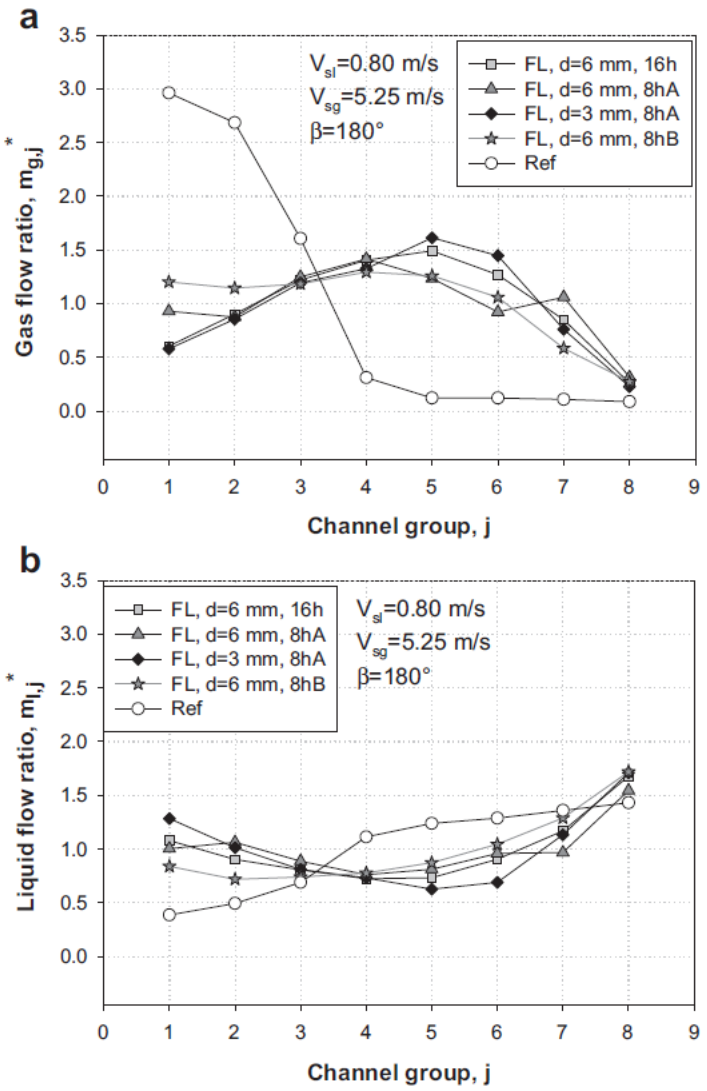

Fig. 5. a and b. Gas and liquid flow ratios inside parallel channels. Comparison between Reference, 16 holes and 8 holes working modes (8hA and 8hB).

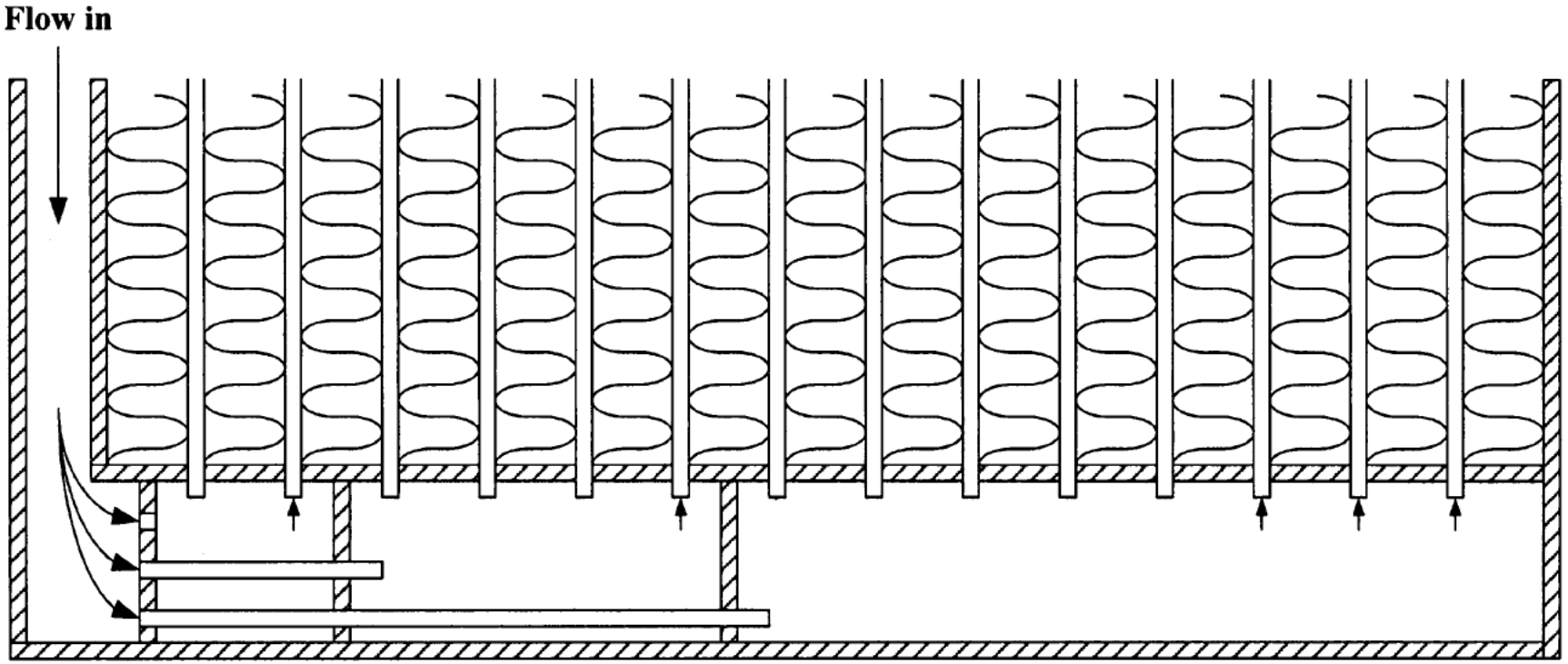

Figure 19 Front view of heat exchanger [16].

[16] Chiba, T., and Toshihara, T., Heat Exchanger with a Distribution Device Capable of Uniformly Distributing a Medium to a Plurality of Exchanger Tubes, U.S. Patent No. 5,901,785, 1999.

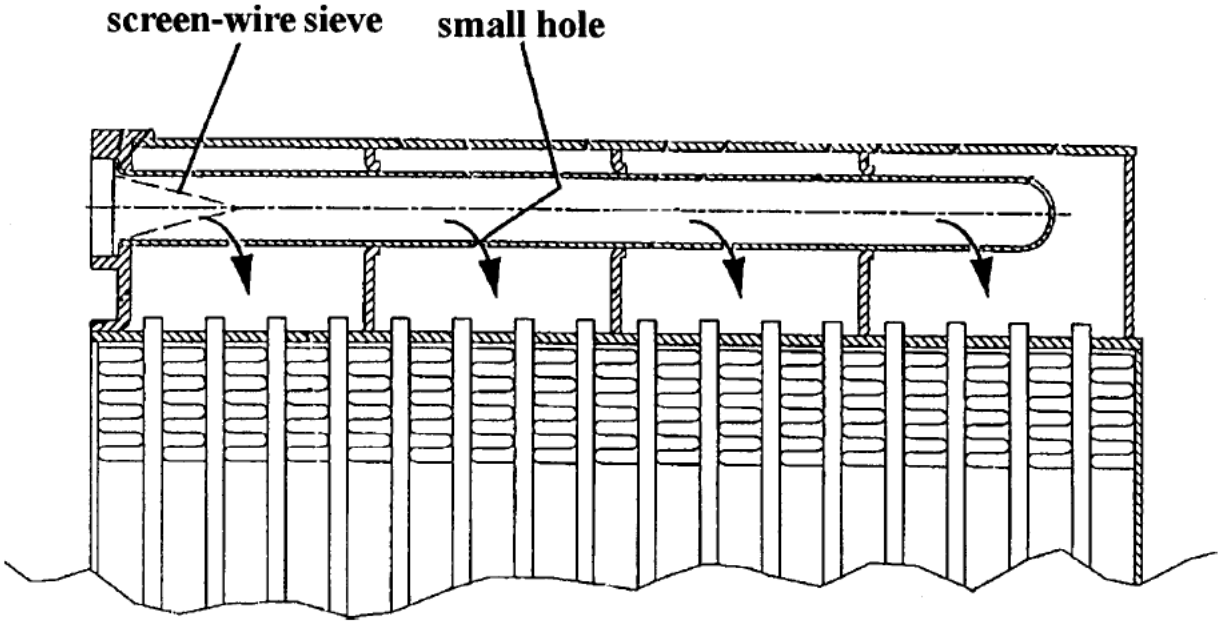

Figure 20 Inlet distributor tube with sieve-mesh distribution [5].

[5] Haussmann, R., Distributing/Collecting Tank for the at Least Dual Flow Evaporator of a Motor Vehicle Air Conditioning System, U.S. Patent No. 6,199,401 B1, 2001.

Osthues, J., Petz, M., and Zeitvogel, B., Plate Heat Exchanger with a Refrigerant Distributor, U.S. Patent No. 5,806,586, 1998.

- The flow distribution in the header of these inventions [23–25] depends on the shape, size, space of the holes, and the small distributor tube diameter. Among these, the small distributor tube diameter is a dominant parameter that strongly influences the two-phase flow characteristics in the tube. These designs will require modification if the operating conditions (total number of tubes, the refrigerant flow rate, or the inlet vapor quality) change.

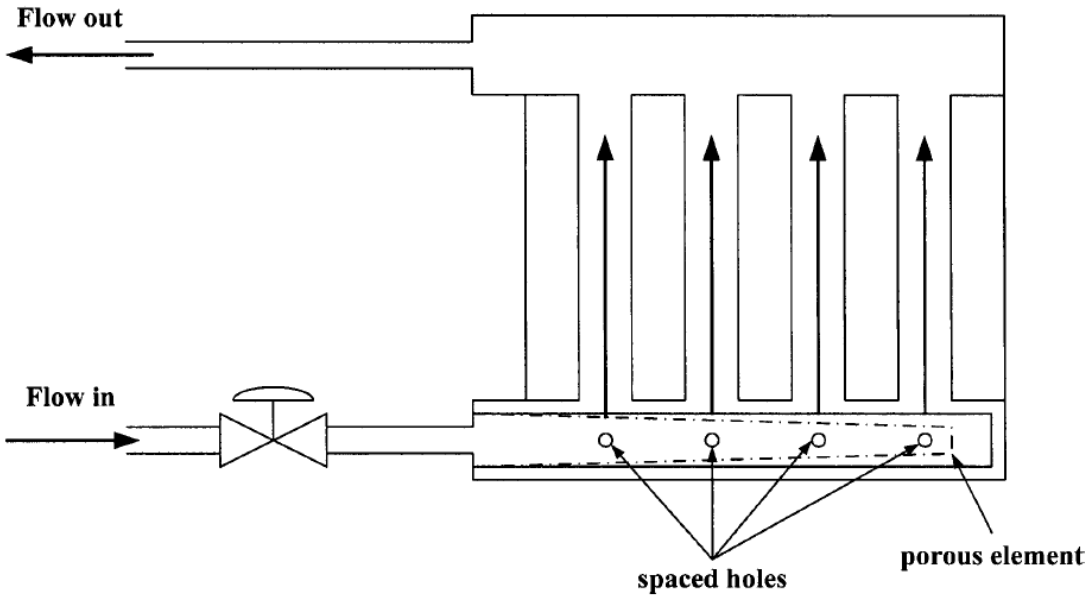

Figure 21 Schematic diagram of a conventional plate evaporator [25].

- Each separating plate has a hole (51a–53a) that serves as a flow distribution orifice, which distributes to that chamber and feeds the refrigerant to the next chamber. The orifice diameter in the plates is decreased as the distance from the refrigerant inlet is increased. The flow distribution in the header depends on the location and number of throttle plates and orifice size. The design must be modified for a different total number of tubes or other operating conditions.

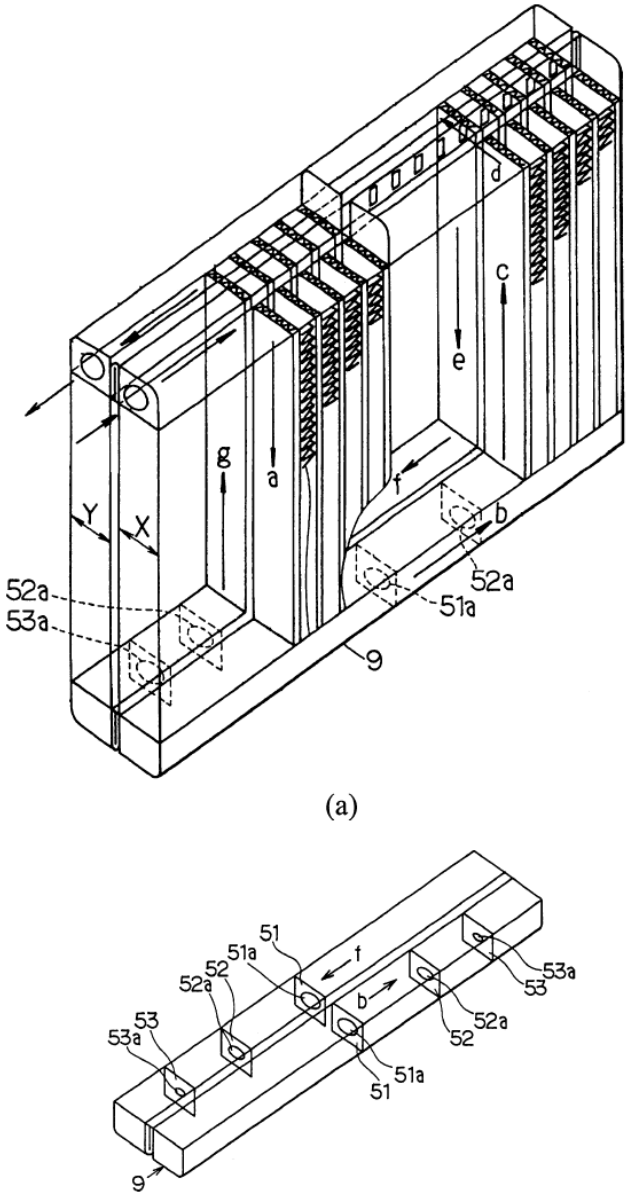

[30] Nagasawa, T., Torigoe, E., and Makihara, M., Refrigerant Evaporator with Refrigerant Distribution, U.S. Patent No. 6,449,979 B1, 2002.

Figure 22 Distributor concept described by Nagasawa et al. [30]: (a) schematic perspective view of the evaporator, (b) schematic perspective view showing a lower tank portion.

Ayub, Z. H., Distributor for Plate Heat Exchangers, U.S. Patent No. 6,179,051 B1, 2001.

- The angled grooves in the distributor and the outer walls form a passage (49) to distribute the fluid flow into the respective channels (15) associated with each plate passage in the exchanger.

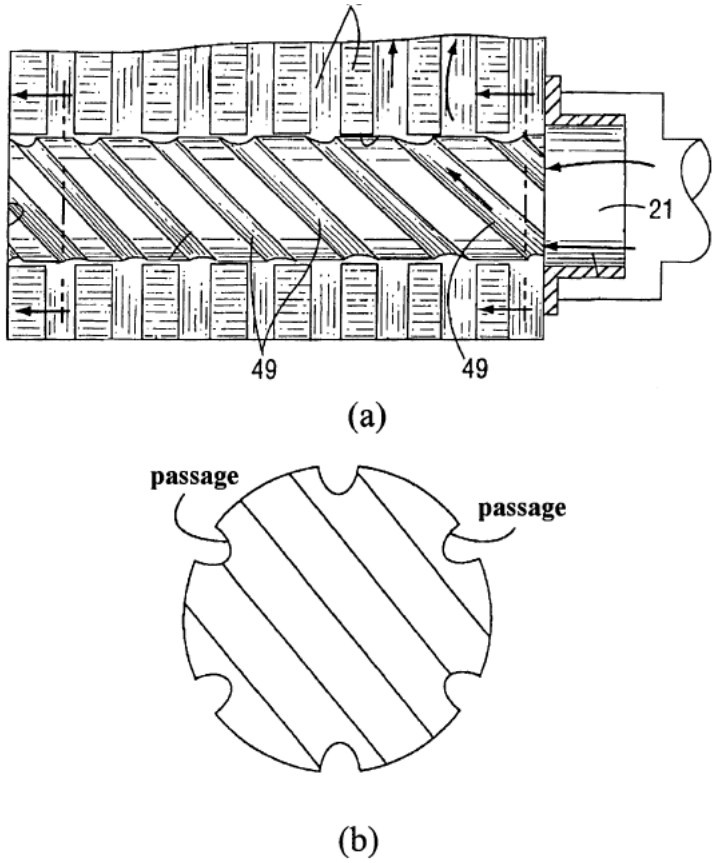

Figure 23 (a) Schematic cross-sectional view of an inlet port of heat exchanger, (b) cross-sectional view of flow distributor [31].

Improvement via homogenization

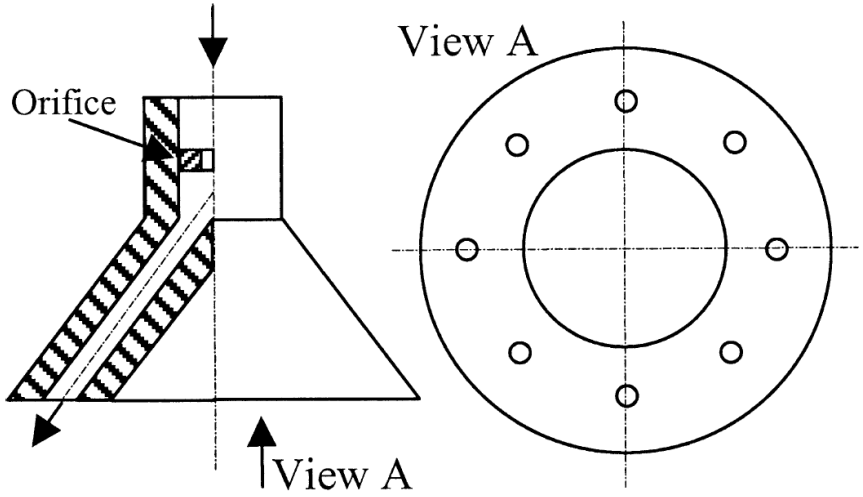

Figure 8 Typical conical distributor based on flow homogenization.

Developing Adiabatic Two Phase Flow in Headers — Distribution Issue in Parallel Flow Microchannel Heat Exchangers, Heat Transfer, Engng., 25(3):61–68, 2004

Improvement via separation, downward arrangement

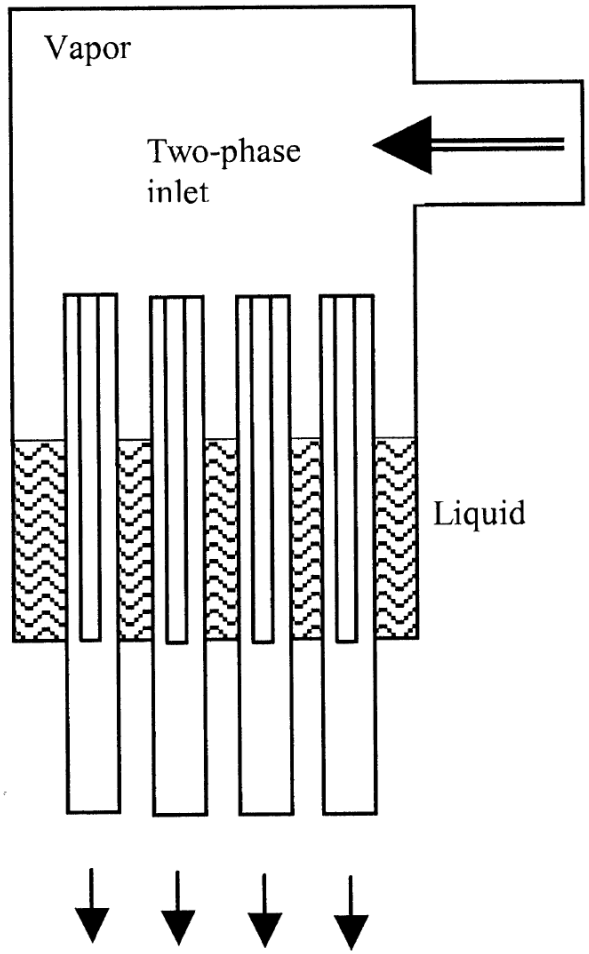

Figure 9 Distributor based on full separation and equal distribution of each phase.

Improving two-phase refrigerant distribution in the manifold of the refrigeration system, Applied Thermal Engineering 28 (2008) 2126–2135; R-134a, inlet pressure of 173.5 kPa and mass flux of 130–145 kg/m2 s.

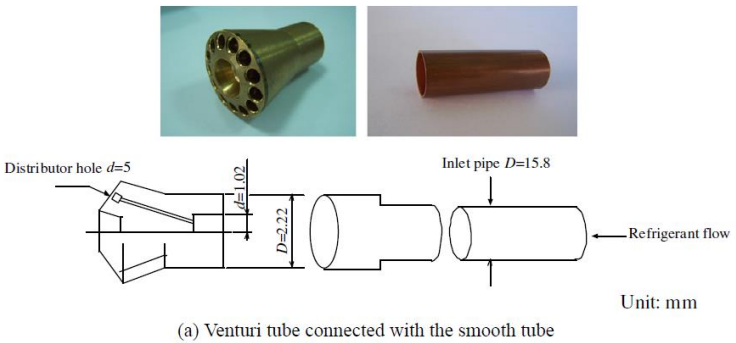

(a) Venturi tube connected with the smooth tube

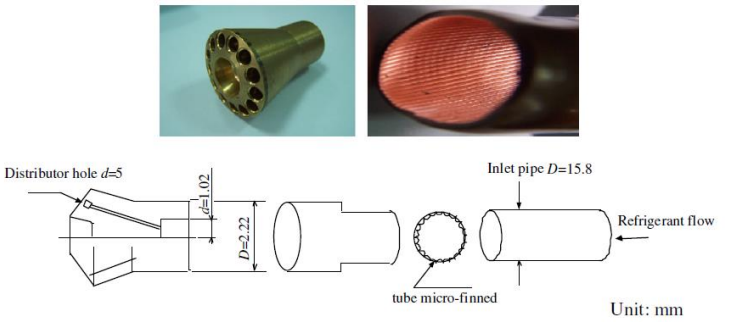

(b) Venturi tube connected with internally spirally micro-finned tube

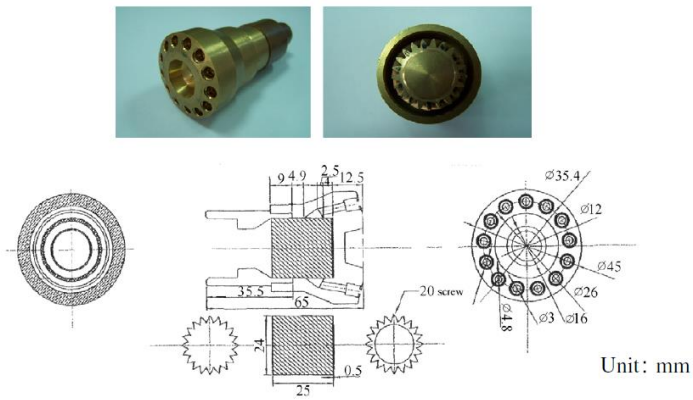

(c) distributor within a roller

Fig. 3. Sectional view and photograph of the distributors used in the present study.

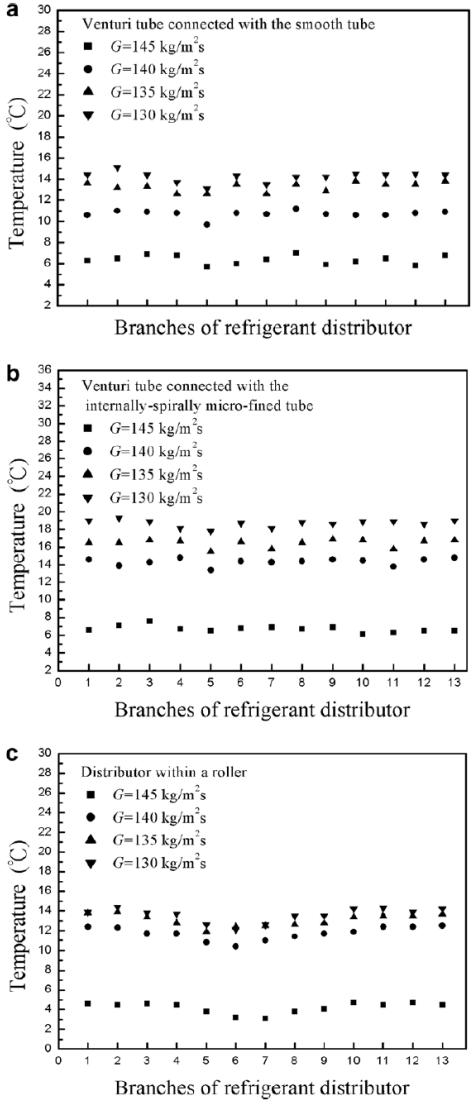

Fig. 4. Outer-wall temperature distributions of the outlet in the manifold for (a) the Venturi tube connected with the smooth tube, (b) the Venturi tube connected with the internally–spirally micro-fined tube and (c) the distributor within a roller.

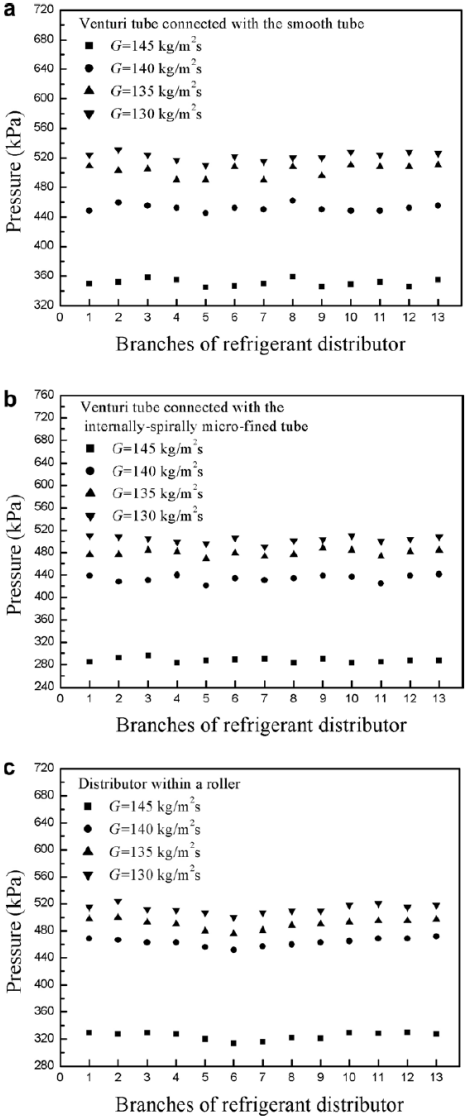

Fig. 5. Pressure distributions of the outlet in the manifold for (a) the Venturi tube connected with the smooth tube, (b) the Venturi tube connected with the internally–spirally micro-fined tube and (c) the distributor within a roller.

New approach to improve performance by venting periodic reverse vapor flow in microchannel evaporator, Int. J. Refrig., 36 (2013) 2187-2195

Vapor venting provided a 5% increase of cooling capacity and 3% of COP when operated at identical test conditions, while the maximum COP improvement was approximately 10%-12% when capacity is matched by reduction of compressor speed.

Table 1 – Cycle configurations with different valve setups.

Cycle	Bypass valve	Venting valve
DX	Closed	Closed
FGB	Open	Closed
FGBR	Open	Open

FGB: flash gas bypass
FGBR: revised flash gas bypass

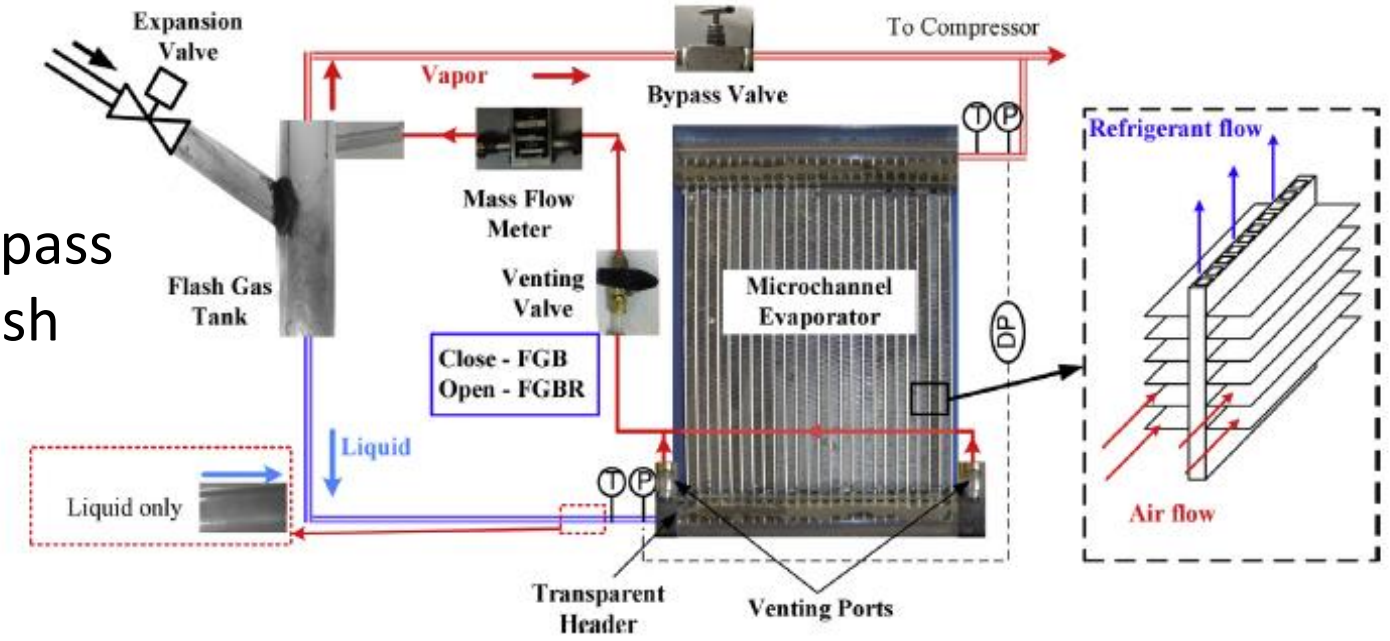

Fig. 2 – Detailed layout of the revised flash gas bypass with venting reverse vapor flow.

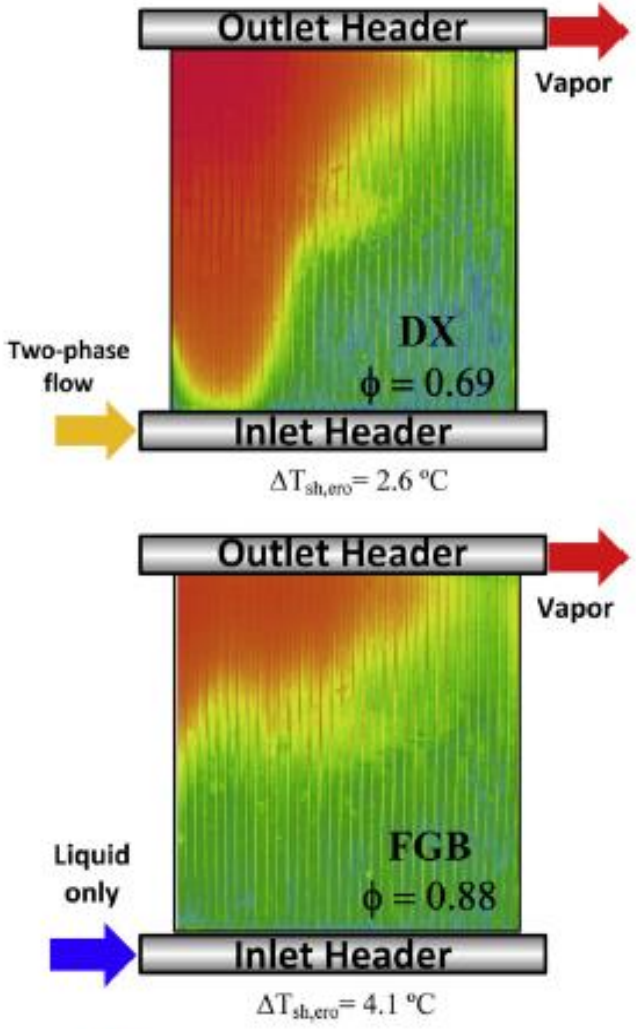

Fig. 3 – Infrared images of the low pressure evaporator in DX and FGB modes.

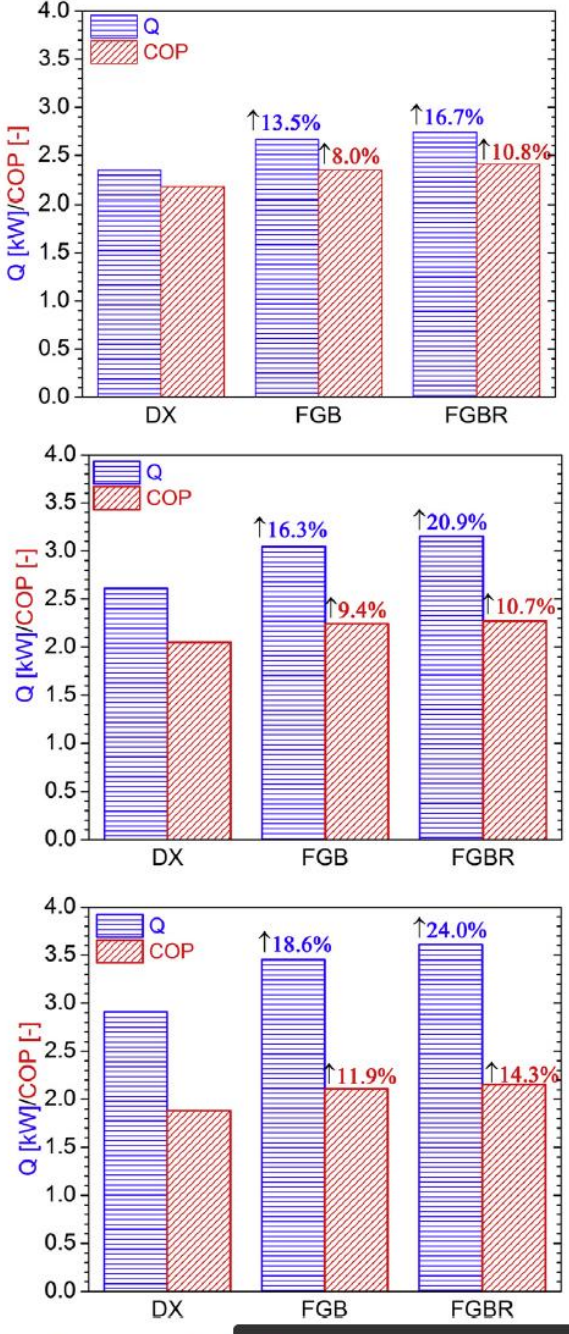

Fig. 3 – Comparison of A
operating cycles at the fix
(2) 35/35 °C (3) 43/43 °C.

Experimental verification of a condenser with liquid vapor separation in an air conditioning system, applied thermal engng., 51, 2013, 48-54.

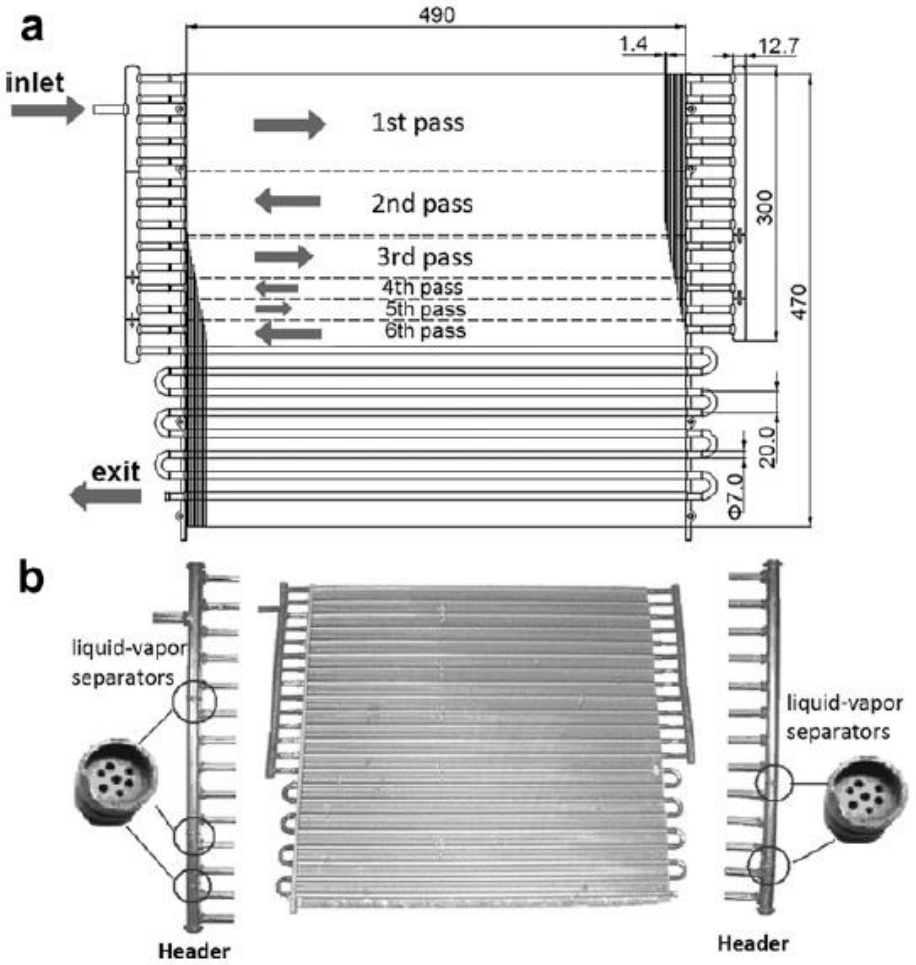

Fig. 1. (a). Schematic of liquid–vapor separation condenser. (b). Picture of LSC and the headers with the liquid–vapor separator.

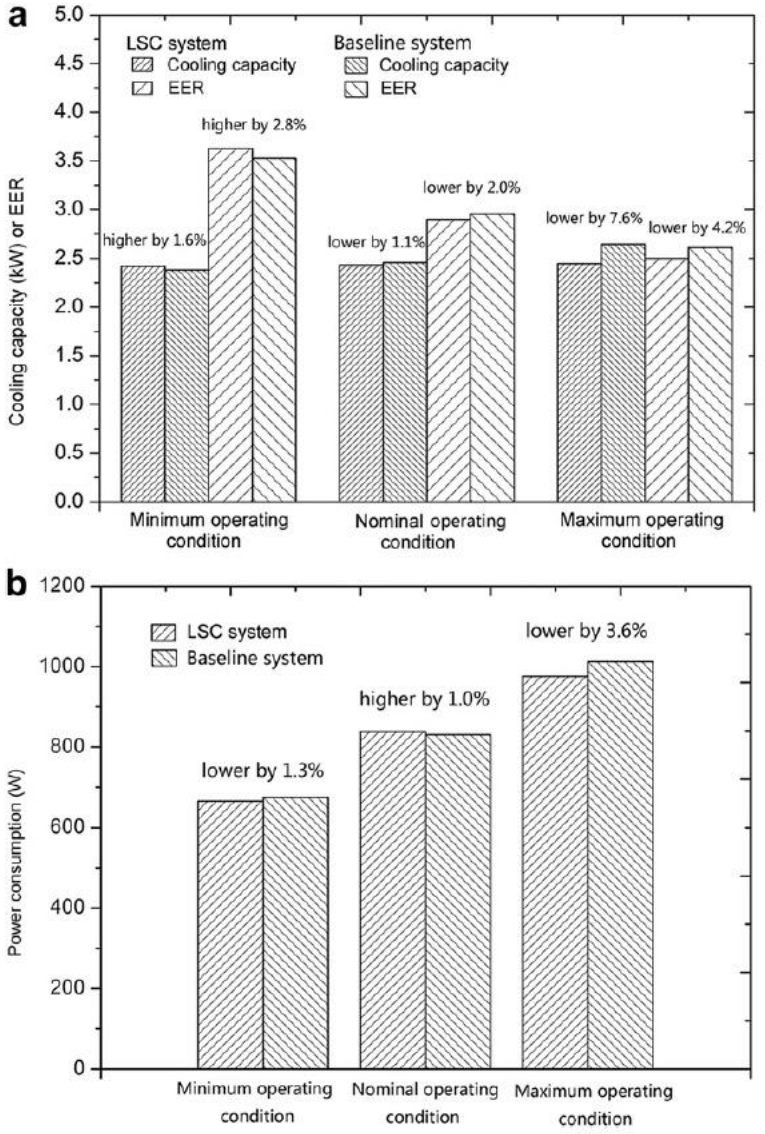

Fig. 4. (a) Cooling capacity and EER of the two systems. (b) Power consumption of the two systems.

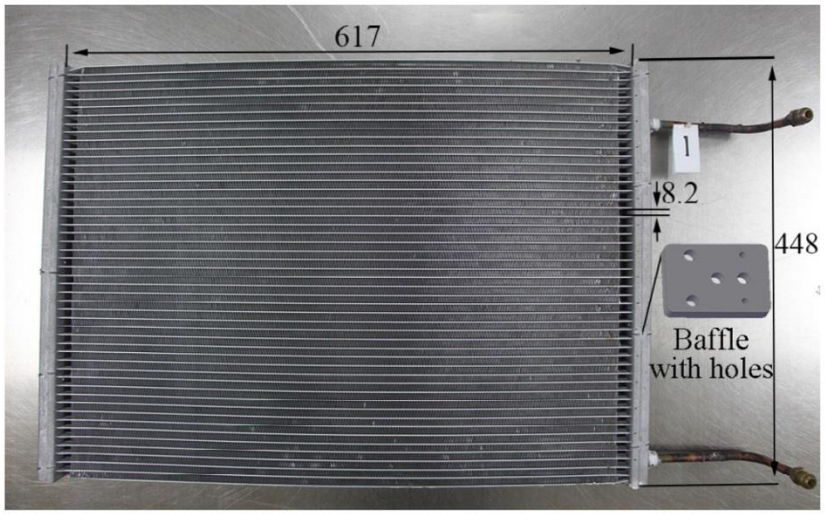

(a)

(b)

Fig. 1 – (a and b) Double-row liquid–vapor separation microchannel condenser.

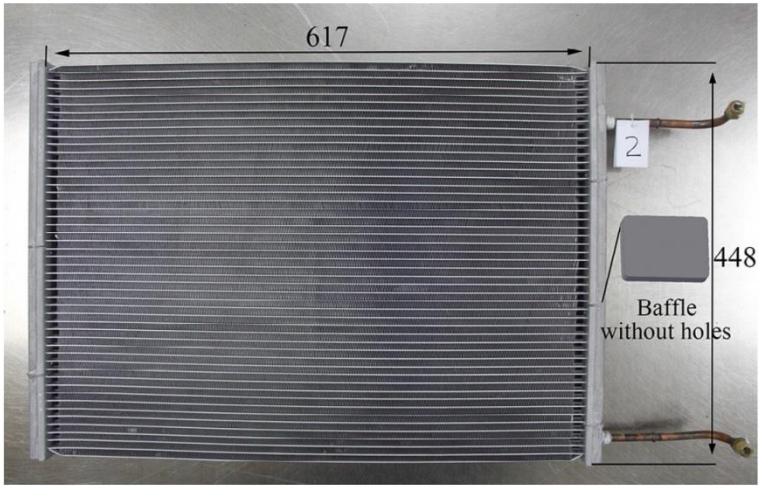

Fig. 2 – Double-row parallel-flow microchannel condenser.

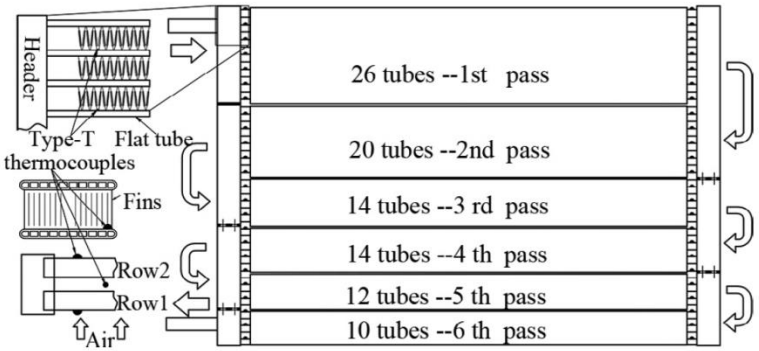

Fig. 3 – Tube pass scheme and thermocouple arrangement.

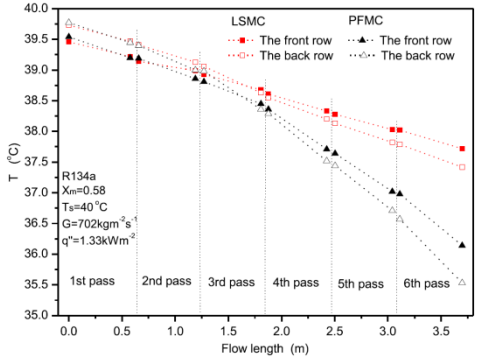

Fig. 5 – Tube wall temperatures along the flow length.

Experimental investigation on the thermodynamic performance of double-row liquid–vapor separation microchannel condenser, Int. j. Refrig., Vol. 67, 2016, pp. 373-382.

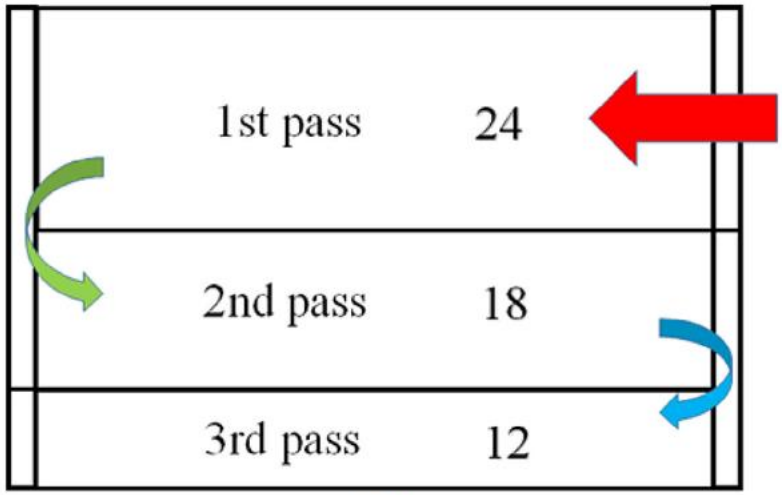

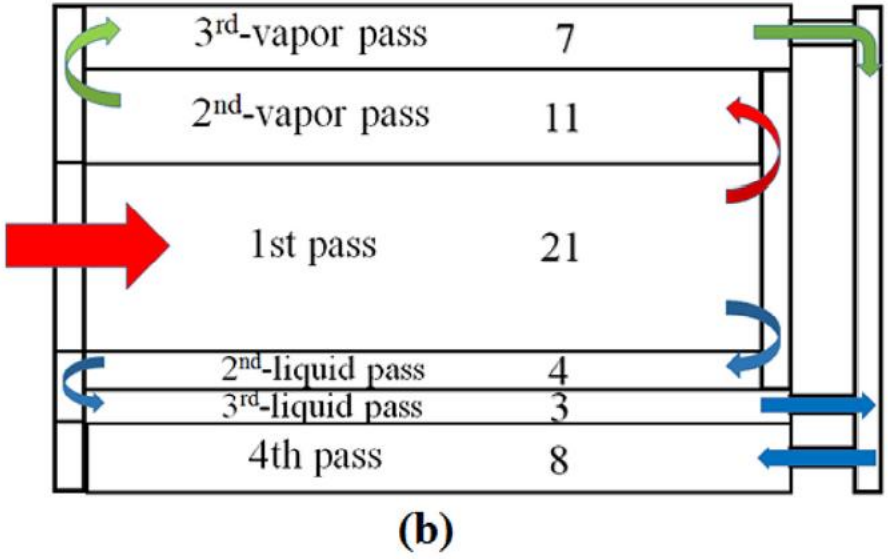

Fig. 4 – Schematic of the condensers: (a) Baseline condenser; (b) Separation condenser

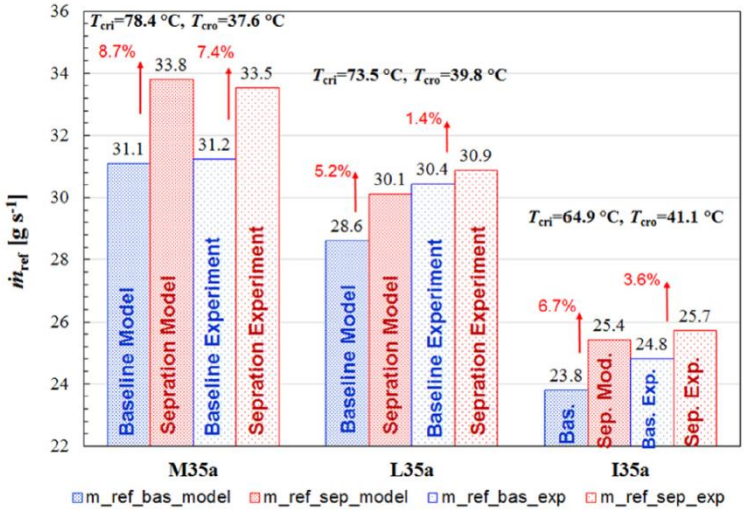

Fig. 10 – Mass flow rate $\dot{m}_{ref}$ for the two condensers at the same T_{cri} and T_{cro}, at three operating conditions.

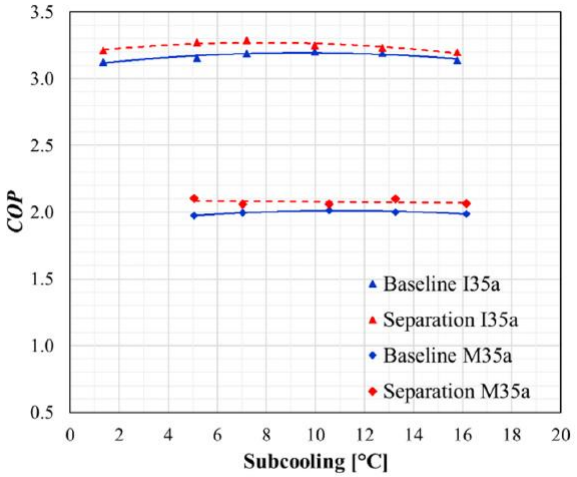

Fig. 12 – COP comparison for refrigeration systems with baseline condenser and separation condenser at superheat of 10 K and at the matched capacity.

Improvement of condenser performance by phase separation confirmed experimentally and by modeling, Int. J. Refrig., Vol. 78 (2017) 60–67.

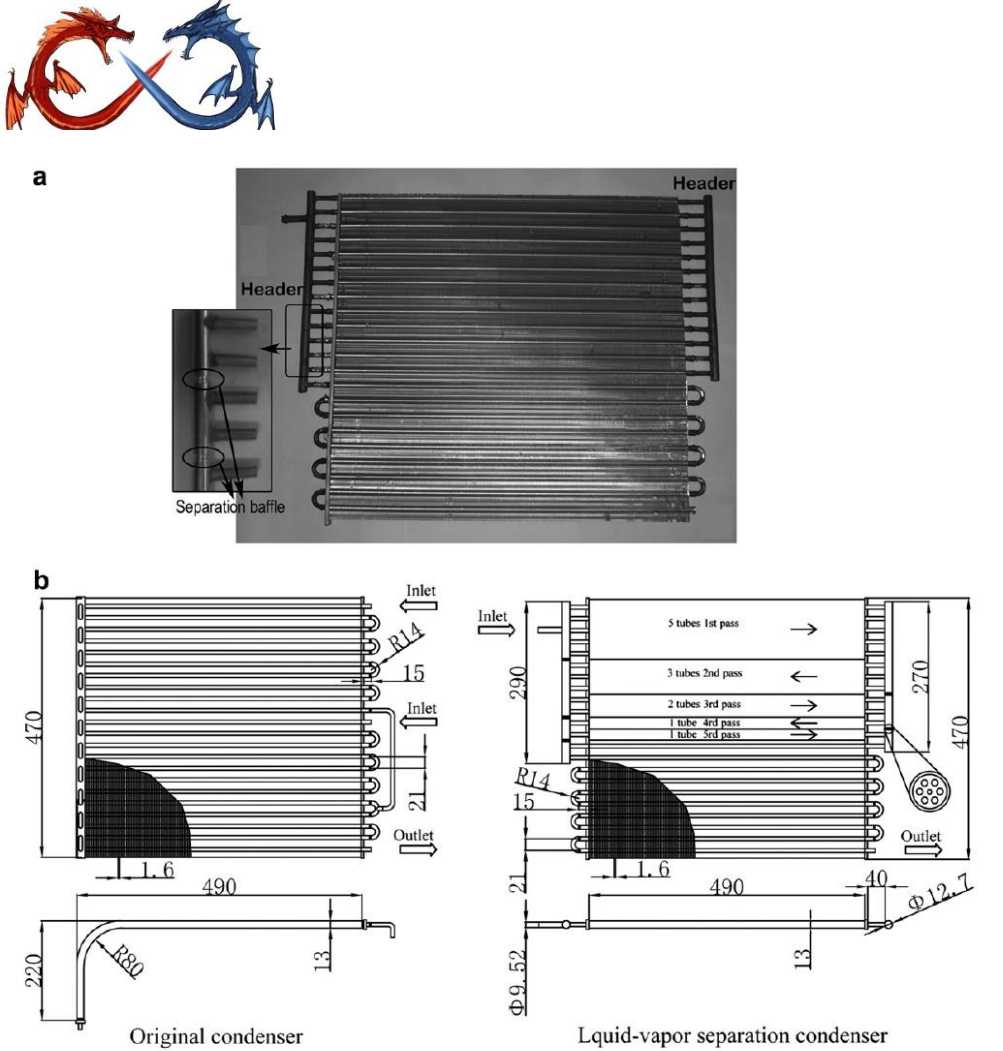

Fig. 2 – (a) Picture of the condenser with liquid–vapor separation baffles. (b) Schematics of the heat exchangers.

Performances of a split-type air conditioner employing a condenser with liquidevapor separation baffles, Int. J. Refrig., (2012), 278-289

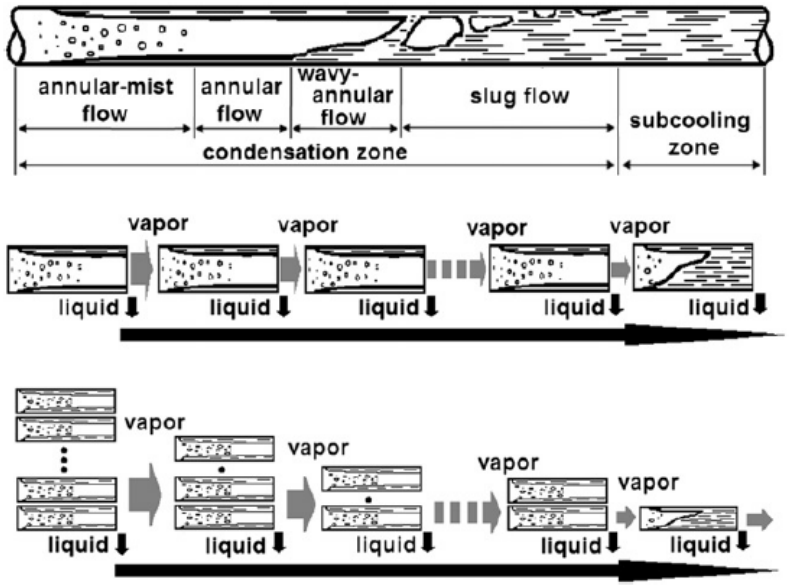

Fig. 1 – Schematics diagram of liquid–vapor separation condenser.

The results showed that the enhanced condenser unit could supply the equivalent cooling capacity and energy efficiency ratio (EER) as those of the baseline one at the standard cooling condition when it had only 63.1% condenser heat transfer area and 80.3% charge amount of the baseline unit. With the optimal capillary tube length of 700 mm, the cooling capacity of the LSC unit just decreases by 2.9% as well as EER by 2.3% while charge is added to 18% more than the charge at the maximum EER.

Visualization of flow distribution in rectangular and triangular header geometries, Int. J. Refrig, 76 (2017) 170–183

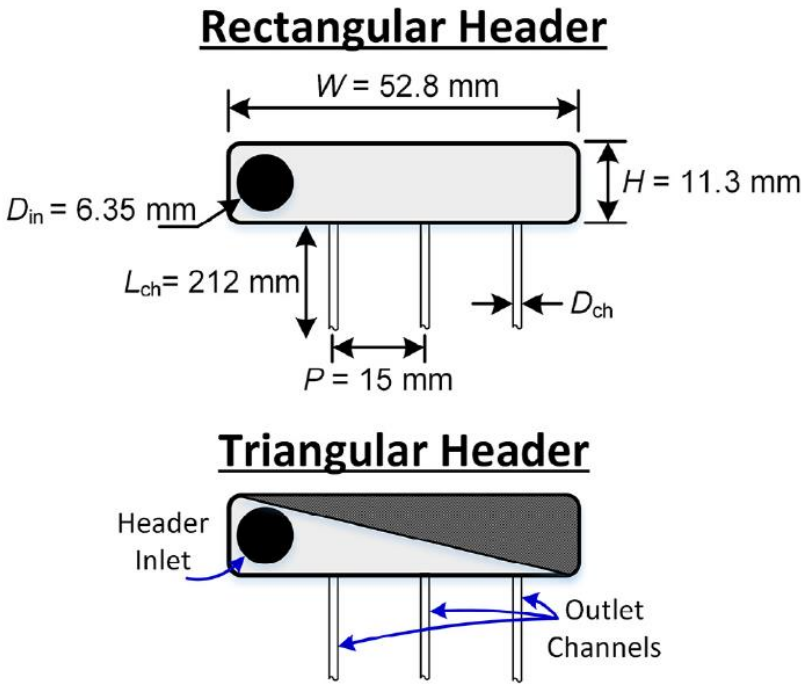

Fig. 2 – Schematic of header geometries tested with key dimensions.

Table 3 – Important operational and geometric parameters.

Parameter	Values
Inlet Quality	0.05–0.35
Average Channel Mass Flux	50.0–300 kg m^{-2} s^{-1}
Outlet Channel Diameter	1–3 mm
Inlet Mass Flux	2.60–200 kg m^{-2} s^{-1}
Feeder Tube Diameter	6.35 mm
Rectangular Header Dimensions ($L \times W \times H$)	52.8 mm × 3.50 mm × 11.3 mm

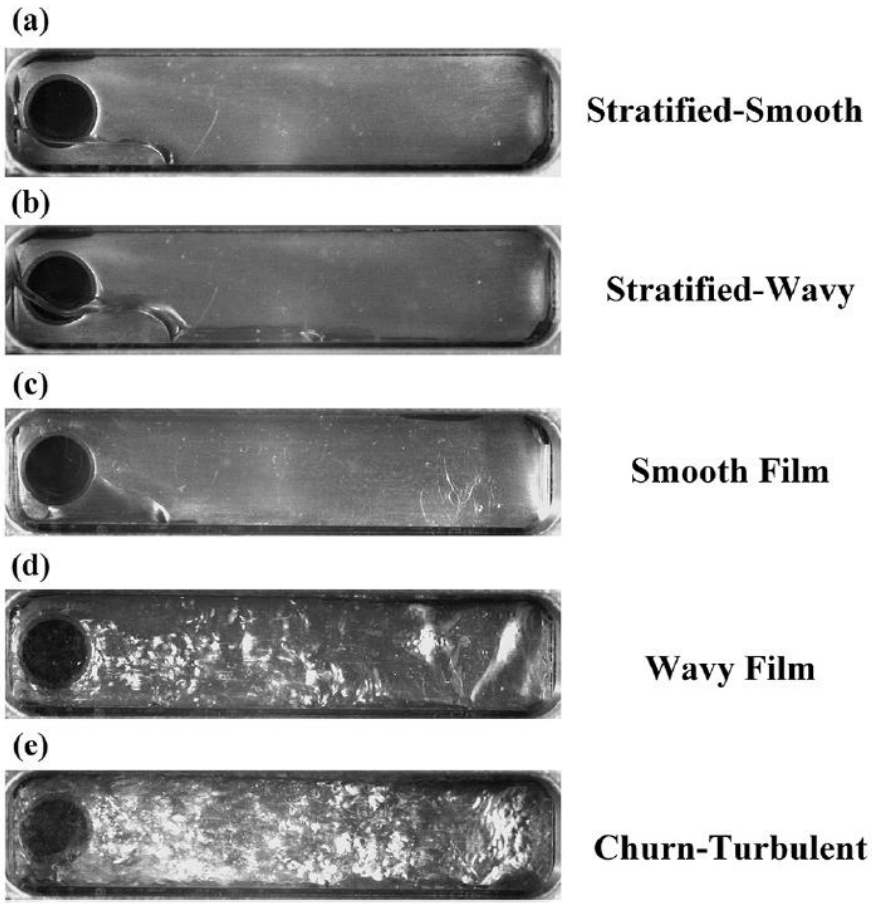

Fig. 3 – Photographs of flow regimes observed in the rectangular header.

Air-water system

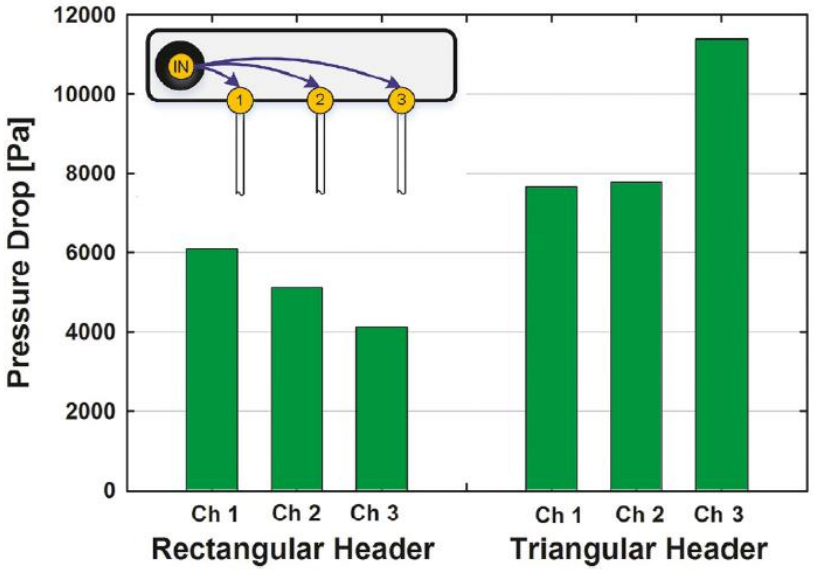

Fig. 13 – Pressure drop between the header inlet and the channel entrances. Data collected at an inlet quality of 0.20 and an average channel mass flux of 300 kg m^{-2} s^{-1}.

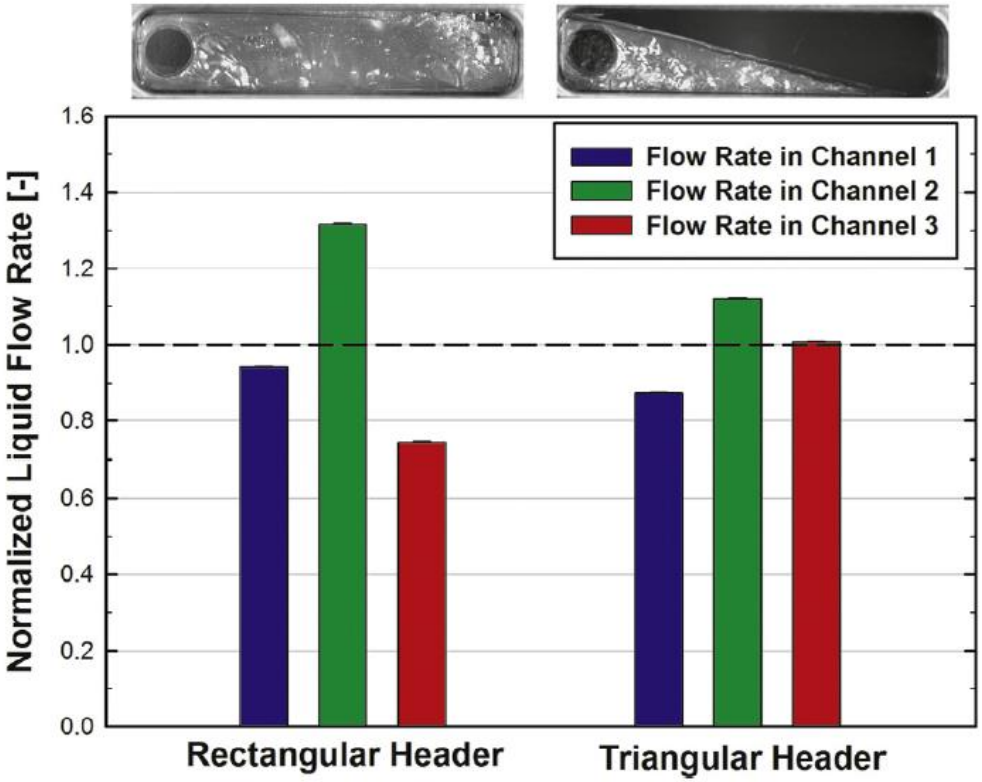

Fig. 11 – Normalized liquid flow rates for the rectangular and triangular headers connected to 2-mm diameter outlet channels. Images of the header flow regime for this condition are shown above the plot.

Influence factors of flow distribution and a feeder tube compensation method in multicircuit evaporators, Int. J. Refrig., 73 (2017) 11–23.

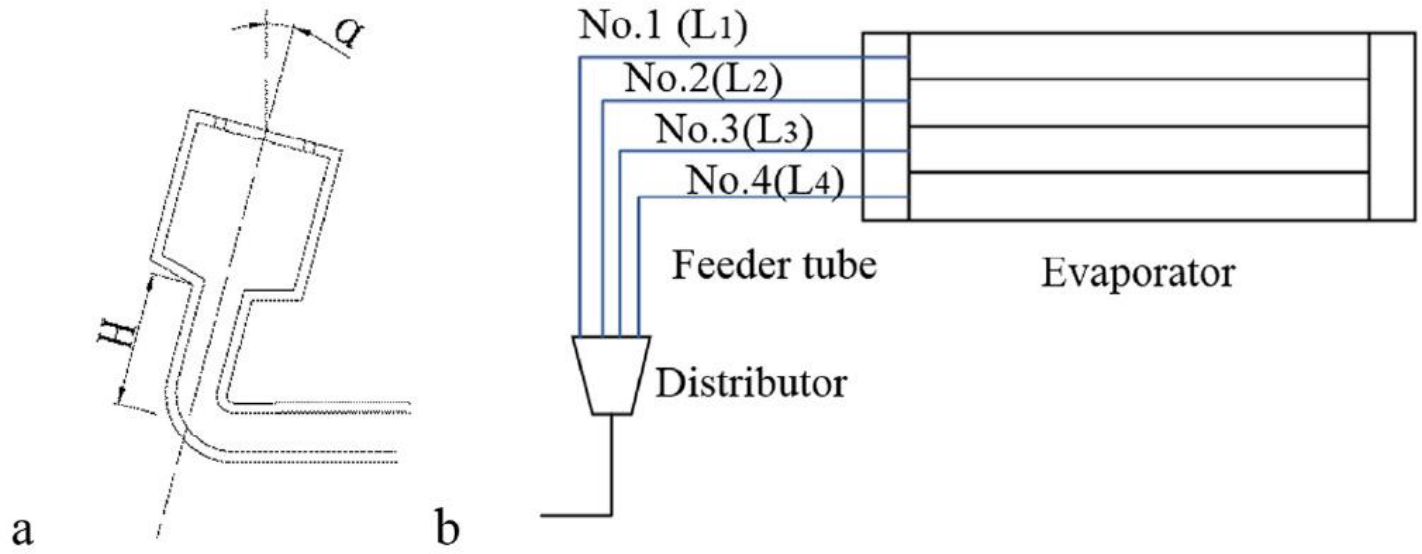

Table 1 – Test samples configuration.

Sample	L_1/mm	L_2/mm	L_3/mm	L_4/mm	H/ mm
1	300	300	300	300	200
2	300	300	300	300	100
3	300	300	300	300	50
4	500	400	400	300	200
5	700	500	500	300	200
6	300	300	400	400	200

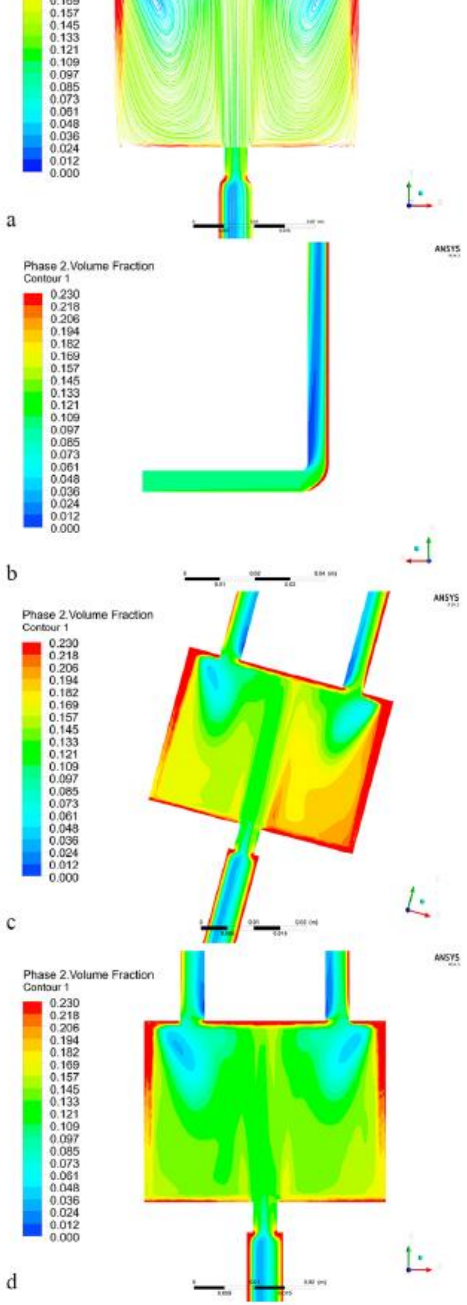

Fig. 7 – Flow behavior for distributor: (a) pathlines in the distributor, liquid phase volume fraction (b) in inlet tube, (c) in the distributor with vertical installation, (d) in the distributor with inclination installation.

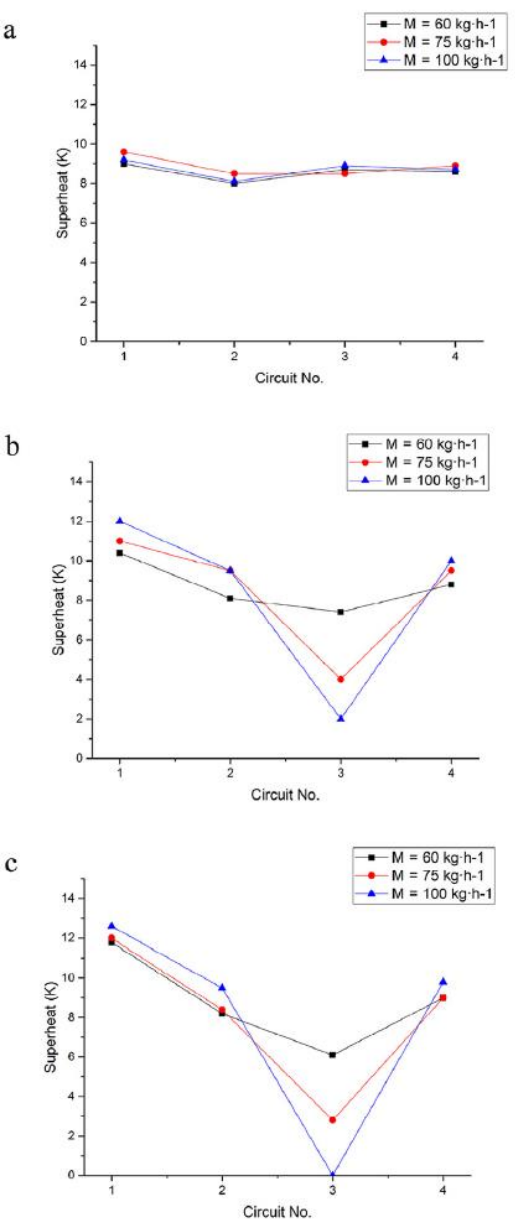

Fig. 3 – Superheat distribution performance in four evaporator circuits for (a) sample 1 with H = 200 mm, (b) sample 2 with H = 100 mm, and (c) sample 3 with H = 50 mm.

Enhanced condensation heat transfer for dielectric fluid within microchannel heat sink,Int. J. Heat Mass Transfer, 106 (2017) 518–525

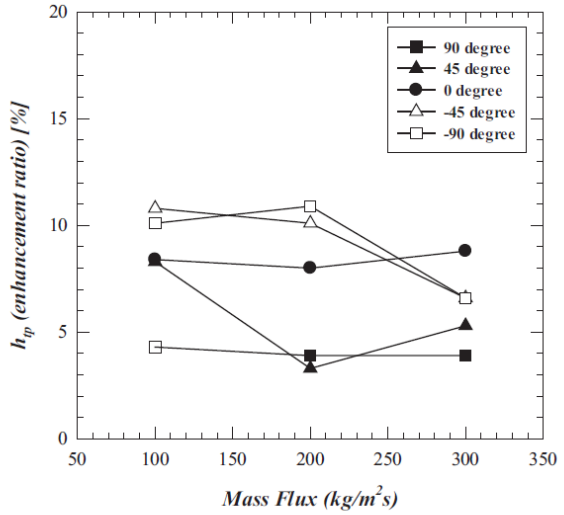

(a) Enhancement ratio of average heat transfer coefficient

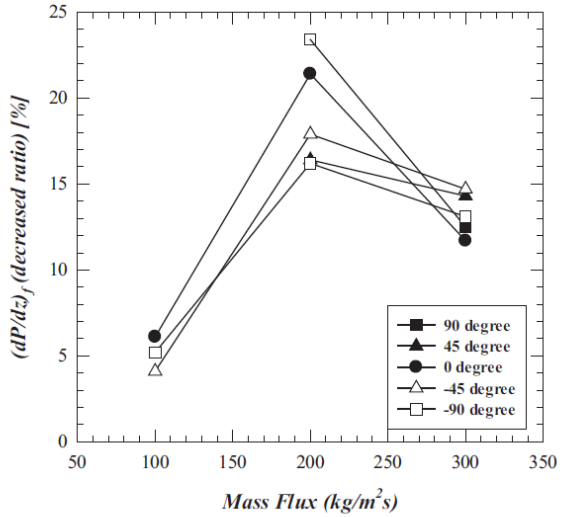

(b) Reduction ratio of average pressure drop.

Fig. 8. Ratios of heat transfer enhancement and pressure drop reduction between micro-drainage channel and conventional channel for all mass flux and orientations.

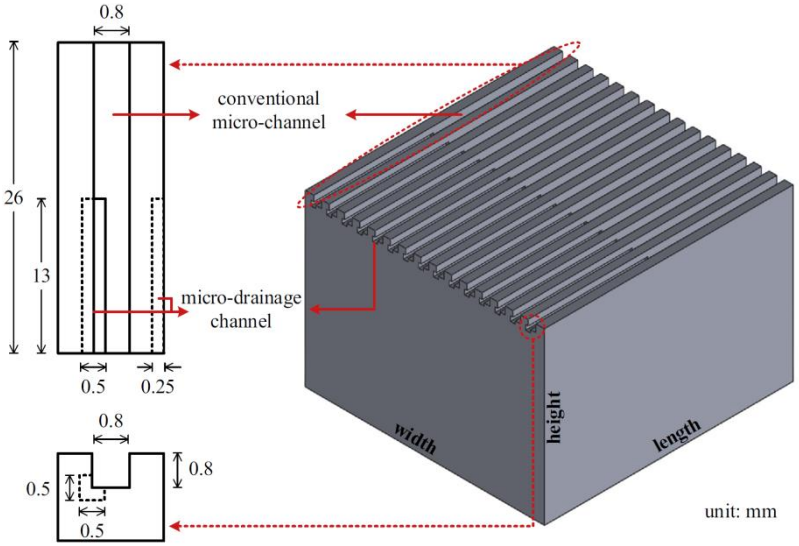

Fig. 2. Micro-channel cheat sink with micro-drainage channel.

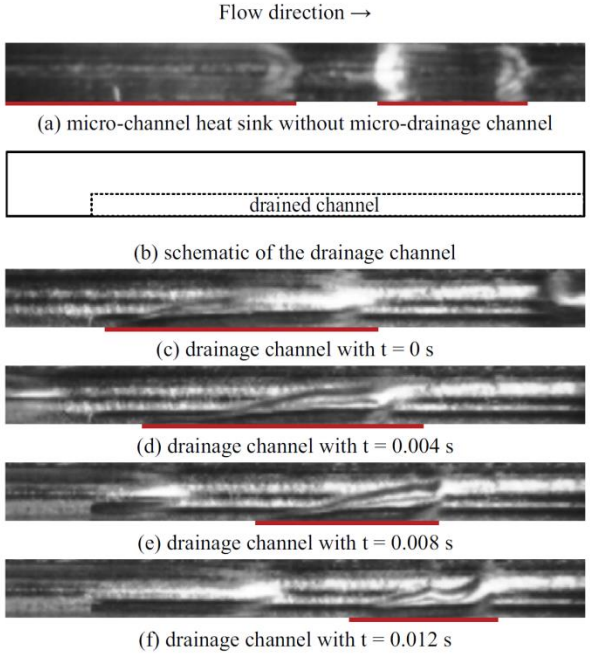

(a) micro-channel heat sink without micro-drainage channel

(b) schematic of the drainage channel

(c) drainage channel with t = 0 s

(d) drainage channel with t = 0.004 s

(e) drainage channel with t = 0.008 s

(f) drainage channel with t = 0.012 s

Fig. 4. Flow pattern for microchhanel heat sink with and without micro drainage subject to horizontal arrangement ($G = 100\ kg\ m^{-2}\ s^{-1}$, $\theta = 0°$, $x_{avg} = 0.19$).

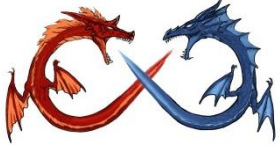

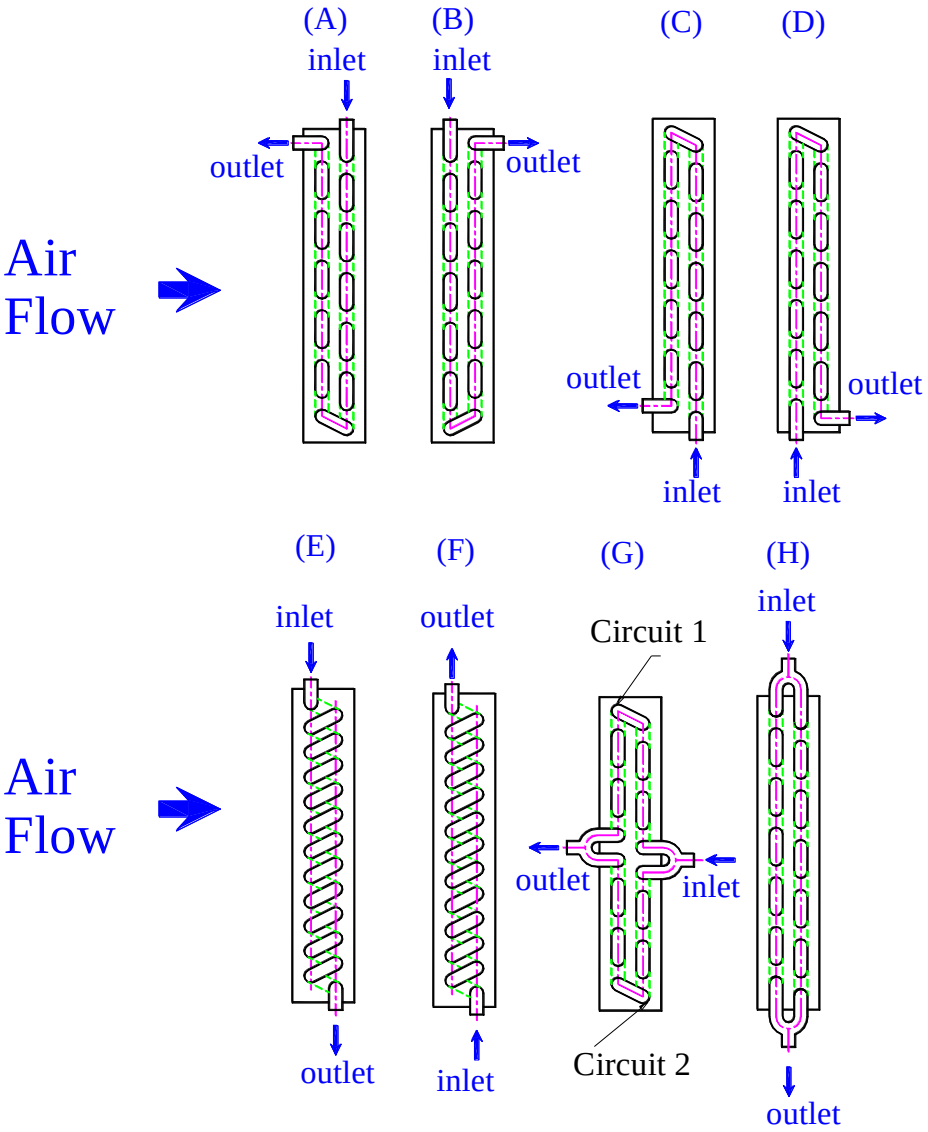
Air Flow
(A)
inlet
outlet
(B)
inlet
outlet
(C)
outlet
inlet
(D)
outlet
inlet
Air Flow
(E)
inlet
outlet
(F)
outlet
inlet
(G)
Circuit 1
outlet
inlet
Circuit 2
(H)
inlet
outlet

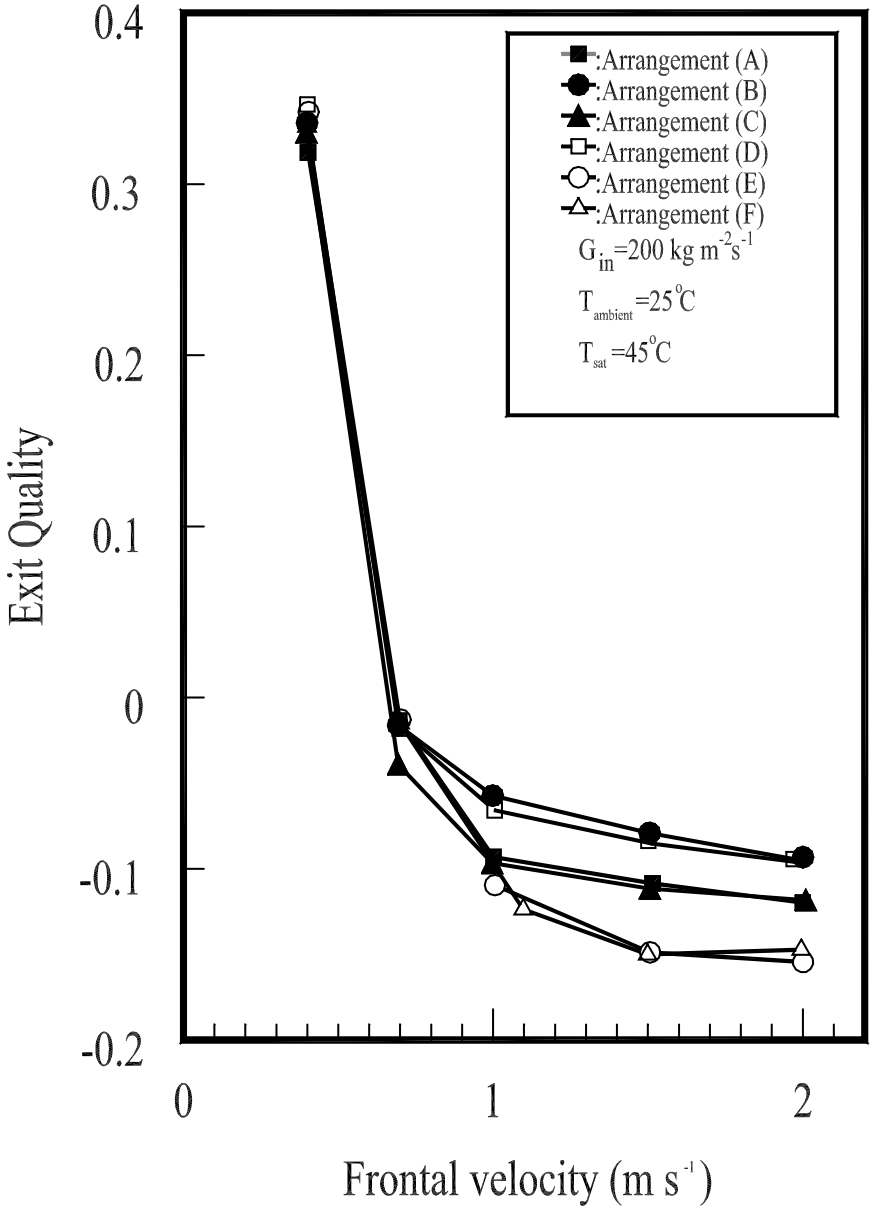
:Arrangement (A)
:Arrangement (B)
:Arrangement (C)
:Arrangement (D)
:Arrangement (E)
:Arrangement (F)
G_{in}=200 kg $m^{-2}s^{-1}$
$T_{ambient}$=25°C
T_{sat}=45°C
Exit Quality
0.4
0.3
0.2
0.1
0
-0.1
-0.2
0
1
2
Frontal velocity (m s^{-1})

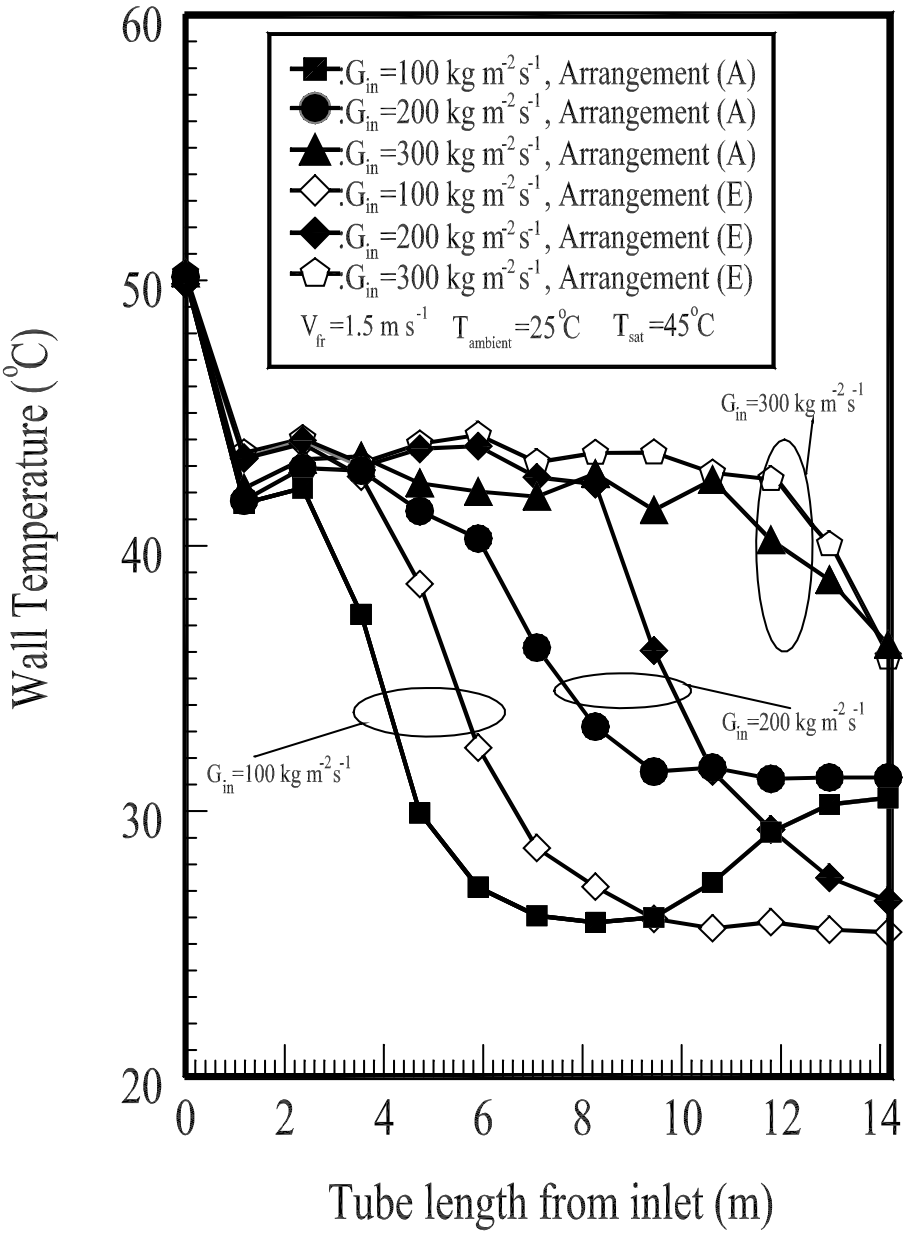
:G_{in}=100 kg m^{-2}s^{-1}, Arrangement (A)
:G_{in}=200 kg m^{-2}s^{-1}, Arrangement (A)
:G_{in}=300 kg m^{-2}s^{-1}, Arrangement (A)
:G_{in}=100 kg m^{-2}s^{-1}, Arrangement (E)
:G_{in}=200 kg m^{-2}s^{-1}, Arrangement (E)
:G_{in}=300 kg m^{-2}s^{-1}, Arrangement (E)
V_{fr}=1.5 m s^{-1} $T_{ambient}$=25°C T_{sat}=45°C
G_{in}=300 kg m^{-2}s^{-1}
G_{in}=200 kg m^{-2}s^{-1}
G_{in}=100 kg m^{-2}s^{-1}
Wall Temperature (°C)
60
50
40
30
20
0
2
4
6
8
10
12
14
Tube length from inlet (m)

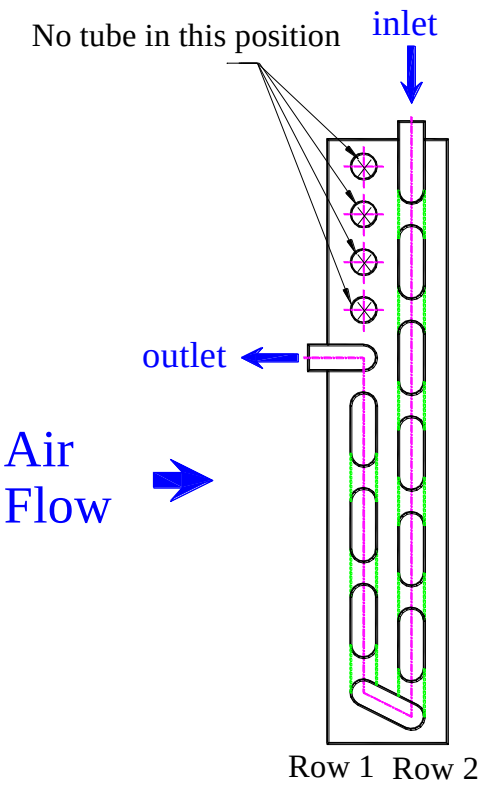
No tube in this position
inlet
outlet
Row 1
Row 2

Air Flow

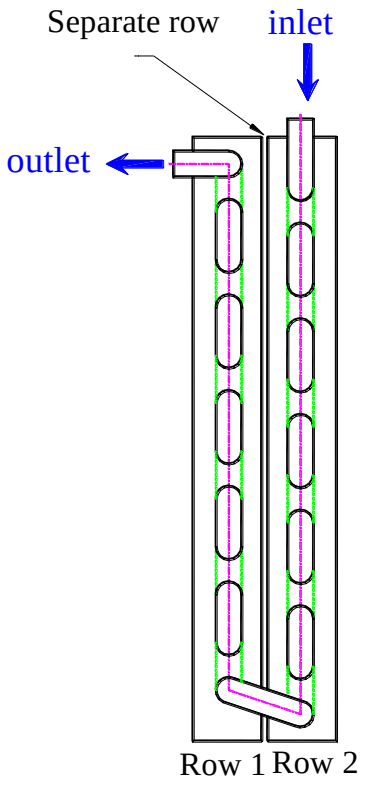
Separate row
inlet
outlet
Row 1
Row 2

Performance of a finned-tube evaporator optimized for different refrigerants and its effect on system efficiency, Int. J. Refrig, 28 (2005) 820–827

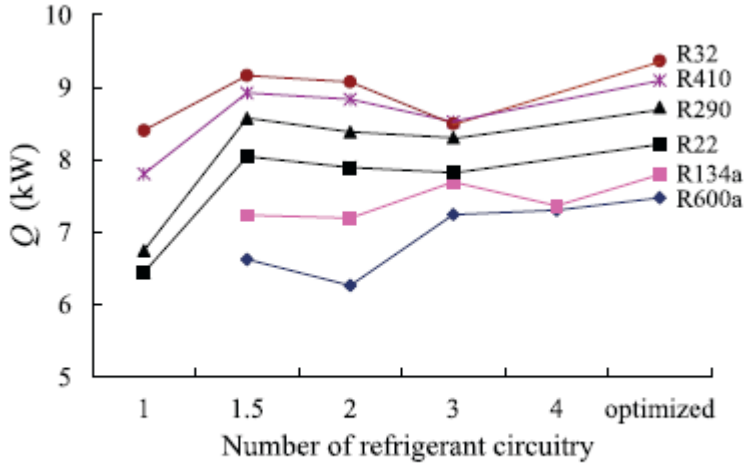

Fig. 4. Evaporator capacities for manually developed and ISHED1-optimized circuitry designs.

Table 2
Evaporator design information

Items	Unit	Value
Tube length	mm	500
Tube inside diameter	mm	9.2
Tube outside diameter	mm	10.0
Tube spacing	mm	25.4
Tube row spacing	mm	22.2
Number of tubes per row		12
Number of depth rows		3
Fin thickness	mm	0.2
Fin spacing	mm	2
Tube inner surface		Smooth
Fin geometry		Louver
Air volumetric flow rate	$m^3\ min^{-1}$	25.5

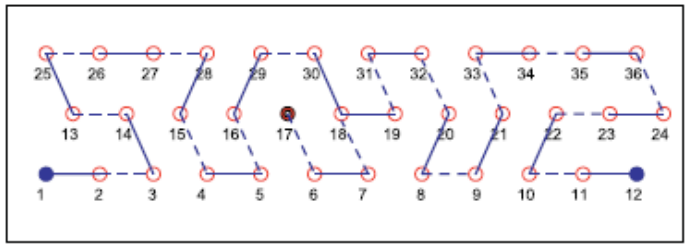

1.5 Circuits

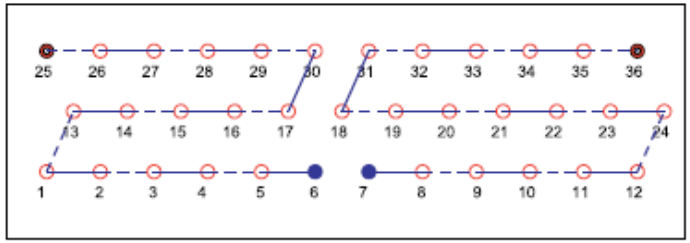

2 Circuits

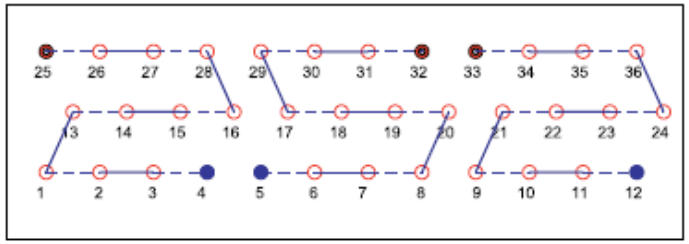

3 Circuits

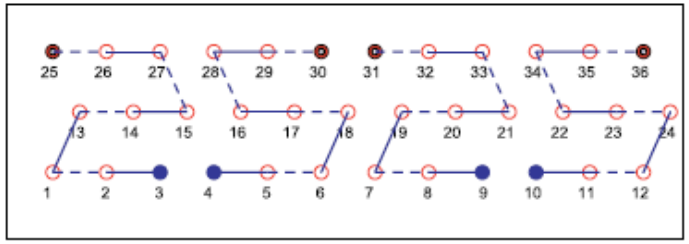

4 Circuits

Fig. 3. Manually developed 1.5, 2, 3, and 4-circuit designs (side view; circles denote tubes; continuous lines indicate return bends on the near side of the heat exchanger, broken lines indicate return bends on the far side, full circles indicate outlet tubes).

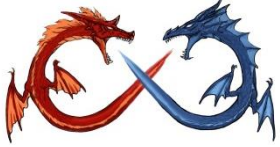

Concluding Remarks

- Flow distribution is highly dependent on the flow pattern in header.
- Normally placing higher resistance at downstream (heat exchanger tubes..) would provide better flow distribution.
- Flow distribution also depends on the upstream conditions into the header.
- Geometric dimensions plays essential role in flow distribution. Inlet location into the header also influences the flow distribution appreciably.
- Flow direction/header direction also affects the flow distribution.
- Normally inlet quality imposes very minor influence of flow distribution, however, if a restriction is added to produced mist flow, better flow distribution occurs.
- Some liquid/vapor separation mechanism can effectively improve the distribution either in evaporator or condenser.

感謝聆聽

敬請賜教

王啟川
Tel: +886-3-5712121 ext. 55105
E-mail:ccwang@mail.nctu.edu.tw